INFORMATION TO USERS

This manuscript has been reproduced from the microfilm master. UMI films the text directly from the original or copy submitted. Thus, some thesis and dissertation copies are in typewriter face, while others may be from any type of computer printer.

The quality of this reproduction is dependent upon the quality of the copy submitted. Broken or indistinct print, colored or poor quality illustrations and photographs, print bleedthrough, substandard margins, and improper alignment can adversely affect reproduction.

In the unlikely event that the author did not send UMI a complete manuscript and there are missing pages, these will be noted. Also, if unauthorized copyright material had to be removed, a note will indicate the deletion.

Oversize materials (e.g., maps, drawings, charts) are reproduced by sectioning the original, beginning at the upper left-hand corner and continuing from left to right in equal sections with small overlaps. Each original is also photographed in one exposure and is included in reduced form at the back of the book.

Photographs included in the original manuscript have been reproduced xerographically in this copy. Higher quality 6" x 9" black and white photographic prints are available for any photographs or illustrations appearing in this copy for an additional charge. Contact UMI directly to order.

U·M·I

University Microfilms International
A Bell & Howell Information Company
300 North Zeeb Road, Ann Arbor, MI 48106-1346 USA
313/761-4700 800/521-0600

Order Number 9408509

Accretion disk boundary layers

Popham, Robert George, Ph.D.

The University of Arizona, 1993

U·M·I
300 N. Zeeb Rd.
Ann Arbor, MI 48106

ACCRETION DISK BOUNDARY LAYERS

by

Robert George Popham

A Dissertation Submitted to the Faculty of the

DEPARTMENT OF ASTRONOMY

In Partial Fulfillment of the Requirements
For the Degree of

DOCTOR OF PHILOSOPHY

In the Graduate College

THE UNIVERSITY OF ARIZONA

1 9 9 3

THE UNIVERSITY OF ARIZONA
GRADUATE COLLEGE

As members of the Final Examination Committee, we certify that we have read the dissertation prepared by Robert George Popham

entitled Accretion Disk Boundary Layers

and recommend that it be accepted as fulfilling the dissertation requirement for the Degree of Doctor of Philosophy

R. Narayan	8-26-93
	Date
W. Kley	8/26/93
	Date
James W. Liebert	8/26/93
	Date
Lubow Nelson	8/26/93
	Date
	Date

Final approval and acceptance of this dissertation is contingent upon the candidate's submission of the final copy of the dissertation to the Graduate College.

I hereby certify that I have read this dissertation prepared under my direction and recommend that it be accepted as fulfilling the dissertation requirement.

R. Narayan	8-26-93
Dissertation Director	Date

STATEMENT BY AUTHOR

This dissertation has been submitted in partial fulfillment of requirements for an advanced degree at The University of Arizona and is deposited in the University Library to be made available to borrowers under rules of the Library.

Brief quotations from this dissertation are allowable without special permission, provided that accurate acknowledgment of source is made. Requests for permission for extended quotation from or reproduction of this manuscript in whole or in part may be granted by the head of the major department or the Dean of the Graduate College when in his or her judgment the proposed use of the material is in the interests of scholarship. In all other instances, however, permission must be obtained from the author.

SIGNED: Robert G. Popham

ACKNOWLEDGEMENTS

I have truly enjoyed my time as a graduate student, and this mostly due to the people with whom I have spent it. My graduate career has been somewhat unusual in that it has been split almost evenly between the University of Arizona and the Center for Astrophysics. The graduate students at both institutions have been good friends and colleagues, and have made the past five years much more enjoyable and interesting. In particular, my hiking companions at Steward and the "golf" group at CfA have enlivened some of my time spent away from work. The move from one institution to another has gone much more smoothly than expected, and this has largely been due to the extra effort of the people in the two astronomy department offices, Helen Bluestein and Michelle Santos at Steward and Christina Doyle and Beth Tracy at CfA. Joy Facio at Steward has been especially helpful in keeping track of my somewhat complex financial matters. Also, the members of my class at Steward, Sally Oey, Kim McLeod, Brian McLeod, and Dante Minniti, and my former officemate, James Lowenthal, have always been willing to help when I needed to do things at Steward remotely.

A number of people have been generous with their time and expertise, and have helped me complete the work presented in this thesis. Several people have served in the capacity of local experts on various topics; these include Jim Liebert and Richard Wade at Steward and George Rybicki, Scott Kenyon, and Lee Hartmann at CfA. In addition, some outside experts have also provided useful comments and discussions on this work, including Marek Abramowicz, Bohdan Paczyński, and especially Jim Pringle.

Finally, much of the credit for the work presented here, and for my development as a researcher, must go to my advisor and collaborator, Ramesh Narayan. I have worked with Ramesh throughout my graduate student career, and I feel that my decision to work with him was one of the best I have ever made. As an advisor, as a teacher, and as a collaborator, he has been exceptionally good. If I can live up to his example with even half his energy, I will consider my career in astronomy a great success.

TABLE OF CONTENTS

TABLE OF CONTENTS – *Continued*

TABLE OF CONTENTS – *Continued*

LIST OF FIGURES

LIST OF FIGURES – *Continued*

LIST OF TABLES

ABSTRACT

We examine the nature of the boundary layer in α-viscous accretion disks. The boundary layer is the interface between the disk and the accreting central star or black hole. We develop two models for the boundary layer by expanding and generalizing the standard disk equations, and then solving our new set of equations numerically using a relaxation method.

First, we use a model which includes a polytropic equation of state to examine the disk dynamics. This allows us to ignore the energetics and radiative transfer and simplifies the problem considerably. We find two types of boundary layer solutions with this model, depending on the rotation rate of the accreting star. One of these is a new type of solutions in which the angular momentum accretion rate can be small or negative. These solutions allow accretion to continue even after the star spins up to breakup speed.

We apply a causally-limited viscosity prescription to our solutions, and find that it prevents the radial velocities from becoming supersonic in the boundary layer, thus preserving causality. We apply the same prescription to a model for disks around black holes, and find that it allows us to calculate solutions for reasonable values of α, where none existed before.

We develop a more complete model, which includes the energetics and radiative transfer of the boundary layer, for comparison with observations. We apply this model to cataclysmic variables, and find that the nature of the boundary layer in these systems depends strongly on the optical depth, which in turn depends largely on the mass accretion rate and the rotation rate of the accreting star. The

dependence of our results on the accretion rate agrees well with X-ray observations of these systems. We also apply the model to accretion disks in pre-main sequence stars, such as T Tauri and FU Orionis stars, and find that the temperatures and radial widths of the boundary layer in our solutions agree well with those inferred from observations.

3. INTRODUCTION

3.1 Accretion Disks in Astrophysics

3.1.1 *The Role of Accretion Disks in Astrophysics*

Accretion disks are produced when a relatively dense, compact object gravitationally attracts lower-density viscous gas (see Frank, King, & Raine 1985). This gas has some angular momentum relative to the dense object, and thus begins to revolve around it in an orbit. As the orbiting gas accumulates, viscosity spreads it into a disk and causes it to lose angular momentum, which is transported outward through the disk. As a result, the gas spirals inward, or accretes, onto the central dense object. Some of the gravitational potential energy lost by the infalling gas is dissipated by viscosity and subsequently radiated by the disk, often producing large luminosities.

A wide variety of accreting systems have been observed in a variety of contexts in astrophysics. Usually, the dense central object which accretes matter is either a star or a stellar remnant, such as a white dwarf, neutron star, or black hole. The gas which accretes onto it often comes from a companion star; usually, this companion star overflows its Roche lobe and loses matter from its outer layers to the accreting star. Such a system is known as an accreting binary. In other cases, the accreting gas comes from the surrounding medium. One common example of this is the accreting pre-main sequence stars, which are generally thought to be accreting gas from the dense cloud from which they have recently formed. Another

example occurs in the active galactic nuclei, which have "central engines" which are thought to consist of a supermassive black hole which accretes nearby gas and even nearby stars, after disrupting them by tidal forces.

Our own solar system is thought to have formed from an accretion disk similar to those seen in present-day pre-main sequence accretors. Accreting binaries have been observed throughout our galaxy and have contributed greatly to our understanding of stellar evolution. Active galactic nuclei occur in some nearby galaxies, and extend throughout the observable universe; in fact, they are the most distant objects yet observed. Thus, accretion disks are fundamental to astrophysical processes occurring on a wide range of scales, including some of the most important topics of current astrophysical research.

3.1.2 *Past Theoretical Work on Accretion Disks*

Pringle (1981) and Shapiro & Teukolsky (1983) have reviewed the history of accretion disk theory. The earliest discussions of disks were motivated by the observation that the planets of the solar system lie in a plane, suggesting that they formed from a disk of matter. This "nebular hypothesis" was advanced by Laplace. The role of viscosity in the evolution of a disk of gas was studied by Peek (1942), von Wiezsäcker (1943, 1948), and Lüst (1952). These studies determined the basic dynamical behavior of such a disk: viscosity would cause the mass to flow inward toward the central object as angular momentum flowed outward.

The motivation for using accretion disks in astronomy was the discovery and identification of several stellar X-ray sources in the 1960s. Shklovskii (1966) suggested that these X-rays might be produced by matter flowing from an ordinary

main-sequence star onto a neutron star. Prendergast & Burbidge (1968) showed that such matter would form a disk around the compact star.

The modern theory of accretion disks appeared a few years later in work by Pringle & Rees (1972), Novikov & Thorne (1973), Lynden-Bell & Pringle (1974), and, most notably, Shakura & Sunyaev (1973). These papers developed the basic accretion disk model, and by making several simplifying assumptions, arrived at analytic expressions for the radial variation of the basic disk properties such as temperature, thickness, and density. None of these papers managed to identify the source of the viscosity responsible for accretion in the disk; it was suggested that poorly understood phenomena such as turbulence might be responsible. Nonetheless, Shakura & Sunyaev (1973) suggested a simple parametrization, the "α-prescription", for the viscosity coefficient, and showed that in fact the emission from the disk surface was largely independent of viscosity. The Shakura-Sunyaev model did not address the boundary layer, the interface between the accretion disk and the central accreting object. In fact, the analytic expressions derived for various disk quantities became unphysical if applied near the inner edge of the disk. This was a direct result of some of the assumptions made by Shakura and Sunyaev: in particular, the assumption that the rotation of the disk was purely Keplerian.

In the years since the development of the basic disk model, the theory of accretion disks has advanced in various directions. Much effort has gone into the development of disk instability models to explain the outbursts observed in various accreting systems (Smak 1984, Lin & Shields 1986, Huang & Wheeler 1989, Clarke, Lin, & Pringle 1990). Other studies have examined how the spectra of accretion disks should differ from blackbody or stellar spectra (Wade 1984, 1988, Shaviv &

Wehrse 1989, Hubeny 1990). In the last few years, there has been renewed effort to explain the source of the viscosity in accretion disks (Balbus & Hawley 1991, 1992, Hawley & Balbus 1991, 1992, Ryu & Goodman 1992, Goodman 1993). Finally, a few authors have explored the nature of the boundary layer region; this work will be discussed in section 3.2.

3.1.3 *Observations of Accretion Disks*

Since the initial identification of stellar X-ray sources as accreting binaries by Shklovskii (1966) and Prendergast & Burbidge (1968), observations of accretion disks have advanced enormously. Much of this progress has been made through X-ray observations by HEAO-1, *Einstein*, EXOSAT, and ROSAT. Unlike a star, the surface of an accretion disk has a wide range of temperatures, so that it radiates at a wide range of wavelengths. Thus, the development of infrared detectors, and ultraviolet observations using IUE, have greatly enhanced our ability to study accreting systems. This has been particularly important in studying accreting systems such as the pre-main sequence accretors, where the accreting star is not a compact stellar remnant, These increasing observational capabilities have led to the discovery of hundreds of new accreting systems, and allowed detailed study of their basic properties and behavior over time.

The brightest X-ray sources in the sky are the X-ray binaries, accreting binary systems in which the accreting object is a neutron star or a black hole (see Watson & King 1991 for a review). Several classes of these systems have been recognized. Some systems have low-mass companions which are losing mass by Roche lobe overflow; others have high-mass companions which lose mass through a stellar wind. Some of

the neutron stars in these systems have strong magnetic fields on the order of 10^{12} G; these include most of the neutron stars with high-mass companions and a few of those with low-mass companions. The presence of a strong magnetic field greatly alters the nature of the accretion onto these stars (Ghosh, Lamb, & Pethick 1977, Ghosh & Lamb 1979a,b). In general, the star's magnetosphere disrupts the inner portions of the accretion disk, and channels the accreting matter onto the magnetic poles. This produces bright polar caps which cause the system to appear to pulsate as the neutron star rotates. The variation of the pulsation period can then be used to examine the spin evolution of the neutron star. Other X-ray binaries show distinctive spectral features or dynamical evidence which suggest that they contain accreting black hole accretors (McClintock 1991).

Another important class of accreting binaries is the cataclysmic variables (CVs) (see Horne 1991 for a review of CV observations). These systems consist of an accreting white dwarf and a low-mass companion which is losing mass via Roche lobe overflow. The mass accretion rates are generally inferred to range from $10^{-11}\,M_\odot\ yr^{-1}$ to $10^{-7}\,M_\odot\ yr^{-1}$ (Patterson 1984). Many CVs emit X-rays, usually in far smaller quantities than the X-ray binaries (Cordova and Mason 1983). Perhaps the most notable feature of the CVs is their wide variety of eruptive events and other time-variable behavior. These include classical and dwarf novae, each of which can be divided into several subtypes (Wade and Ward 1985). Some CVs also have white dwarfs with strong magnetic fields, which may disrupt part or all of the accretion disk. As with the magnetized neutron stars in X-ray binaries, the rotation rates of such systems can be observed. This is not true of the non-magnetized white

dwarfs in most CVs, which makes it difficult to study the spin evolution of these systems.

Several other classes of accreting binaries also exist, some of which contain a main-sequence star which is accreting mass. These include some symbiotic stars (Kenyon 1986), in which a mass-losing giant star provides a very high accretion rate of around $10^{-4}\,M_\odot\ yr^{-1}$, and Algol-type binaries, which consist of two main-sequence stars.

Another major class of accreting systems is the pre-main sequence accretors, which are stars in the process of formation. Lynden-Bell & Pringle (1974) originally made the suggestion that the FU Orionis stars were accreting from a disk. This suggestion was confirmed by Hartmann & Kenyon (1985); later, Adams, Lada, & Shu (1987) and Kenyon & Hartmann (1987) also argued that T Tauri stars were disk accretors. T Tauri stars are low-mass stars with moderate accretion rates around $10^{-7}\,M_\odot\ yr^{-1}$ (Basri & Bertout 1991). FU Orionis stars appear to be similar to T Tauri stars, but have higher accretion rates $\sim 10^{-4}\,M_\odot\ yr^{-1}$, and seem to be undergoing outbursts which may be similar to the dwarf nova outbursts observed in many CVs (Hartmann *et al.* 1991). Herbig Ae/Be stars are thought to be a higher-mass analogue to the T Tauri stars, with accretion rates of around $10^{-5}\,M_\odot\ yr^{-1}$ (Hillenbrand *et al.* 1992).

The third major class of accreting systems are active galactic nuclei. These systems include the most luminous objects known in the universe. Nonetheless, many of them also show rapid variability, implying that the source of the luminosity is quite compact. These facts taken together have supported the view, originally proposed by Lynden-Bell (1969), that the luminosity of these systems is produced

by accretion. The accreting object is generally assumed to be a supermassive black hole, with a mass on the order of 10^8 $M_\odot$ (Rees 1984). The accreting gas is supplied by the surrounding interstellar medium, or by stars which come close to the black hole and are ripped apart by its tidal forces (Rees 1988). The nature of the accretion process in these objects is not well understood. In this thesis, we limit our work to the first two classes of accreting objects: accreting binaries and accreting pre-main sequence stars.

3.2 Boundary Layers in Accretion Disks

3.2.1 *The Importance of Boundary Layers to Studies of Accretion Disks*

The boundary layer is the interface between the accretion disk and the accreting central object. In general, the inner regions of the disk are rotating quite rapidly, but the central object may be rotating slowly or not at all. Thus, the rotational velocity of the accreting material must decrease rapidly as it moves through the boundary layer. The rapid rotation of the inner disk material supports it against the gravity of the central object. As the rotational velocity decreases, that support is lost, and the material must be supported by a radial pressure gradient, as in a star.

As the accreting material moves through the disk, it dissipates only half of the gravitational potential energy it loses as it falls toward the central object. The remainder of the energy is retained in the material in the form of rotational kinetic energy; as the rotational velocity decreases, much of this rotational kinetic energy is rapidly lost in the boundary layer region. This energy is dissipated by viscosity

and radiated away, as in the rest of the disk. Thus, the small boundary layer region may radiate just as much energy as the much larger disk.

The boundary layer imparts both mass and angular momentum to the central object. Of the gravitational potential energy lost by the accreting material, the portion which is not radiated away by the disk and boundary layer goes into spinning up the star. As the central object spins up, the rotating material loses less kinetic energy, and the boundary layer luminosity decreases substantially. The spin rate of the star also has important evolutionary implications. Some authors have suggested that when the star spins up to breakup speed, it cannot accrete any more mass; rather, this mass is ejected by some mechanism (Lynden-Bell & Pringle 1974, Shu *et al.* 1988). This would limit the mass that can be added by accretion, which would have profound consequences for star formation, where it is often suggested that solar-type stars gain much of their mass by accretion through a disk. Also, many accreting white dwarfs might be unable to reach the Chandrasekhar limit, which would have important consequences for theories of production of Type I supernovae and formation of neutron stars by accretion induced collapse.

Accreting systems are generally distinguished by their high-energy radiation and rapid temporal variations. In many cases, the boundary layer may be responsible for these characteristics. The large release of energy in a relatively small region suggests that the boundary layer will be hotter than the disk, and will produce more high-energy radiation. The rapid variations experienced by the accreting material within the boundary layer make it the most likely region for the occurrence of instabilities and time-variable phenomena. The boundary layer region will also be

important in determining the spin evolution of accreting objects. These considerations make it clear that the boundary layer is likely to be quite complex, but also quite important to our understanding of accretion disks and accreting systems.

3.2.2 *Past Theoretical Work on Boundary Layers*

Despite the clear importance of the boundary layer to studies of accretion disks, there have been relatively few efforts to understand it. The first examination of the boundary layer was made by Lynden-Bell & Pringle (1974), who derived some approximate relations for the size and temperature of the region. They also discussed the spin-up of the central star and the consequences of spinning it up to breakup.

In the following years, X-ray observations of cataclysmic variables motivated several studies of boundary layers in these systems. Most of these studies were based on a local analysis, and attempted to find approximate values for the boundary layer temperature and size. After a few CVs were detected in soft X-rays, Pringle (1977) estimated that a CV with a 1 $M_\odot$ white dwarf accreting $1.6 \times 10^{-8}\, M_\odot\ yr^{-1}$ should have a boundary layer temperature of about 5×10^5 K. He assumed that the boundary layer in such a system would be optically thick, and estimated that the radial size of the boundary layer would then be about equal to its height, since this would be the distance over which radiation would diffuse before reaching the disk surface.

Later, CVs were also observed in hard X-rays. Pringle & Savonije (1979) suggested that these hard X-rays could be produced by a boundary layer which was optically thin, and contained one or more shocks which produced the required high

temperatures. They noted that the boundary layer would have to be optically thin for the hard X-rays to escape, and that this would require a low accretion rate. Also, they suggested that in order to produce sufficiently hard X-rays, the shocks in the boundary layer would need to be quite strong, i.e., not too oblique to the flow. Tylenda (1981) proposed an alternate model for the production of hard X-rays. In his scenario, the high temperatures are produced in an optically thin boundary layer due to inefficient cooling, which for the most part is only by free-free emission. Nonetheless, this analysis, like all the other boundary layer studies up to this point, was based only on local considerations, rather than self-consistent calculations of the boundary layer structure and energetics.

The first attempt to determine the radial structure of the boundary layer was made by Regev (1983), who used the method of matched asymptotic expansions. In this approach, one identifies a small parameter in the boundary layer, e.g. $\epsilon = H/R_*$, and writes down the equations to leading order in ϵ. One then solves the simplified equations in the boundary layer region and matches the solution asymptotically to the star and the disk with appropriate boundary conditions. The method has been applied to cataclysmic variables (Regev and Hougerat 1988, Regev and Shara 1989) and to T Tauri stars (Bertout and Regev 1992). Although the matched asymptotic expansion method is reasonable in principle, in practice it seems to run into problems. For instance, in some cases with perfectly well-posed boundary conditions, the method fails to find any solution. Also, some of the solutions published so far have unphysical features such as a large radiative flux flowing into the star, or have required the authors to invoke *ad hoc* mass loss in order to get rid of some of the boundary layer luminosity. In Chapter 10, we compare our

models of boundary layers to those recently published by Bertout & Regev (1992), and discuss some of the problems of the matched asymptotic method.

Numerical work on boundary layers began to appear in the mid-1980s. Papaloizou & Stanley (1986) used a polytropic equation of state to construct a model of the boundary layer dynamics. In general, they found that the radial velocity increases rapidly in the boundary layer, so that the surface density of the accreting material becomes rather low. They also found evidence for boundary layer oscillations, which they argued might well be the cause of the quasi-periodic intensity oscillations observed in some accreting systems. They also adopted a viscosity prescription modified from the standard α-prescription of Shakura & Sunyaev (1973). In the standard α-prescription, the disk vertical pressure scale height is used as the limiting value of the turbulent length scale. Papaloizou & Stanley replaced this length scale with a prescription that essentially uses the minimum of the vertical and radial pressure scale heights. This serves to reduce the viscosity in the boundary layer region, where the radial pressure scale height is quite small. The purpose of this reduction in viscosity was to reduce the radial velocity of the accreting material, which in many cases exceeds the local sound speed in the boundary layer. As first noted by Pringle (1977), the radial velocity in the boundary layer should be subsonic so that the disk does not lose causal contact with the central object. Nonetheless, even with the reduced viscosity, Papaloizou & Stanley found that the radial velocity still became supersonic in some cases.

Kley (1989,1991) developed a two-dimensional (in the $R - z$ plane), time-dependent simulation of a boundary layer. He used a constant viscosity coefficient rather than the α-prescription, and treated ra[illegible]n transport in the flux-limited

diffusion approximation. After integrating for a few dynamical times, these calculations produce near-steady-state models. The models tend to have supersonic radial infall because of the large viscosity coefficient used. This can presumably be corrected by modifying the viscosity prescription, but it is not clear if the calculations will then be able to maintain adequate radial resolution to resolve the subsonic boundary layer. So far, only optically thick boundary layers have been simulated. Optically thin models would be most interesting, but these tend to be quite complex and may be difficult to resolve in a multi-dimensional simulation.

3.2.3 *Observations of Boundary Layers*

Boundary layers have proven to be almost as difficult to observe as they are to model. One reason for this is the large number of emitting regions which contribute to the spectra of accreting objects; these can include the accreting star, the disk, the "bright spot" at the outer edge of the disk, the mass-losing companion star, winds from the stars or the disk, and the boundary layer itself. Another problem is that in many cataclysmic variables (CVs), most of the boundary layer emission is in the form of extreme ultraviolet (EUV) radiation. Observations in the EUV are extremely difficult because the opacity of neutral hydrogen is very high at these wavelengths, so that observations are generally only possible in the solar neighborhood. Despite these difficulties, emission believed to arise from the boundary layer region has been observed both in CVs and pre-main sequence accretors.

Many CVs were detected in both soft and hard X-rays by the *HEAO-1* and *Einstein* satellites; these observations were summarized by Cordova and Mason (1983). As discussed in section 3.2.2, the origin of both the soft and hard X-ray

emission was interpreted to be the boundary layer region (Pringle 1977, Pringle & Savonije 1979, Tylenda 1981). Ferland *et al.* (1982) argued that soft X-ray fluxes in CVs were substantially lower than expected, so that far fewer CVs than expected had actually been detected in soft X-rays. Patterson & Raymond (1985a), using observations of a large number of CVs, showed that the ratio of X-ray to optical flux was strongly anti-correlated with the mass accretion rate, so that systems with low accretion rates had large X-ray fluxes. They argued, based on the proposal by Tylenda (1981), that this correlation was due to a transition between optically thin boundary layers, which exist in systems with low accretion rates and have substantial hard X-ray fluxes, and optically thick boundary layers, which are in high accretion rate systems. In these systems, the large optical depth of the boundary layer converts the hard X-rays into very soft X-rays and EUV radiation. Patterson & Raymond (1985b) also argued that the small numbers of CVs detected in soft X-rays were approximately as predicted by boundary layer theory, and that the apparent discrepancy noted by Ferland *et al.* (1982) was due to inappropriate choices of boundary layer parameters. The soft X-ray flux is particularly sensitive to the boundary layer temperature because only the high-energy end of the boundary layer spectrum, where the flux is falling off rapidly, contributes to the soft X-rays.

Emission attributed to the boundary layer has also been observed from T Tauri stars. In these stars this emission takes the form of "veiling" in the optical and ultraviolet spectra, excess continuum emission which fills in the absorption lines from the central star (Hartigan *et al.* 1989, 1991). This excess emission is substantially bluer than the stellar photospheric emission, and the ratio of the excess flux to the stellar flux ranges from ~ 0.1 to ~ 10. The source of the emission

has been modeled as a very simple boundary layer consisting of a slab of gas with a single temperature and density. These models have yielded estimates for the size and temperature of the boundary layers in several T Tauri systems; the temperatures generally range from $\sim$ 7000 to 10,000 K, and the sizes from about 1% to 10% of the stellar radius (Bertout *et al.* 1988, Basri & Bertout 1989, Hartigan *et al.* 1991).

Observations of FU Orionis stars have shown less evidence for boundary layer emission. Kenyon *et al.* (1989) observed three FU Orionis stars in the ultraviolet and found no significant veiling of the stellar absorption lines, indicating that the emission from the boundary layer at these wavelengths is far weaker than expected.

Boundary layer emission has also been observed in some symbiotic stars (Kenyon *et al.* 1991, Mikołajewska and Kenyon 1992), which are binary systems where the accreting star is a main-sequence star. Accretion rates are quite large in these systems, $\sim 10^{-5} - 10^{-4}\,M_\odot\ yr^{-1}$, and the boundary layer appears to be quite hot, sometimes exceeding 100,000 K.

3.3 Organization and Summary

3.3.1 *Spin-up in Accreting White Dwarfs*

The work presented in this dissertation began with a consideration of the spin evolution of accreting white dwarfs (Narayan & Popham 1989), which is presented in Chapter 4. Since disk accretion imparts both mass and angular momentum to the white dwarf, it should spin up steadily as it accretes. Eventually, if it continues to accrete, it should reach breakup. This may not happen if the white dwarf has a

substantial magnetic field, since the interaction of the field lines with the surrounding disk will alter the normal steady spin-up rate. This mechanism was described by Ghosh & Lamb (1979a,b) with application to accreting magnetic neutron stars. As the star spins up, the disk slows down the field lines and exerts a braking torque on the star, which cancels some of the angular momentum added by the accreting material. Eventually the star spins up to an equilibrium spin rate, for which the two torques balance each other, allowing the star to accrete mass without spinning up any further.

In Chapter 4, we present the results of a calculation in which we followed the spin-up of accreting white dwarfs of various initial masses and magnetic fields for specified values of the mass accretion rate. We integrated the net torque forward in time to follow the changes in the mass and angular momentum of the white dwarf. Throughout the evolution, we kept track of the structure of the white dwarf by interpolating from calculations of the structure of rotating white dwarfs made by Hachisu (1986), assuming that the white dwarf rotates rigidly. Eventually, the white dwarfs in the calculations either reached the Chandrasekhar limit and collapsed, or reached breakup rotation speed. Both results had some interesting implications; the collapse of the white dwarf might produce a Type I supernova explosion, or, in the case of an oxygen-neon-magnesium white dwarf, it might produce a neutron star by accretion-induced collapse (Nomoto 1987). The latter case would potentially provide a way to produce millisecond pulsars in close, circular binary systems, which would appear to be impossible if the neutron star were formed in the conventional way, by a Type II supernova explosion. Alternatively, if the white dwarf spun up

to breakup, its future evolution would be even less certain, since it was unknown whether accretion could continue in such a situation.

We found that only white dwarfs with high magnetic fields $B \gtrsim 10^6 G$, and those which have initial masses very close to the Chandrasekhar mass, can collapse before they spin up to breakup speed. If the magnetic flux and angular momentum are conserved in the collapse, these white dwarfs could produce neutron stars with magnetic fields $B \gtrsim 10^{11} G$ and spin periods $\sim 0.15 - 100$ ms. The minimum spin period for a neutron star is about 1 ms, so some of these white dwarfs would form "fizzlers" (Gold 1975, Shapiro & Lightman 1976); that is, they would be unable to collapse directly to neutron star densities without first losing additional angular momentum.

The vast majority of accreting white dwarfs, those without high magnetic fields or very high initial masses, would reach breakup after accreting $0.1 - 0.15\,M_\odot$. Their subsequent fate would be uncertain: if they could somehow continue to accrete mass without accreting additional angular momentum, they would eventually reach the Chandrasekhar mass and collapse. In fact, above about one solar mass, the breakup value of angular momentum for white dwarfs decreases as their mass increases. Thus, to continue accreting mass once it reaches breakup, a massive white dwarf would have to lose angular momentum. Some authors have suggested that continued accretion will be impossible, and that the mass which would have been accreted will instead be ejected in some fashion (Lynden-Bell & Pringle 1974, Shu *et al.* 1988).

3.3.2 *Dynamics of Boundary Layers Around Rotating Stars: Can Accretion Continue onto a Star Rotating at Breakup?*

This work (Popham & Narayan 1991), presented in Chapter 5, addressed the question raised in Chapter 4, namely, what happens when an accreting star reaches breakup? Clearly, the key to this question is the boundary layer region, where the disk encounters the rapidly rotating star. In order to examine the boundary layer structure, we set up the dynamical equations for the radial and angular momentum of the accretion flow. In the usual disk equations, it is assumed that gravity is balanced by centrifugal force, so that the radial momentum equation is simply $\Omega = \Omega_K$. Since the angular velocity profile is known, the angular momentum equation is also quite simple, and generally assumes that the angular momentum accretion rate is just the Keplerian rate, which is simply the mass accretion rate multiplied by the Keplerian specific angular momentum at the stellar surface.

Clearly, these assumptions are insufficient for a study of the boundary layer. Since the means of support against gravity changes from rotation to pressure gradient in the boundary layer region, we added a pressure gradient term to the radial momentum equation, along with a term to account for radial acceleration as the accreting material moves through the boundary layer. As in the standard disk model, the angular momentum equation includes two terms: angular momentum advected by the infalling material, and angular momentum transported by the viscous torque. However, since we were interested in how the angular momentum accretion rate varies as the star spins up, we did not assume that it is given by the Keplerian rate. Also, since we were not assuming $\Omega = \Omega_K$, both the radial and angular momentum equations become differential equations.

We then attempted to solve these coupled differential equations, providing boundary conditions which included a condition that the angular velocity match

the stellar rotation rate at the stellar surface. In order to simplify the problem, we confined ourselves to the dynamics of the flow by using a polytropic equation of state, which allowed us to write the dynamical equations in a fairly simple form, without including the energetics and radiative transfer. Also, rather than dividing the problem into various regions of disk, boundary layer, and star, we used the same equations to describe the entire accretion flow. We also assumed that the flow was axisymmetric and in a steady state. We found that in fact the differential equations were very stiff, and that they could not be solved using an initial-value integrator. Instead, we solved the equations as a boundary-value problem using a relaxation method.

We found two basic types of solutions. For stars rotating below breakup speed, we found solutions which in most respects matched the conventional picture of the boundary layer. The angular velocity dropped from approximately Keplerian to the stellar rotation rate in a very narrow layer. The star accreted angular momentum at a rate very close to the Keplerian rate. One aspect of the solutions was surprising: the radial velocity of the accretion flow became supersonic for commonly used values of α, the factor in the viscosity coefficient.

The second type of solution corresponds to stars rotating at breakup. Here the angular velocity never reaches a maximum, but simply becomes constant as the flow reaches the stellar surface. This allows viscosity to transport angular momentum from the star out into the disk, which cannot occur in the first type of solution, since the maximum in the angular velocity between the disk and star is a point at which there is no shear and thus no viscous angular momentum transport. In the breakup solutions, the viscous torque can remove large amounts of angular

momentum which can cancel or exceed the angular momentum added by the accreting material, allowing solutions in which the central star accretes mass while losing angular momentum. Clearly, these are exactly the solutions required to solve the problem posed in Chapter 4. The existence of these solutions means that accreting white dwarfs, or other accreting stars, can continue to accrete even after they have spun up to breakup. This implies that accreting white dwarfs can collapse even if they do not have the high magnetic fields or initial masses required to keep them from reaching breakup. Another important implication is that accreting protostars can accrete arbitrarily large amounts of mass from the surrounding medium without ever encountering any sort of angular momentum barrier. Paczyński (1991) independently reached the same conclusion.

We found that the angular momentum accretion rate varies as a function of the rotation rate of the central star, and that this variation differs greatly between the two types of solutions. For the slowly rotating solutions, the angular momentum accretion rate, in units of the Keplerian rate at the stellar surface, remains nearly constant as the star spins up, and always stays slightly larger than the Keplerian rate. Note that the equatorial radius of the star increases as the star spins up, so that the Keplerian angular momentum accretion rate at the stellar surface also increases. It should also be noted that our definition of the stellar surface is fairly arbitrary; we take the stellar radius to be the point at which the disk height is one tenth of the radius. In the breakup solutions, the angular momentum accretion rate decreases very rapidly as the star spins up, and quickly becomes negative. This means that there should be a tightly defined rotation rate for which the star can accrete without spinning up or down. For most stars, this would be the rotation

rate at which the star accretes little or no angular momentum; however, the star is also gaining mass, which may produce changes in its moment of inertia, requiring a nonzero angular momentum accretion rate. For instance, massive white dwarfs would be contracting rapidly as they gained mass, which would tend to spin them up, so that a negative angular momentum accretion rate would be required.

Finally, we found that these results do not depend on the fact that the breakup solutions have subsonic radial velocities in the boundary layer, while the slowly rotating solutions have supersonic radial velocities. In order to demonstrate this, we calculated solutions using $\alpha = 10^{-4}$, and found that both types of solutions then remained subsonic. Nonetheless, the other characteristics of the solutions remained very similar to the solutions calculated with $\alpha = 0.1$.

3.3.3 *Supersonic Radial Velocities and Causally Limited Viscosity*

Although the basic nature of our slowly rotating solutions appears not to depend on whether the radial velocities in the boundary layer are subsonic or supersonic, the presence of supersonic radial velocities for conventional values of α presents a problem with regard to causality. The disk must be aware of the star and its characteristics, since our formulation of the problem uses the stellar rotation rate as a boundary condition, and assumes that the angular momentum accretion rate is the same at all radii in the disk. The existence of a supersonic zone between the disk and star would prevent communication between the two regions. This constraint on boundary layer radial velocities was first pointed out by Pringle (1977).

We found that the problem of supersonic velocities was caused by the viscosity prescription and its lack of any provision for causality (Popham & Narayan 1992);

our solution to this problem is persented in Chapter 6. Shear viscosity in accretion disks is usually assumed to arise through turbulent diffusion of angular momentum. The standard diffusion equation includes no causal limit comparing the bulk flow velocity to the maximum velocity of the diffusive elements. The usual α-viscosity prescription sets the viscosity coefficient $\nu = \alpha c_s H$, where c_s is the sound speed, assumed to be the highest transport speed for the turbulent fluid elements, and H is the disk height, assumed to be the largest length scale over which the turbulent elements travel. Note that this prescription also contains no causal limit.

In order to enforce causality, we introduced a factor $(1 - v_R^2/v_t^2)^2$ into the viscosity coefficient, where v_t is the velocity of the turbulent elements. This correction factor is analogous to that used by Levermore & Pomraning (1981) in their flux-limited diffusion theory, which has become widely accepted in radiative transfer applications. The form of the factor was derived by Narayan (1992), who studied a simple steady-state system of particles with a distribution of velocities undergoing diffusion in a moving medium. The factor serves to reduce the viscosity coefficient as the radial velocity approaches the turbulent transport speed.

We also added an additional factor to the expression for the viscosity coefficient. Rather than using the disk height H, which is the vertical pressure scale height, as the limiting turbulent length scale, this factor, $1/(1/H + 1/H_p)$, essentially uses the lesser of the radial and vertical pressure scale heights, where $H_p = P/|dP/dR|$ is the radial pressure scale height. This factor was proposed and used by Papaloizou & Stanley (1986) in an effort to solve the problem of supersonic radial velocities; it failed to do so in some cases.

Introducing both factors into our viscosity coefficient, we calculated slowly rotating solutions for $v_t = 0.8c_s$ and for $v_t = 1.2c_s$. We found that the radial velocities in these solutions always stayed below the turbulent transport speed v_t, even when values of α as large as unity were used. Thus, the solutions always maintained viscous communication between the star and the disk, even though some of the solutions for $v_t = 1.2c_s$ had radial velocities exceeding the sound speed. This resolved the causality problems found in the earlier slowly rotating solutions. In other respects, the new solutions were quite similar to the earlier solutions; in particular, the relation between the angular momentum accretion rate and the stellar rotation rate remained almost identical to its earlier form.

3.3.4 *Black Hole Accretion with Causally-Limited Viscosity*

In Chapter 7, which has just been completed and has not yet been submitted for publication, we incorporate the causally-limited viscosity introduced in Chapter 6 into polytropic models of accretion disks around black holes. The black hole disks discussed in this chapter are rather different from the disks examined in the other chapters, which have a central accreting star. Unlike a star, a black hole does not require the accreting gas to match its rotation rate at its surface. Instead, the infalling gas accelerates until it reaches a sonic point, where its radial velocity exceeds the sound speed, and from this point on, the gas basically falls freely into the black hole.

The Shakura & Sunyaev (1973) disk model was intended for black hole disks, but it assumed that a purely Keplerian disk extended all the way in to the black hole event horizon. Later, Paczyński and Bisnovatyi-Kogan (1981) and Muchotrzeb

and Paczyński (1982) added pressure gradients and radial acceleration to the radial momentum equation, and also expanded the energy equation used by Shakura and Sunyaev to include radial transport of energy. These "slim disk" equations provided a much more realistic model for the accretion flow, particularly in the region near the sonic point. These authors obtained solutions for the flow in which the sonic point was just inside the radius of the last stable orbit at $R = 3R_g = 6GM/c^2$; however, they were unable to obtain solutions with values of α, the parameter used in the viscosity coefficient, larger than ~ 0.03 (Muchotrzeb 1983). This was a serious problem, since the best indications of the value of α, in CV disks where dwarf novae outbursts have occurred, suggest values of $\alpha \sim 0.1 - 1$. Thus, up to now, no self-consistent models of black hole accretion have been found when "reasonable" values of α are used.

We have created simple polytropic models of disk accretion onto black holes, using the disk equations presented in Chapter 5. We have incorporated into these models the causally-limited viscosity prescription presented in Chapter 6. This prescription was able to solve the problem of supersonic radial velocities in the boundary layer region in standard accretion disks around stars. We do not use the full general relativistic equations; instead, we adopt the pseudo-Newtonian "Paczyński potential" $\Phi = -GM/(R - R_g)$ introduced by Paczyński and Wiita (1980). This potential was used to approximate general relativistic effects in the previous work on the subject, and so we retain it here in order to allow comparison with that work.

Using our causally limited viscosity, we have been able to find solutions for black hole disks for values of α up to and including $\alpha = 1$. Like the earlier solutions

of Muchotrzeb & Paczyński (1982), these solutions have sonic points inside $3R_g$. Our causally limited viscosity prescription reduces the viscosity as the radial velocity of the gas approaches the sound speed. At the sonic point, and inside it, the viscosity is assumed to be zero, and the gas basically free-falls down to the event horizon while conserving angular momentum. We believe that these are the first self-consistent solutions for disks around black holes calculated using the generally accepted values of α near unity.

3.3.5 *Boundary Layer Models Including Energetics and Radiative Transfer: Modeling Cataclysmic Variables*

Although our polytropic models were excellent tools for understanding the dynamics of boundary layers, they also illustrated that it should be possible to construct a complete boundary layer model, including energetics and radiative transfer, for comparison with observations of various types of accreting systems. Such a model (Narayan & Popham 1993) is presented in Chapter 8. It allows us to find temperatures, sizes, and optical depths, and to synthesize continuum spectra for comparison with observations. It also allows us to examine how the observable boundary layer parameters vary as the accretion rate, stellar mass, radius, and rotation rate change.

In order to construct such a model, we must first abandon the polytropic equation of state and replace it with a more standard equation of state which includes gas pressure and radiation pressure. In addition, we must include an energy equation, which describes the balance of sources and losses of energy at each radius in the disk. The standard disk equations use a simple energy equation in which

energy dissipated by viscosity is radiated by the disk surface at the same disk radius at which it was dissipated. In the boundary layer, one cannot be so certain that such a local balance will exist. The boundary layer region dissipates a huge amount of energy, up to half of the total accretion energy, and yet it may do so in a very narrow region, the radial extent of which may in fact be smaller than its height. Thus, much of the boundary layer energy may be radiated in the radial direction rather than vertically. Also, if the accreting material falls inward rapidly, it may carry with it a substantial amount of energy. Thus, we use the "slim disk" energy equation of Muchotrzeb & Paczyński (1982) and Abramowicz *et al.* (1988), which includes terms for radial radiative and advective energy transport, as well as the usual viscous dissipation and vertical radiation terms.

In general, we cannot assume that the disk will be optically thick, so that the standard diffusion approximation to the radial and vertical fluxes must be replaced by some more explicit radiative transfer equations. We adopt a simple two-stream approximation for the radial radiative transfer; this prescription includes both absorption and scattering of radiation. In the vertical direction, we adopt a relation between the vertical flux and the disk midplane temperature and optical depth derived by Hubeny (1990). This relation basically reduces to the diffusion approximation for optically thick regions, but also gives the appropriate flux in optically thin regions.

The addition of the energy equation and two equations describing the radial radiative transfer increases the number of coupled differential equations to five. We solve these equations using a relaxation code, and specifying the stellar mass, radius, rotation rate, and effective temperature, and the mass and angular momentum

accretion rates. In this chapter we present solutions for a cataclysmic variable, where the accreting star is a white dwarf. We use a single set of white dwarf parameters: a $1\,M_\odot$ white dwarf with a radius of 5×10^8 cm, and an effective temperature of 20,000 K. This corresponds to a fairly massive, compact white dwarf. We then calculate boundary layers for four accretion rates: $10^{-7.5}$, $10^{-8.5}$, $10^{-9.5}$, and $10^{-10.5}\,M_\odot\ yr^{-1}$, which span the wide range of accretion rates inferred from observed cataclysmic variables.

At high accretion rates, $10^{-7.5}$ and $10^{-8.5}\,M_\odot\ yr^{-1}$, we find that the boundary layer is optically thick in the vertical direction. The effective temperature of the boundary layer region in these solutions is in the $100,000 - 300,000$ K range. The boundary layer really has two radial widths; the angular velocity decreases rapidly over a fairly narrow region which we call the "dynamical width" of the boundary layer. The boundary layer energy is also dissipated in this narrow zone, but much of it is radiated outward in the radial direction, and then radiated from the disk surface farther from the star. For observational purposes, the boundary layer is thus substantially wider than the dynamical width; we refer to this larger region from which the energy is radiated as the "thermal width" of the boundary layer. For these accretion rates, the dynamical width is about 1% of the stellar radius, while the thermal width is closer to 10% of the stellar radius. Both widths increase with larger accretion rates.

At low accretion rates, $10^{-9.5}$ and $10^{-10.5}\,M_\odot\ yr^{-1}$, the boundary layer becomes optically thin. This has a profound effect on the character of the region. The cooling, by free-free emission, is quite ineffective, and the gas becomes very hot. This effect was predicted by Tylenda (1981), who made a local analysis of the

boundary layer energetics using the standard disk assumption that dissipated energy is radiated locally. We find that in addition to the effects of inefficient cooling, the energy transport terms play an important role in the boundary layer region. Much of the energy dissipated in the boundary layer goes directly into the entropy of the gas, and this energy is finally released when the gas reaches the stellar surface, where it condenses and cools rapidly. Again, most of the energy then goes into outward radial flux, which travels across the optically thin boundary layer zone, and is absorbed by the optically thick material just outside of the boundary layer, where it is subsequently radiated from the disk surface. The optically thin boundary layers are thus substantially more complex than their optically thick counterparts. The central temperature in these solutions reaches $1 - 2 \times 10^8$ K, in the optically thin region, but the effective temperature in the same region is less than 100,000 K because the cooling is so inefficient. The high boundary layer temperatures and correspondingly high viscosity coefficients result in a very wide boundary layer; in these solutions the angular velocity decreases gradually over a dynamical width of about $0.2 - 0.5$ stellar radii. The thermal width is only about 50% larger than the dynamical width, since the zone which radiates most of the energy sits at the outer edge of the extensive optically thin region. Finally, in these solutions, the boundary layer width increases as the accretion rate decreases, since the boundary layer continues to get hotter and wider as the optical depth gets even smaller.

These results correspond quite well to X-ray observations of cataclysmic variables (CVs), which were analyzed and discussed by Patterson & Raymond (1985a,b). They found that the ratio of X-ray to optical flux was anti-correlated with the inferred accretion rate in a large sample of CVs observed with the *Einstein* satellite.

They also argued that a transition between optically thin boundary layers at low accretion rates and optically thick boundary layers at high accretion rates could account for such a correlation. This argument was based on the Tylenda (1981) analysis and on simple estimates for the accretion rate at which such a transition might take place. Our results provide a self-consistent model of the boundary layer which includes the dynamics, energetics, and radiative transfer, and which appears to account for the correlation quite well. In our solutions, the transition to a hot optically thin boundary layer occurs at an accretion rate around $10^{-9.5}\,M_\odot\ yr^{-1}$, which agrees reasonably well with the observations.

3.3.6 *Optically Thick Boundary Layers in Cataclysmic Variables*

Chapter 9, which consists of unpublished work, supplements the cataclysmic variable boundary layer solutions presented in Chapter 8. It examines optically thick boundary layers around white dwarfs, and discusses three major topics. All of the boundary layer solutions calculated for this chapter have an accretion rate of $10^{-7.5}\,M_\odot\ yr^{-1}$, and a white dwarf of mass $1\,M_\odot$ and radius 5×10^8 cm, rotating at about half of breakup speed.

The first topic examined in Chapter 9 is the dependence of the boundary layer structure upon the stellar parameters of the accreting star, such as the mass, radius, and rotation rate. In this case, the accreting star is a white dwarf, so the mass and radius vary in a well-defined way, and can be treated as a single parameter. Since this is a preliminary version of this work, we have used approximate radii at each value of the white dwarf mass. We calculated solutions for masses of $0.6 - 1.0\,M_\odot$, with corresponding radii of $9 - 5 \times 10^8$ cm, and found that as the mass

decreases and the radius increases, the boundary layer becomes cooler, but shows no real qualitative changes. The rotation rate of the accreting star produced more significant changes, due in part to the dramatic effect it has on the boundary layer luminosity. Our solution for a nonrotating star had a large luminosity and a wider boundary layer than the solutions for more rapidly rotating stars. On the other hand, our solution for a star rotating at its maximum speed showed only a very small boundary layer luminosity, with a correspondingly small peak in the effective temperature in the boundary layer region.

Next, Chapter 9 examines the "breakup branch" of boundary layer solutions, which were discussed in Chapter 5 for the polytropic disk solutions, but were not discussed in Chapter 8 with full disk solutions including an energy equation. We show that the breakup branch does exist when the full disk equations are used, and that they are quite similar to the breakup branch solutions from Chapter 5. In particular, they include solutions with small and even negative values of the angular momentum accretion rate, which allow stars to continue accreting even after they have spun up to breakup. A very interesting aspect of these solutions is that the effective temperature increases substantially as the angular momentum accretion rate decreases; this occurs because energy which was going into spinning up the star is now being dissipated and radiated by the disk. Also, the breakup branch solutions have large surface densities in the boundary layer region and are optically thick, even for accretion rates as low as $10^{-10.5}\,M_\odot\ yr^{-1}$.

Finally, this chapter addresses the energetics of the boundary layer region. First, we discuss the energy balance in the boundary layer region. In the dynamical boundary layer, radiation in the radial direction removes most of the boundary layer

luminosity and carries it outward. The luminosity is subsequently absorbed and reradiated from the disk surface in the thermal boundary layer; thus the dominant energy terms here are the radial flux, which is a source of energy, and the vertical flux, which radiates that energy away. Next, we examine the total luminosity of the boundary layer and disk. The commonly used expression for the boundary layer luminosity has been shown by Kluzniak (1987) to be incorrect, since it neglects the energy that goes into spinning up the star. In Chapter 9 and Appendix C, we derive the correct expression for the luminosity of the boundary layer. The total luminosity of the disk and boundary layer taken together depends on the mass and radius of the accreting star, the stellar rotation rate, and the accretion rates of both mass and angular momentum. We compare the predicted values of the total luminosity to the values from our solutions, and find that they agree well, and that the boundary layer luminosity does depend on the stellar rotation rate and angular momentum accretion rate as predicted by the new expression.

3.3.7 *Boundary Layer Models Including Energetics and Radiative Transfer: Modeling Pre-Main Sequence Stars*

This work (Popham *et al.* 1993), presented in Chapter 10, applies the same disk and boundary layer model used in Chapters 8 and 9 to boundary layers around accreting pre-main sequence stars. The only major difference in the modeling procedure is that whereas the CV boundary layer models used a simple Kramers opacity along with electron scattering, the pre-main sequence models use a tabulated opacity which includes H and H^- free-free and bound-free absorption and electron scattering. This is necessary because we expect the pre-main sequence boundary layers to be substantially cooler than those in CVs.

The stellar parameters and accretion rates used in this work are chosen to resemble the values estimated from observational studies of T Tauri and FU Orionis stars. These studies have generally estimated masses around $1\,M_\odot$, radii ranging from $2 - 7R_\odot$, surface temperatures of $3000 - 5000$ K, and mass accretion rates of about $10^{-7}\,M_\odot$ yr^{-1} in T Tauri stars and $10^{-4}\,M_\odot$ yr^{-1} in FU Ori stars. As in Chapter 8, the goal of this chapter is to explore the basic structure of boundary layers around stars with these parameters, and to examine how that structure depends on the accretion rate. Accordingly, we calculate models for accretion rates of 10^{-7}, 10^{-6}, 10^{-5}, and $10^{-4}\,M_\odot$ yr^{-1}. All of these models use stellar radii of $2 - 2.5R_\odot$ except the $10^{-4}\,M_\odot$ yr^{-1} solution, which uses a star with a radius of about $4.5R_\odot$. All of these solutions used $\alpha = 0.1$; we also calculated a solution at $10^{-4}\,M_\odot$ yr^{-1} with $\alpha = 0.001$, which had a stellar radius of about $6.5R_\odot$.

We find that the boundary layers in all of these solutions are optically thick. The effective temperature of the boundary layer ranges from about 8500 K in the $10^{-7}\,M_\odot$ yr^{-1} solution to about 17,000 K in the 10^{-5} and $10^{-4}\,M_\odot$ yr^{-1} solutions. In the $10^{-4}\,M_\odot$ yr^{-1}, $\alpha = 0.001$ solution, the boundary layer is cooler, around $7000 - 10,000$ K. As in the optically thick CV solutions, the boundary layers have distinct dynamical and thermal widths, and these widths increase as the accretion rate increases. In the $10^{-7}\,M_\odot$ yr^{-1} solution, the dynamical width is about 2% of the stellar radius, while the thermal width is about 20% of the stellar radius. In the $10^{-4}\,M_\odot$ yr^{-1} solution, the dynamical width has reached about 30% of the stellar radius, and the thermal width is so large that it is difficult to distinguish from the disk. Finally, in the $10^{-4}\,M_\odot$ yr^{-1}, $\alpha = 0.001$ solution, even the dynamical width has become larger than the stellar radius.

We also calculate spectra for the various solutions. These are simple blackbody spectra calculated using the effective temperature at each radius in the boundary layer and disk. In general, as the accretion rate increases, the boundary layer and disk get hotter, and the spectrum gets bluer. The interesting feature in the spectra is that as the accretion rate increases, the boundary layer and disk components become more difficult to distinguish. The spectrum of the $10^{-7}\,M_\odot\ yr^{-1}$ solution clearly has two components with an inflection between them, but the distinction between the two components fades as the accretion rate increases, until at $10^{-4}\,M_\odot\ yr^{-1}$, they seem to have merged into one. The $10^{-4}\,M_\odot\ yr^{-1}$, $\alpha = 0.001$ spectrum also has just one component, but has very little ultraviolet flux, since the boundary layer is cooler.

These results agree reasonably well with observations. Basri & Bertout (1989) and Hartigan *et al.* (1991) estimated boundary layer temperatures of 7000 to 10,000 K and boundary layer widths of 1-10% of the stellar radius from spectra of T Tauri stars. Our $10^{-7}\,M_\odot\ yr^{-1}$ boundary layer has a maximum effective temperature of about 8500 K, and has a thermal width of about 20% of the stellar radius; however, the portion of the thermal boundary layer with an effective temperature above 7000 K is only a few percent of a stellar radius wide. For FU Orionis stars, maximum temperatures of $\sim 7000K$ have been estimated from observations (Kenyon, Hartmann, & Hewett 1988). Thermal instability models for the outbursts of these stars suggest that $\alpha \simeq 0.001$. Our $10^{-4}\,M_\odot\ yr^{-1}$, $\alpha = 0.001$ solution has a boundary layer temperature of about 7000 K; it is interesting that the $10^{-4}\,M_\odot\ yr^{-1}$, $\alpha = 0.1$ model has a much hotter boundary layer, suggesting that small values of α are favored, although this may depend strongly on our other choices of parameters.

3.4 Plans for Future Work

This work began with an examination of spin-up in accreting white dwarfs (Chapter 4), which led us to explore the dynamics of the boundary layer and the importance of the viscosity prescription (Chapters 5, 6, and 7). More recently, we have developed a more complete model of the boundary layer which includes energetics and simple radiative transfer, and applied it to cataclysmic variables and pre-main sequence accretion disks (Chapters 8, 9, and 10). None of these studies has led us to a dead end; rather, each has answered some old questions and raised some new ones, which we hope to answer in the near future. We also hope to apply our boundary layer solution method to other kinds of accreting systems. Finally, we hope to expand the method itself to make it applicable to different types of physical situations.

One immediate goal for the near future is to refine the calculations presented in Chapter 9. For the most part, this involves using more accurate white dwarf masses and radii, rather than the approximate values we have used in the current calculations. This should have only a small effect on the solutions. This work provides more information about the optically thick boundary layer solutions presented in Chapter 8; we subsequently hope to do something similar with our optically thin solutions, which are more difficult to calculate, but also more interesting.

Another objective is to try to apply some of our results to modeling individual accreting stars, both cataclysmic variables and pre-main sequence stars. Our work so far has been oriented toward finding solutions and examining how they vary as a function of the mass accretion rate and the stellar parameters. It would be interesting to see how well we can match the boundary layer emission from individual

systems and constrain the system parameters. One difficulty is that the rotation rates of nonmagnetic CVs and some pre-main sequence stars are unknown.

We would also like to expand our work beyond CVs and pre-main sequence stars to include systems with neutron star and black hole accretors, such as X-ray binaries and possibly active galactic nuclei. In particular, the black hole solutions presented in Chapter 7 may constitute a significant step forward in that they may resolve a problem which has hindered progress in the field for more than a decade. We hope to find black hole solutions using the full disk equations and including the effects of general relativity and radiation forces. Such solutions would be valuable for understanding black hole binaries, where it might help in distinguishing them from neutron star systems, and active galactic nuclei. Another area which deserves further exploration includes main-sequence accretors such as the symbiotic stars and possibly some Algol-type systems.

Finally, we would like to improve upon the model for the boundary layer which is presented in this work. One area which we have already explored briefly is the inclusion of the vertical disk structure in our calculations. We do this by calculating the vertical structure at each radial grid point, and using it to adjust the approximate relations used to describe the vertical structure in the standard vertically-averaged disk equations. Also, a better knowledge of the vertical radiative transfer allows us to calculate more accurate spectra for comparison with observations. Of course, a more complete approach to understanding the combined radial and vertical structure of the boundary layer and disk is to perform a two-dimensional calculation. This would be computationally demanding because of the high resolution which would be required in the boundary layer, particularly in optically thin

solutions.

Another important area for future work might be the development of a time-dependent model of the boundary layer region. This would allow us to study the effects of a sudden increase in the mass transfer rate upon the boundary layer. It would also allow us to examine the transition from the slowly-rotating branch of solutions to the breakup branch in greater detail. Finally, it might also be useful in looking for boundary layer instabilities which could be responsible for some of the rapid brightness variations seen in all types of accreting systems.

A final area into which our models could be expanded would be the inclusion of magnetic fields. This would significantly increase the complexity of the calculations, but it would also permit study of a number of interesting types of accreting systems.

4. ANGULAR MOMENTUM OF ACCRETING WHITE DWARFS: IMPLICATIONS FOR MILLISECOND PULSAR FORMATION

Abstract

We examine the evolution of the angular momentum and angular velocity of uniformly rotating magnetized white dwarfs (WDs) accreting at a constant rate from a thin disk. Depending on the initial mass of the WD, its field strength, and mass accretion rate, the end result is one of the following. Case I: The central density of the WD exceeds the critical density for collapse and a rapidly rotating neutron star is formed directly. Case II: The WD collapses first to a "fizzler", and later becomes a neutron star. Case III: The WD attains the maximum angular momentum allowed for its mass; in order to accrete any more mass and collapse the WD must lose angular momentum, but the mechanism by which it might do this is not clear. The number of systems that lead to low-field short-period neutron stars, similar to the known millisecond pulsars, is small, unless Case III can produce collapse.

4.1 Introduction

Neutron stars with low-mass companions ($\lesssim 1\,M_\odot$) are common in the Galaxy. There are $\sim 10^5$ millisecond pulsars (MSPs) and related low-mass binary pulsars in the disk of the Galaxy (Kulkarni & Narayan 1988) and $\sim 10^2$ low-mass X-ray binaries. There may be even greater numbers, relative to the mass content, in the globular clusters (e.g. Grindlay & Bailyn 1988). The formation of these systems is difficult to understand in a standard Type II supernova scenario. Because the

companion has a low mass, the supernova explosion will normally eject more than half the total mass of the pre-explosion system, and the binary will be disrupted. Moreover, even if the system remains bound, it will still receive a substantial velocity, $\gtrsim 100$ km s^{-1}, both from the recoil and from any asymmetry in the explosion (e.g. Dewey & Cordes 1988). The binary would then move to much higher z in the disk than is observed.

An attractive alternative method for forming low-mass binary neutron stars involves the accretion-induced collapse (AIC) of an oxygen-neon-magnesium white dwarf (WD), or possibly a carbon-oxygen WD (van den Heuvel 1977, Helfand, Ruderman, & Shaham 1983, Chanmugam & Brecher 1987, Nomoto 1987). Because very little mass is lost during AIC, the binary is not disrupted, nor does it receive a significant recoil velocity. Along with mass, an accreting WD also acquires angular momentum, but the effect of this has only been discussed qualitatively (e.g. Grindlay and Bailyn 1988). We have carried out a quantitative calculation to determine the spin history of accreting WDs for a variety of conditions.

4.2 Input Physics

4.2.1 *Torque on a White Dwarf from an Accretion Disk*

We use the model developed by Ghosh & Lamb (1979a,b) and improved by Wang (1987), where the torque consists of two parts. There is a material torque, which always tends to spin up the WD, given by the mass accretion rate $\dot{M}$ multiplied by the specific angular momentum at the inner edge of the disk. The inner edge occurs at the stellar surface when the WD field is weak, but is farther out

when the field is strong. An additional magnetic torque results from the interaction of the disk and the magnetic field of the WD. Field lines that penetrate the disk outside the corotation radius are swept backward and slow the star down, and those that pass inside the corotation radius spin the star up. The net magnetic torque can be positive or negative, depending on the angular velocity of the WD.

4.2.2 *Structure of Rotating White Dwarfs*

Hachisu (1986) has investigated the structure of rotating Chandrasekhar WDs for three assumed rotation laws, viz. constant Ω, constant ΩR, and constant ΩR^2, where R is the radius in cylindrical coordinates. For each law, he has calculated the mass M, angular momentum J, angular velocity Ω, and equatorial radius R_e, as functions of the central density and the rotational flattening. We use the results corresponding to constant Ω, i.e. uniform rotation. This is likely to be a good description of WDs with strong fields since the field will probably eliminate internal shears. For weak fields, the accretion disk will extend down to the surface of the star and the angular momentum will be deposited directly in the outer equatorial layers. Consequently, the outer regions of the star may spin faster than the inside. The closest approximation to this in Hachisu's models is the one with constant Ω.

Uniformly rotating WDs are possible only for M and J that lie within a bounded area in the $M - J$ plane. At each M, there is a maximum value of J at which the outer equatorial layers of the WD are supported entirely by centrifugal forces and the star is on the verge of break-up. We refer to this limit as "critical rotation." In addition, an O-Ne-Mg WD will collapse if the central density reaches the electron capture threshold for Mg at $\rho_c = 10^{9.5}$ g cm^{-3} (Shapiro & Teukolsky

1983); this places a limit on M at each value of J, which we refer to as the "collapse line". These two limits are shown in Figure 4.1.

4.2.3 *Restrictions on Initial M, $\dot{M}$, and B*

Oxygen-neon-magnesium WDs are formed with masses in the range $1.2 - 1.37\,M_\odot$ from $8 - 10\,M_\odot$ progenitors (Nomoto 1984). These WDs can potentially become neutron stars through AIC if the mass accretion rate lies within one of the ranges $\dot{M} < 10^{-9}\,M_\odot\ \mathrm{yr}^{-1}$ or $\dot{M} > 4 \times 10^{-8}\,M_\odot\ \mathrm{yr}^{-1}$ (Nomoto 1987); intermediate rates, $10^{-9}\,M_\odot\ \mathrm{yr}^{-1} < \dot{M} < 4 \times 10^{-8}\,M_\odot\ \mathrm{yr}^{-1}$, produce off-center helium detonation, leading to a "dim" Type I supernova. Furthermore, if $\dot{M} < 10^{-9}\,M_\odot\ \mathrm{yr}^{-1}$, the accreted mass may be ejected in novae or similar eruption events (Paczyński & Zytkow 1978). Thus, it is possible that AIC occurs only when the accretion rate exceeds $4 \times 10^{-8}\,M_\odot\ \mathrm{yr}^{-1}$. Such large $\dot{M}$ may occur with a secondary of around $1\,M_\odot$ ascending the giant branch (Webbink, Rappaport, & Savonije 1983). In our calculations, we consider, for completeness, mass loss rates ranging from 10^{-10} to $10^{-7}\,M_\odot\ \mathrm{yr}^{-1}$, and assume that none of the mass or angular momentum is lost from the system.

We specify the WD field strength by the magnetic flux, BR_e^2, which we assume to be conserved during the evolution and collapse. We consider fluxes in the range 10^{21}–5×10^{24} G cm^2, corresponding to WD fields of about 10^4 to 5×10^7 G and neutron star fields of 10^9 to 5×10^{12} G for radii of $10^{8.5}$ cm and 10^6 cm, respectively.

4.3 Results

Each of our calculations is specified by three parameters, the initial mass of the WD, M_i, the magnetic flux BR_e^2, and the accretion rate $\dot{M}$. The initial angular velocity of the WD is taken to be zero. Rather than M_i, a more useful parameter is the initial mass deficit from the critical mass for collapse (for $J = 0$), viz. $\Delta M = 1.39 - M_i$. According to Nomoto (1984), O-Ne-Mg WDs can have $\Delta M \sim 0 - 0.17\,\mathrm{M}_\odot$; we have considered three representative values in this range, $\Delta M = 0.15, 0.03, 0.01\,\mathrm{M}_\odot$.

At the end of each calculation the WD reaches either the collapse line (Cases I, II) or critical rotation (Case III). We subdivide the systems which collapse according to their final angular momentum. If $J < 6 \times 10^{48}\,\mathrm{g\ cm^2\ s^{-1}} \equiv J^*$, a neutron star is directly formed (Case I), while if $J > J^*$, the collapse is halted midway by centrifugal forces (Case II) in a state called a "fizzler" (Gold 1975, Shapiro & Lightman 1976). Our assumed value of J^* corresponds to a neutron star moment of inertia of 10^{45} g cm^2 and a limiting neutron star spin period of 1 ms.

For most of the allowed range of ΔM of O-Ne-Mg WDs, the evolution is similar to the case $\Delta M = 0.15\,\mathrm{M}_\odot$ shown in Fig. 4.1 and Table 1. If the field is weak, the WD undergoes Case III evolution, reaching critical rotation after accreting $\sim$0.1–$0.15\,\mathrm{M}_\odot$ of material. If the field is sufficiently strong, then the WD reaches the collapse line either in Case I or II. The magnetic torque starts off positive, since the star is spinning more slowly than most of the disk, but quickly becomes negative; the star actually loses angular momentum during most of the accretion. The stronger the field, the lower the final J of the WD at collapse; the final J is essentially independent of ΔM. This is because for strong fields the WD quickly reaches

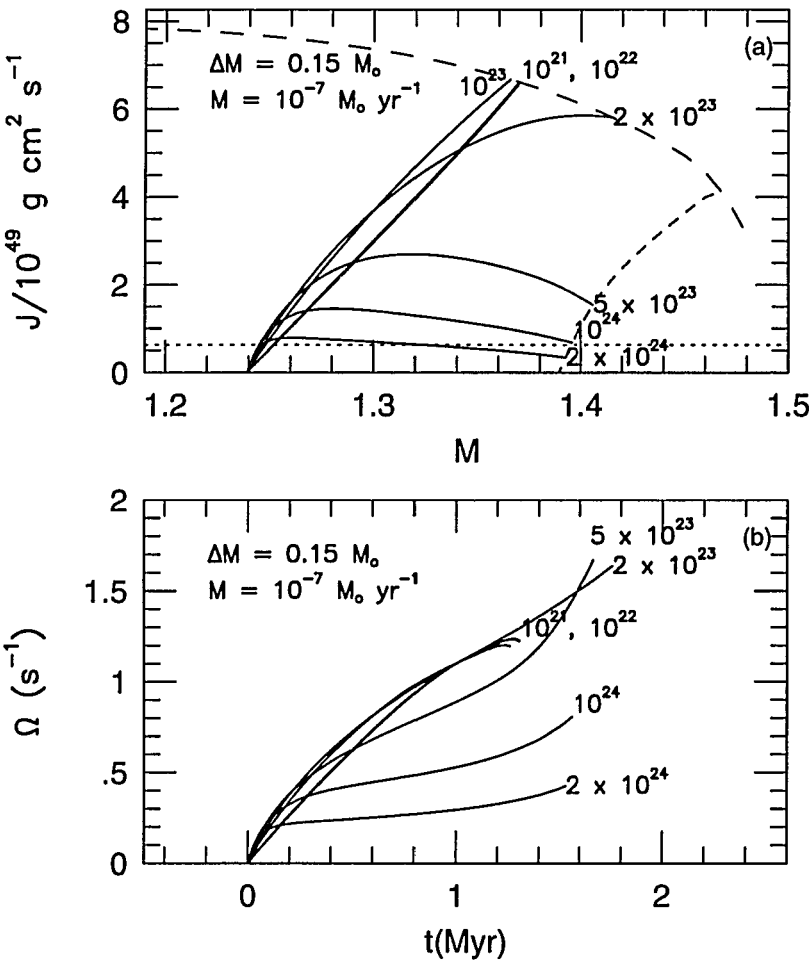

Fig. 4.1—(a) The solid lines show the evolutionary tracks in the M–J plane for accreting WDs that have initial $\Delta M = 0.15\,\mathrm{M}_\odot$ for $\dot{M} = 10^{-7}\,\mathrm{M}_\odot\ \mathrm{yr}^{-1}$. Each curve is labeled by the conserved magnetic flux BR_e^2 in units of G·cm^2. The short-dashed line shows the "collapse line" and the long-dashed line corresponds to "critical rotation". The dotted line represents the marginal angular momentum J^* that separates case I evolution from case II. Of the seven fluxes shown, 2×10^{24} corresponds to case I, 10^{24} and 5×10^{23} lead to case II, and all the others to case III. (b) Variation of angular velocity with time for the cases shown in Fig. 4.1 (a). The horizontal axis has been scaled so as to correspond exactly to the mass axis in Fig. 4.1 (a). For cases I and II the labels give the flux as well as the rotation period of the resulting neutron star. Case II, where the collapse fizzles due to centrifugal forces, is expected to occur for periods less than 1 ms.

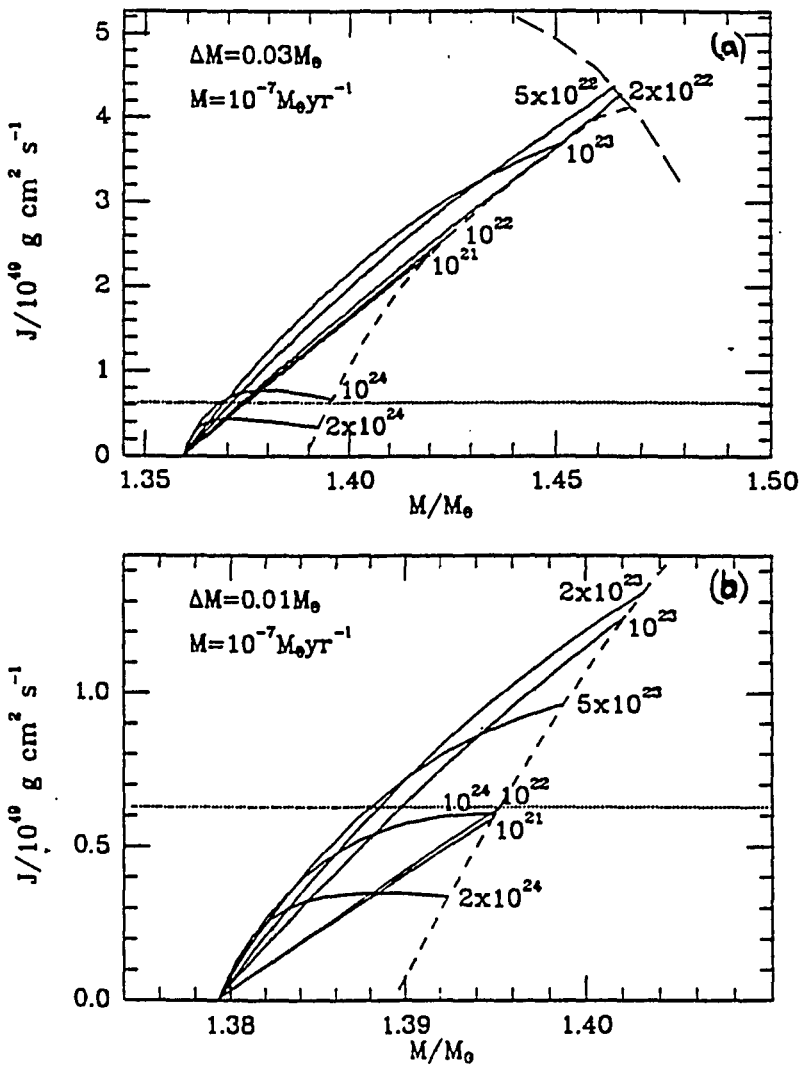

Fig. 4.2—(a) Similar to Fig. 4.1 (a), but with $\Delta M = 0.03\,\mathrm{M}_\odot$. (b) Similar to Fig. 4.1 (a), but with $\Delta M = 0.01\,\mathrm{M}_\odot$.

TABLE 1

SUMMARIZED RESULTS OF THE END STATES OF ACCRETING WHITE DWARFS[1]

ΔM	$\dot{M}$	$BR^2 = 10^{21}$	2×10^{21}	5×10^{21}	10^{22}	2×10^{22}	5×10^{22}
0.15	10^{-10}	c:0.100	c:0.103	c:0.053	f:0.30	f:0.73	n:1.84
0.15	10^{-9}	c:0.097	c:0.098	c:0.102	c:0.099	f:0.16	f:0.50
0.15	10^{-8}	c:0.097	c:0.097	c:0.098	c:0.099	c:0.103	c:0.079
0.15	10^{-7}	c:0.097	c:0.097	c:0.097	c:0.097	c:0.098	c:0.101
0.03	10^{-10}	c:0.003	c:0.001	f:0.25	f:0.40	f:0.75	n:1.84
0.03	10^{-9}	f:0.24	c:0.002	c:0.003	f:0.19	f:0.28	f:0.56
0.03	10^{-8}	f:0.27	f:0.26	f:0.22	c:0.003	c:0.003	f:0.23
0.03	10^{-7}	f:0.27	f:0.27	f:0.26	f:0.25	f:0.20	c:0.003
0.01	10^{-10}	f:0.74	f:0.56	f:0.48	f:0.59	f:0.74	n:1.85
0.01	10^{-9}	n:1.03	f:0.76	f:0.63	f:0.50	f:0.49	f:0.72
0.01	10^{-8}	n:1.09	n:1.07	f:0.98	f:0.80	f:0.59	f:0.48
0.01	10^{-7}	n:1.10	n:1.09	n:1.08	n:1.04	f:0.95	f:0.67
ΔM	$\dot{M}$	$BR^2 = 10^{23}$	2×10^{23}	5×10^{23}	10^{24}	2×10^{24}	5×10^{24}
0.15	10^{-10}	n:3.44	n:6.28	n:12.3	n:19.7	n:32.2	n:64.2
0.15	10^{-9}	n:1.09	n:2.13	n:4.79	n:8.47	n:13.6	n:25.7
0.15	10^{-8}	f:0.25	f:0.61	n:1.59	n:3.00	n:5.50	n:11.0
0.15	10^{-7}	c:0.101	c:0.052	f:0.41	f:0.93	n:1.85	n:4.19
0.03	10^{-10}	n:3.44	n:6.28	n:12.3	n:19.7	n:32.2	n:64.2
0.03	10^{-9}	n:1.10	n:2.13	n:4.79	n:8.47	n:13.6	n:25.7
0.03	10^{-8}	f:0.36	f:0.65	n:1.59	n:3.00	n:5.50	n:11.0
0.03	10^{-7}	f:0.17	f:0.25	f:0.49	f:0.94	n:1.85	n:4.19
0.01	10^{-10}	n:3.44	n:6.28	n:12.3	n:19.7	n:32.2	n:64.2
0.01	10^{-9}	n:1.17	n:2.14	n:4.79	n:8.47	n:13.6	n:25.7
0.01	10^{-8}	f:0.55	f:0.79	n:1.62	n:3.00	n:5.50	n:11.0
0.01	10^{-7}	f:0.52	f:0.48	f:0.66	n:1.04	n:1.86	n:4.19

[1]For each combination of ΔM, $\dot{M}$ and BR^2, the final state is indicated by a letter and a number, with the following meanings:

- c: White dwarf reaches critical rotation; the number refers to $1.467\,M_\odot - M_{\rm final}$, which is the mass that the white dwarf needs to accrete to reach the intersection of the collapse line and critical rotation line.
- f: White dwarf collapses to a fizzler; the number refers to the rotation "period" in ms *if* a standard neutron star could form directly.
- n: White dwarf collapses to a neutron star; the number refers to the rotation period in ms.

and follows a track for which the material and magnetic torques cancel each other. This situation is similar to the equilibrium period reached by neutron stars. The variation of angular velocity Ω with time is shown in Figure 4.1 (b). Interestingly, even while J is decreasing, Ω continues to increase because the moment of inertia of the WD decreases with increasing mass.

The dependence on magnetic field is somewhat different for smaller values of ΔM. For $\Delta M \sim 0.025 - 0.035\,\mathrm{M}_\odot$, low and high field WDs reach the collapse line, but intermediate field WDs attain critical rotation (Figure 4.2 (a); Table 1). For $\Delta M \lesssim 0.025\,\mathrm{M}_\odot$, all WDs reach the collapse line (Fig. 4.2 (b); Table 1).

4.4 Discussion

Of the possible outcomes for accreting O-Ne-Mg WDs, Case I, where AIC leads directly to a neutron star, is probably the easiest to understand. However, as we see from Table 1, unless ΔM is very small, this occurs for only a small subset of highly magnetized WDs, producing neutron stars with correspondingly strong fields. The combination of strong field and millisecond period in these neutron stars will lead to a rapid loss of rotational energy, producing a luminosity $\sim 4 \times 10^{43} B_{12}^2 / P_{\rm ms}^4 \sim 10^{39}$–$10^{44}$ erg s^{-1} in magnetic dipole radiation for a time $\sim 30 P_{\rm ms}^2 / B_{12}^2 \sim 10$–$10^5$ yr, where $B_{12} = B/10^{12}$ G and $P_{\rm ms} = P/1$ ms. For instance, a WD with $BR^2 = 10^{24}$ G cm^2 accreting at a rate of $\dot{M} = 10^{-7}\,\mathrm{M}_\odot\ \mathrm{yr}^{-1}$ will produce a neutron star with a period of $\sim$1 ms and a magnetic field of $\sim 10^{12}$ G. Such a star will lose the bulk of its kinetic energy in about 30 yrs with a luminosity $> 10^{43}$ erg s^{-1}. The resulting "supernova" remnant will be quite spectacular and may be visible even in distant galaxies.

In Case II, the collapse is halted to form a "fizzler". According to Tohline (1984), the details of the collapse and further evolution depend both on the value of the initial ratio of kinetic to potential energy, and on the variation of the adiabatic exponent Γ with density. Fizzlers will lose angular momentum through magnetic dipole radiation and very likely also through gravitational radiation driven by unstable nonaxisymmetric distortions. Thus, fizzlers ultimately become neutron stars with spin periods close to the limiting value ~ 1 ms.

Case III, where the WD reaches critical rotation, is probably the least understood outcome. At critical rotation, the WD is on the verge of losing mass due to centrifugal forces, but more mass is being added by the continuing accretion. It is not clear how the star will respond to this situation. It may develop an extended envelope like a red giant, or it may eject mass, or it may manage to continue accreting more mass. The last option may be possible if angular momentum can be pumped back through the disk; the WD may thus slide down the critical line in the $M - J$ plane until it reaches the critical central density and collapses as a fizzler.

Case III will probably be the most common situation since the majority of WDs have weak fields (Schmidt 1989). What would a binary WD look like when it has attained critical rotation? Since the rotation rates of the star and disk join smoothly, there will be no boundary-layer emission, as indeed may be the case with many cataclysmic variables. Moreover, because of the weak field, there may not be any rotation-induced luminosity modulation, making the rotation rate difficult, if not impossible, to determine observationally. It is possible that some of the known accreting WDs are critically rotating but have not been recognized as such.

MSPs and low-mass X-ray binaries in the Galaxy are characterized by low fields ($\sim 10^8 - 10^{9.5}$ G) and long lifetimes ($\sim 10^9$ yr). If they are formed by AIC, then our results have some interesting implications.

In the simplest scenario, the collapsed neutron star directly becomes a MSP (Chanmugam & Brecher 1987) with fast rotation and low field. The progenitor then has to be a low-field WD. However, we find from our calculations that only a fraction of such WDs, those with small ΔM, reach the collapse line. Furthermore, our calculations are probably optimistic because of our assumption of uniform rotation. More likely, the outer layers of the WD would spin faster than the center and the critical rotation limit would be reached at much smaller J than we have assumed; the range of ΔM that hit the collapse line would then be even smaller. It may be that Cases I and II will not provide enough progenitors to make all the MSPs in the Galaxy, and it may be necessary to invoke AIC in the Case III systems.

In an alternative scenario (e.g. Taam & van den Heuvel 1986), the collapsed neutron star does not directly make a MSP but undergoes field decay and accretion spin-up before it is seen as a MSP. Here, even strong-field WDs can make MSPs and our calculations show that such WDs undergo Case I or II even for large ΔM. However, a basic requirement in this scenario is that the accretion must continue for a long enough time for the field to decay to its final value. This may be a problem since, for reasons discussed in §II*c*, AIC is believed to be possible only when $\dot{M} \gtrsim 4 \times 10^{-8}\,\mathrm{M_\odot yr^{-1}}$. The accretion timescale in such systems will be less than ten million years, which is much shorter than the time needed (> 50 million yr) for a strong initial field of $\sim 10^{12}$ G to decay to $< 10^9$ G. Once again, either

one must restrict oneself to low-field low-ΔM WDs, in which case there may not be enough progenitors, or find a way to induce collapse in Case III systems.

It is thus important, in either scenario, to address the evolution of critically-rotating accreting WDs.

5. DOES ACCRETION CEASE WHEN A STAR APPROACHES BREAKUP?

Abstract

We model a steady-state thin accretion disk around a uniformly-rotating unmagnetized star using a two-dimensional fluid with a polytropic equation of state and α-viscosity. We explicitly include gradients in the radial velocity and the pressure, and numerically solve for the angular velocity profile. We treat the specific angular momentum, j, added to the star as an eigenvalue of the problem that is determined through the boundary conditions. We find that there is a mapping between j and the stellar rotation rate, Ω_*, with the following properties. When Ω_* is somewhat less than the breakup rotation rate of the star, $\Omega_{\rm max}$, we find a class of solutions where the angular velocity of the disk attains a maximum close to the star and then decreases rapidly in a boundary layer to match Ω_*. For a thin disk with thickness ~ 0.01 times the radius and $\alpha = 0.1$, the radial flow of the accreting material briefly becomes supersonic in the boundary layer before being decelerated in a radial shock. For a thicker disk (thickness $\sim$0.1 times radius) with much smaller viscosity ($\alpha = 0.0001$), the flow is subsonic throughout. In either case, j is almost independent of Ω_* and is approximately equal to the Keplerian specific angular momentum at the stellar surface. This agrees with the standard picture of angular momentum transport in thin disks. However, if Ω_* is near break-up, then we find a second class of solutions where the disk angular velocity has no maximum at all but increases monotonically all the way down to the stellar surface; the flow remains subsonic for all choices of disk thickness and α. For these solutions, j decreases

extremely rapidly with increasing Ω_* and even takes on fairly large negative values. Because of this, the spin-up of an accreting star slows down and eventually stops at a rotation rate near break-up. Beyond this point, the star can continue to accrete any amount of matter without actually breaking up. This result has applications in star formation and in the theory of cataclysmic variables. It also eliminates one of the objections to the accretion-induced collapse scenario for the formation of low-mass binary neutron stars.

5.1 Introduction

Accretion disks deliver both mass and angular momentum to their central accreting stars (see Pringle 1981 for a review). In the case of accreting magnetized stars such as the binary x-ray pulsars (cf. Lewin & van den Heuvel 1984 and references therein), one sees direct evidence for the addition of angular momentum in the spin-up of the stars. A feature of these systems is that there is a maximum rotation rate to which the stars are spun-up. Once the star has achieved this rotation, mass accretion can still continue but there is no additional spin-up. This phenomenon has been modeled by Ghosh & Lamb (1979b) who showed that there is a cancellation between the positive torque due to the angular momentum carried in by the accreting material and a negative torque due to the interaction between the stellar magnetic field and the fluid in the accretion disk. The existence of negative feedback from the magnetic torque thus ensures that an accreting magnetized star asymptotically approaches, but does not exceed, a stable "equilibrium" rotation rate.

The situation is less clear in the case of accretion by an *unmagnetized* object. In this case it is generally assumed that the central star receives specific angular momentum from the disk at a rate corresponding approximately to the Keplerian angular momentum at the surface of the star. Further, in the standard picture, there is no opposing torque or negative feedback mechanism. One therefore expects that if accretion were to continue long enough the star would be spun up to and possibly even beyond its maximum allowed rotation rate, $\Omega_{\rm max}$, the so-called "break-up" rate, where the equatorial centrifugal force just balances the force of gravity. What happens beyond this point is not known. Since the star is apparently unable to accept any more mass from the accretion disk, because it cannot accommodate the angular momentum that goes with it, one might imagine that either the accumulating material is ejected through a wind or via jets, or the matter builds up to form a relatively independent envelope around the central star.

The question of what happens when there is continued accretion onto an unmagnetized star close to break-up has become relevant as a result of two recent studies. Shu *et al.* (1988) investigated star-forming disks and argued that the central objects would be quickly spun-up to $\Omega_{\rm max}$. They proposed that such a system would then eject a wind from the circumferential cusp that forms around the rapidly-spinning star. This wind may be collimated to produce the outflows that are seen in star-forming regions. In another study, we (Narayan & Popham 1989) investigated the spin history of accreting white dwarfs and found that unmagnetized white dwarfs attain $\Omega_{\rm max}$ after accreting as little as $\sim 0.1\,{\rm M}_\odot$, assuming that there is no mass loss through nova ejection. Since white dwarfs in cataclysmic variables are thought to accrete several tenths of a solar mass during the course of their evolution, it seems

likely that many of these systems should achieve a spin rate close to $\Omega_{\rm max}$. A question we were unable to answer in the earlier study, and which we pursue in this paper, is: What does an accreting unmagnetized white dwarf, or any other unmagnetized star, do when its spin rate approaches $\Omega_{\rm max}$?

This question is particularly interesting in the case of massive accreting white dwarfs. In these objects, the angular momentum corresponding to break-up, $J_{\rm max}$, *decreases* with increasing mass, M (e.g. Hachisu 1986), because of the steep inverse mass-radius relation. This means that once the white dwarf has achieved a spin rate $\sim \Omega_{\rm max}$, it must actually *lose* angular momentum in order to accrete any more mass. At first glance, it appears impossible for an accretion disk to remove angular momentum from a star while at the same time supplying mass to it — as we mentioned above, the current wisdom is that there is a certain fixed amount of positive angular momentum that is associated with any accreted matter. The main purpose of the present paper is to demonstrate that disks can indeed remove angular momentum from the accreting object.

We construct here steady axisymmetric accretion disk models where we allow the specific angular momentum, j, added to the central star to be a free parameter. We show that j behaves like an eigenvalue that is self-consistently determined by the various boundary conditions that the disk must satisfy. The most important of the boundary conditions is that the rotation rate of the the star, Ω_*, should match that of the disk at the boundary between the two. As a consequence of this condition we find that there is a precise mapping between Ω_* and j. This mapping is such that j is approximately equal to the Keplerian specific angular momentum at the equator of the star whenever Ω_* is somewhat less than $\Omega_{\rm max}$.

This result is in agreement with conventional wisdom. However, we find that j becomes much smaller, and even takes on (quite large) negative values, when Ω_* is close to $\Omega_{\rm max}$. Because of the existence of such negative j solutions, there is a natural negative feedback mechanism, and the central star can continue to accrete any amount of matter even when it approaches $\Omega_{\rm max}$. In this sense, accretion onto an unmagnetized star behaves exactly as in the magnetized case; the only difference is that the "equilibrium" rotation rate here is of order $\Omega_{\rm max}$, whereas in the magnetized systems it is determined by the Keplerian Ω at the magnetospheric radius.

Our results confirm previous work by Pringle (1989) who argued that, even when a star is rotating exactly at break-up, accretion is not prevented. In Pringle's view only a star with $\Omega_* > \Omega_{\rm max}$ can stop accreting. The present work advances these ideas in two ways. First, we construct models that reveal the explicit connection between the stellar rotation rate Ω_* and the accreted specific angular momentum j. Thus, in a sense, we have quantified Pringle's argument. Secondly, we show that solutions with negative j are possible. Thus, a star can lose angular momentum — quite a lot of it if necessary — while at the same time continuing to accrete. We are not aware of any previous work that anticipated this result.

After we had completed this study, we discovered that Paczyński (1991) had independently carried out a similar investigation. Although using a somewhat different approach, Paczyński agrees with most of our conclusions. In particular, he too finds that accretion is not inhibited when a star approaches break-up.

5.2 Theory

5.2.1 *Fluid Model*

A key feature of our approach is that we treat the accretion disk, the boundary layer and the accreting star all as a single fluid system, described by the same set of equations. In order to simplify the analysis, we further assume that the fluid properties can be integrated in the vertical direction, i.e. the direction parallel to the rotation axis, so that the system can be described in terms of an effective two-dimensional fluid. This approximation is routinely made in the theory of thin accretion disks and is clearly valid in the outer parts of our model. It is less clear that the approximation is allowed in the central regions. However, as we show below, the model does represent the star reasonably well, at least near the disk-star interface, and so there is no serious error from this assumption. In any case, we feel that the two-dimensional approximation will not affect the qualitative features of our results.

Assuming that the fluid attains an axisymmetric steady state, its surface density profile is described by a function $\Sigma(R)$, where R is the radial distance from the center of the star. We use the equatorial radius of the star as our unit of length so that $R = 1$ represents the equatorial boundary of the star. As we discuss below, the exact position of the boundary is hard to locate since there is a smooth transition from the star to the disk. We use a particularly simple definition for the edge of the star, viz. that the vertical half-thickness is $H = 0.1$ at $R = 1$ (see equation [18] below). We are confident that the main results are not influenced by this choice.

We take the outer edge of the disk at some large radius, typically $R_{\rm out} = 100$. We have verified that the results are quite insensitive to the choice of $R_{\rm out}$.

The motion of the fluid is described by an angular velocity profile, $\Omega(R)$, and a radial velocity, $v_R(R)$. The latter is taken to be positive when pointed outwards and is therefore negative for accretion. We take our unit of frequency to be such that the Keplerian angular velocity, $\Omega_K(R)$, is unity at $R = 1$, i.e.

$$\Omega_K(R) = R^{-3/2}. \tag{1}$$

We assume that the two-dimensional fluid satisfies a polytropic equation of state,

$$P = K\Sigma^\gamma, \tag{2}$$

where P is the height-integrated pressure, and K and γ are constants. In principle, we could solve our equations for any choice of γ. However, in an attempt to be realistic we have selected $\gamma = 2$ for most of our computations. As we show in Appendix A, this produces the best match between our results and those of a standard thin accretion disk around a white dwarf.

For a steady accretion rate $\dot{M}$, mass conservation gives

$$\dot{M} = -2\pi R v_R \Sigma. \tag{3}$$

Using this, the sound speed, c_s, of the fluid may be written as

$$c_s^2 = \frac{dP}{d\Sigma} = \gamma K \Sigma^{\gamma-1} = C_o^2 (R|v_R|)^{1-\gamma}. \tag{4}$$

The parameter C_o describes a combination of $\dot{M}$ and the fluid constants K and γ. In our calculations we usually selected C_o such that the sound speed at the outer

edge was a fixed fraction X of the local Keplerian velocity, i.e.

$$c_s(R_{\rm out}) = X R_{\rm out}^{-1/2}. \tag{5}$$

Since a typical cataclysmic variable has $c_s/\Omega_K R \sim 0.01$ at the outer edge (cf. Frank, King, & Raine 1985), we set $X = 0.01$ in most of our calculations. As we see from equation (13) below, X is a measure of the relative thickness of the disk.

5.2.2 *Equations of Motion*

The continuity equation has been absorbed into our mapping between c_s and v_R in equation (4), and we do not need an energy equation because of the polytropic assumption. Therefore, the dynamics are completely described by the two components of the equation of motion.

In steady state, the radial equation of motion gives

$$v_R \frac{dv_R}{dR} = (\Omega^2 - \Omega_K^2)R - \frac{1}{\Sigma}\frac{dP}{dR}, \tag{6}$$

which may be rewritten as

$$\frac{dv_R}{dR} = \frac{v_R[(\Omega_K^2 - \Omega^2)R^2 - c_s^2]}{R(c_s^2 - v_R^2)}. \tag{7}$$

The form of the denominator alerts us to the possibility of obtaining a sonic point in the solution. By including pressure terms in the radial equation, we have thus gone beyond the standard theory of thin accretion disks; in fact, an equation similar to eq. (7) is used in the theory of so-called "slim" accretion disks (Abramowicz *et al.* 1988, see also Paczyński & Bisnovatyi-Kogan 1981, Muchotrzeb & Paczyński 1982).

Next we obtain a differential equation for Ω by considering the tangential equation of motion. Let the disk transport angular momentum inwards at a steady rate $\dot{J}$, and let us define

$$j \equiv \dot{J}/\dot{M}. \tag{8}$$

By our choice of units, j is expressed in units of the Keplerian angular momentum at the defined edge of the star. Going back to our discussion in sect. 5.1, the usual assumption is that $j \sim 1$, regardless of the rotation of the star, for disks around unmagnetized stars. We avoid this assumption and treat j as an adjustable parameter — an eigenvalue — whose value is determined by the boundary conditions.

Consider now the angular momentum flow across some radius R in the system. The accreting fluid carries angular momentum inwards at the rate $\dot{M}\Omega R^2$. At the same time, there is an outward flux of angular momentum because of the viscous stress. If the kinematic coefficient of viscosity is ν, then we have the following relation,

$$\dot{M}\Omega R^2 + 2\pi R^2 \nu \Sigma R \frac{d\Omega}{dR} = \dot{J}. \tag{9}$$

Substituting equation (3) for Σ and using equation (8), this can be rewritten as

$$\frac{d\Omega}{dR} = \frac{v_R}{\nu}\left(\Omega - \frac{j}{R^2}\right). \tag{10}$$

For the viscosity, we use the standard α-prescription of Shakura & Sunyaev (1973), which we write in the form

$$\nu(R) = \frac{\alpha c_s^2(R)}{\Omega_K(R)} = \alpha R^{3/2} c_s^2(R). \tag{11}$$

We assumed $\alpha = 0.1$ in most of the calculations.

The differential equations (7) and (10), coupled with the relations (4) and (11), allow us to solve for $v_R(R)$, $\Omega(R)$ and $c_s(R)$, given appropriate boundary conditions. The equations are, however, very stiff and cannot be integrated by any of the standard initial-value integrators. All our results were obtained using a relaxation method (cf. Press *et al.* 1986). Apart from overcoming the stiffness of the equations, the relaxation method was also particularly convenient for handling sonic points in equation (7).

A derived quantity of particular interest is the thickness of the disk, $H(R)$. To calculate this, we obviously need to abandon the two-dimensional approximation and make some assumption regarding the three-dimensional properties of the fluid. This question is discussed in Appendix A, where we show that, for a polytropic fluid with a particular choice of polytropic indices ($\gamma = 2,\ \gamma_3 = 3$), we have the relation

$$\frac{H}{R} = \sqrt{2}\,\frac{c_s}{\Omega_K R} = \sqrt{2}\,R^{1/2} c_s(R). \tag{12}$$

The form of the relation between H and c_s is robust, but the particular coefficient, $\sqrt{2}$, is not to be taken seriously since it depends on somewhat arbitrary assumptions. A relation very similar to eq. (12) was used by Papaloizou & Stanley (1986).

5.2.3 *Outer Boundary Conditions*

Equations (5) and (12) combine to give one of the boundary conditions at the outer edge, viz.

$$\frac{H(R_{\rm out})}{R_{\rm out}} = \sqrt{2}\,X. \tag{13}$$

For our standard choice, $X = 0.01$, the disk is clearly quite thin at the outside. Moreover, for our value of $\gamma = 2$, we have $H/R \propto R^{1/8}$ (see Appendix A) and so

we are assured that, as we move in to smaller radii, the disk remains thin all the way down to the transition zone near the star.

As a second boundary condition at the outer edge, we set

$$\Omega(R_{\rm out}) = \Omega_K(R_{\rm out}) = R_{\rm out}^{-3/2}, \tag{14}$$

so that the disk is constrained to have the rotation rate appropriate to a standard thin disk. In practice, it turned out that the solutions are not sensitive to the choice of $\Omega(R_{\rm out})$. If a somewhat different choice was made for $\Omega(R_{\rm out})$, the solution would settle down to a near-Keplerian $\Omega(R)$ within a short distance from $R_{\rm out}$ and then track $\Omega_K(R)$ except in the region close to the star at $R \sim 1$.

Because of the above comment, $\Omega(R)$ is quite accurately Keplerian near the outer edge. Coupled with equations (4), (10) and (11), this permits us to calculate the infall velocity at the outer edge as well as the constant C_o,

$$v_R = \frac{3}{2}\frac{\nu}{R}\frac{1}{(1-j/R^{1/2})}, \tag{15}$$

$$C_o = c_s(-Rv_R)^{(\gamma-1)/2} = X^\gamma R^{-\gamma/2}\left(\frac{3\alpha R^{3/2}/2}{1-j/R^{1/2}}\right)^{(\gamma-1)/2}. \tag{16}$$

Note that the radial velocity is quite subsonic at the outer edge of the disk.

5.2.4 *Inner Boundary Conditions*

One obvious condition here is that $\Omega(R)$ should equal the rotation rate of the star, Ω_*, at $R = 1$, i.e.

$$\Omega(R) = \Omega_*, \qquad R = 1. \tag{17}$$

Presumably, in a good solution, $\Omega(R)$ will be essentially independent of R and remain equal to Ω_* for $R < 1$, in order to represent the interior of a rigidly-rotating

star. This then brings up a rather subtle point: how do we define the exact location of the boundary between the disk and the star? Unfortunately, there appears to be no unique answer to this since we are treating the disk and the star as a single fluid system.

For the sake of simplicity, we have taken the edge of the star to be *defined* as that radius where the relative thickness reaches a particular (arbitrarily-chosen) value, viz.

$$H(R) = 0.1, \qquad R = 1. \tag{18}$$

The particular value, 0.1, was chosen so as to be larger than the accretion disk thickness by a reasonable factor. Obviously, we do not claim that the point at which $H/R = 0.1$ represents the true stellar edge. We are merely selecting it as a convenient fiducial marker that is likely to be reasonably close to any other better-defined stellar edge. See sect. 5.3.3 for further discussion of this point.

5.3 Results

5.3.1 *Two Solution Branches*

By numerical solution of the equations for the particular choice of parameters, $\gamma = 2$, $X = 0.01$, $\alpha = 0.1$, we discovered two distinct branches of solutions with the following characteristics:

(i) Supersonic Solutions: These solutions have the characteristics of standard thin disks at large R. However, close to the star, they have a sonic radius, R_s, where the conditions $c_s = |v_R| = (\Omega_K^2 - \Omega^2)^{1/2} R$ are satisfied (see equation [7]). For

$R < R_s$, the flow becomes supersonic. In order to match on to the star, the supersonic regime is terminated in a radial standing shock at a shock radius, R_{sh}, inside of which the flow adopts the character of a settling solution and merges with the star. Solutions in this branch usually correspond to stellar rotation rates Ω_* somewhat below unity. The run of Ω, v_R and H of a typical solution of this type is shown in Figure 5.1. This solution corresponds to $j = 1.004$, $\Omega_* = 0.5796$, and has $R_s = 1.00777$, $R_{sh} = 1.00763$. Supersonic solutions can match on to the star only if $R_s \geq 1$. Because of this requirement, we find that they exist only for $j > 1.0005$ (for the assumed γ, X, α).

(ii) Subsonic Solutions: These solutions again behave like thin disks at large R but remain subsonic all the way into the star. They make a fairly abrupt (but continuous) transition from a Keplerian rotation profile, $\Omega(R) \simeq \Omega_K(R)$, to the constant stellar rotation, $\Omega(R) = \Omega_*$, at a radius outside our defined stellar edge. These solutions usually correspond to Ω_* close to unity (the break-up stellar rotation). Figure 5.2 shows a typical member of this solution type and corresponds to $j = 1.004$, $\Omega_* = 0.9142$. Subsonic solutions exist for a range of values of j, including quite large negative values.

The two solutions shown in Figures 5.1 and 5.2 both have the same eigenvalue j and satisfy the same boundary conditions at $R = 1$ and $R = R_{\rm out}$, but have very different stellar rotations, Ω_*. The topological relation between these two branches is revealed by relaxing our inner boundary condition, equation (18), and considering instead a range of values for the height $H(R = 1)$ at the stellar edge. We then obtain Figure 5.3, where we show Ω_* as a function of $H(R = 1)$ for the two solution branches. We find that the two branches meet at a mathematical cusp.

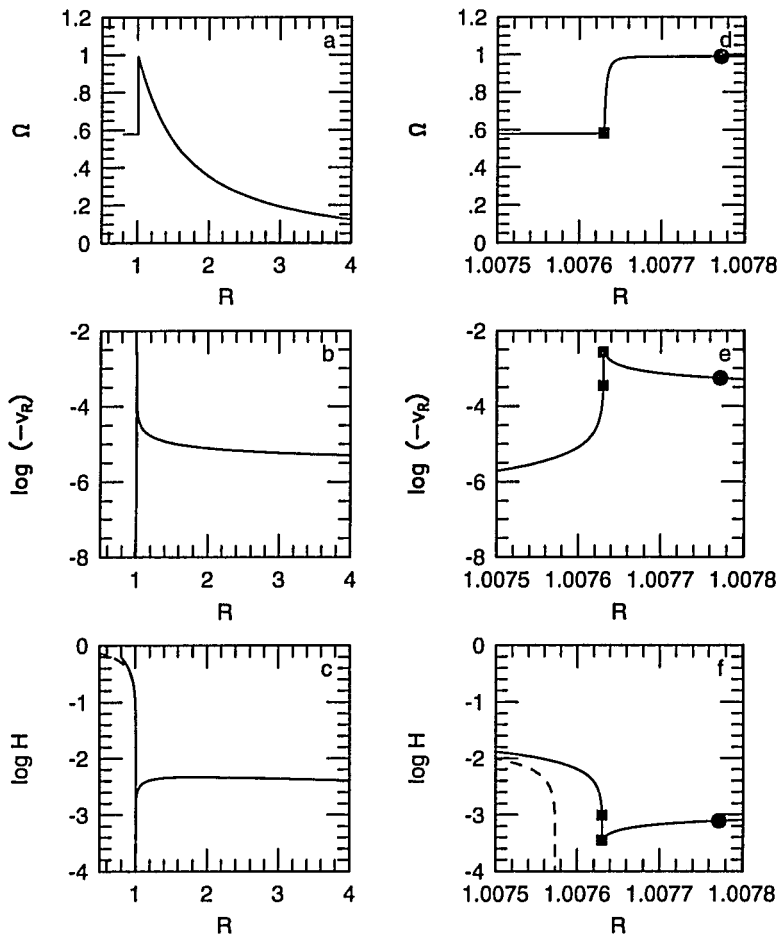

Fig. 5.1—Shows the radial dependence of Ω, v_R, and H for a supersonic disk solution corresponding to $X = 0.01$, $\alpha = 0.1$, $R_{\rm out} = 100$, $j = 1.004$, and $\Omega_* = 0.5796$. a) Ω vs. R; note the abrupt decrease of Ω in a boundary layer from a near-Keplerian value to Ω_*. b) v_R vs. R; $|v_R|$ increases slowly in the Keplerian part of the disk, rises rapidly in the supersonic region, peaks at the shock position, and finally decreases rapidly as the material settles onto the star. c) H vs. R; the disk height decreases gradually in the Keplerian disk, then more rapidly to reach a minimum at the shock position; in the settling region the height increases as the disk joins the star; the dashed line shows H vs. R for a uniformly rotating star in a point-mass potential with the same Ω_*. d)–f) Show the same quantities as a)–c), but with the radial scale expanded to show the structure of the boundary layer; the circles show the position of the sonic point and the squares show the shock. The two squares used for v_R and H show the values on either side of the shock; Ω is continuous across the shock, but $d\Omega/dR$ is not.

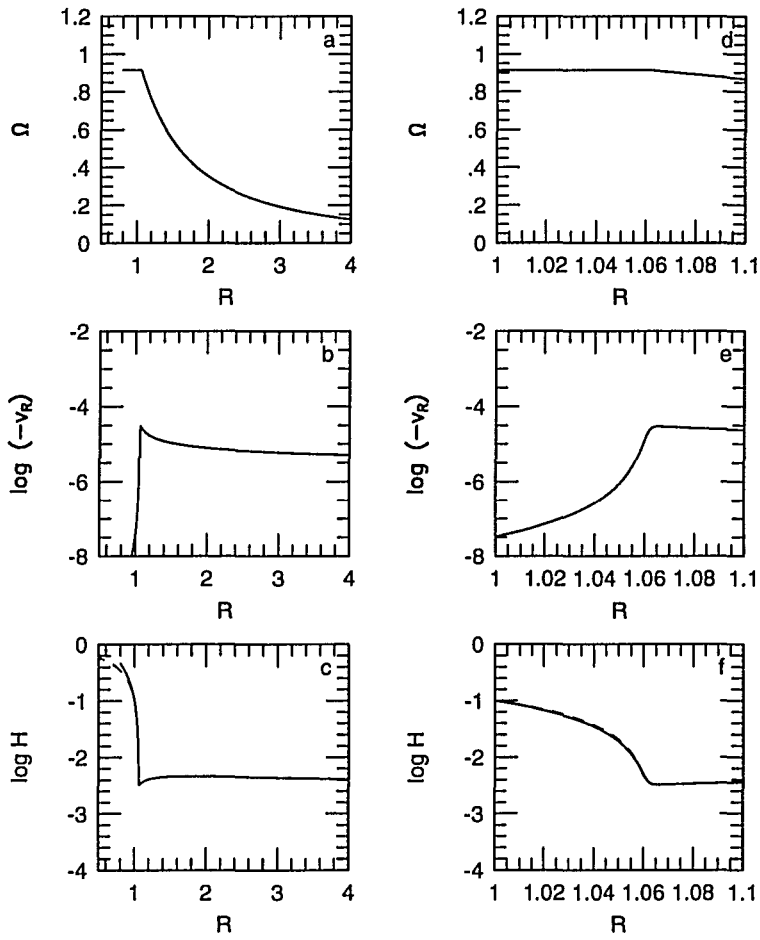

Fig. 5.2—Shows the radial dependence of Ω, v_R, and H for a subsonic disk solution corresponding to $X = 0.01$, $\alpha = 0.1$, $R_{\rm out} = 100$, $j = 1.004$, and $\Omega_* = 0.9142$. a) Ω vs. R; the angular velocity is nearly Keplerian until it reaches Ω_*, and then stays nearly constant in to the stellar surface. b) v_R vs. R; $|v_R|$ reaches a maximum close to the star and decreases in to the stellar surface, but both the maximum and subsequent decrease are far less abrupt than in the supersonic solution shown in Fig. 5.1. c) H vs. R; the disk height reaches a minimum and then increases as the disk meets the star; again the minimum and subsequent rise are less abrupt than their supersonic counterparts; the dashed line shows H vs. R for a uniformly-rotating star in a point-mass potential with the same Ω_*. d)–f) Show Ω, v_R, and H in the region close to the stellar surface. Unlike the supersonic disk in Fig. 5.1, all three quantities and their gradients are continuous.

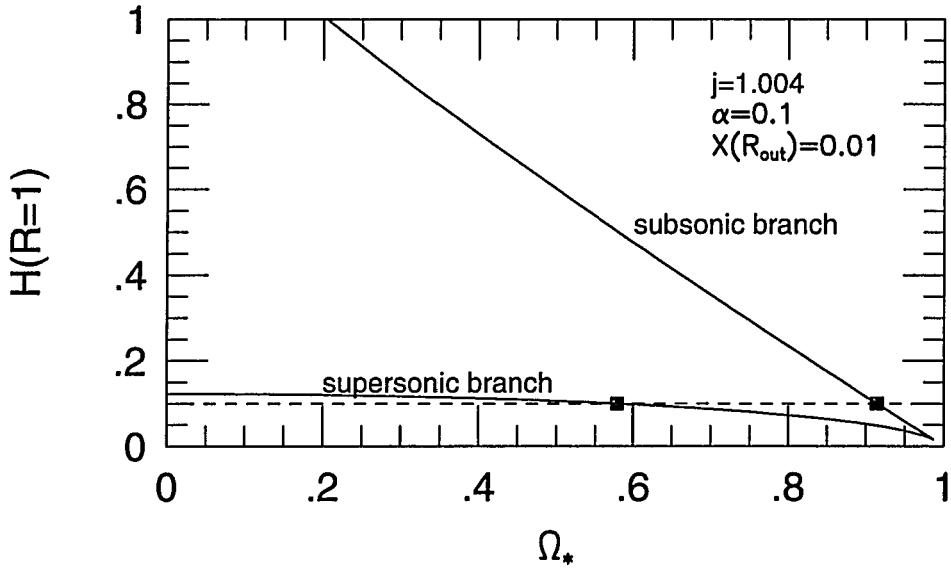

Fig. 5.3—Shows the disk height, H, at the stellar surface, $R = 1$, as a function of the stellar rotation rate Ω_*, for supersonic and subsonic solutions with $X = 0.01$, $\alpha = 0.1$, $R_{\rm out} = 100$, and $j = 1.004$. Note that the two physically distinct solution branches meet at a sharp cusp. Our boundary condition, $H = 0.1$ at $R = 1$, corresponds to the dashed line. The solutions shown in Figures 5.1 and 5.2 are marked by squares.

The solution corresponding to the tip of the cusp may be interpreted either as the last subsonic solution, that barely avoids the sonic point, or as the first supersonic solution, with an infinitesimally weak shock immediately following the sonic point. This particular solution has the smallest allowed value of $H(R = 1)$ for the given value of j. As we move away from the cusp point in Figure 5.3 along the supersonic branch, the solutions have an increasingly larger separation between R_s and R_{sh}, the shock increases in strength, and the stellar rotation rate Ω_* decreases. In fact, even solutions with negative Ω_* (backward-spinning star) are possible.

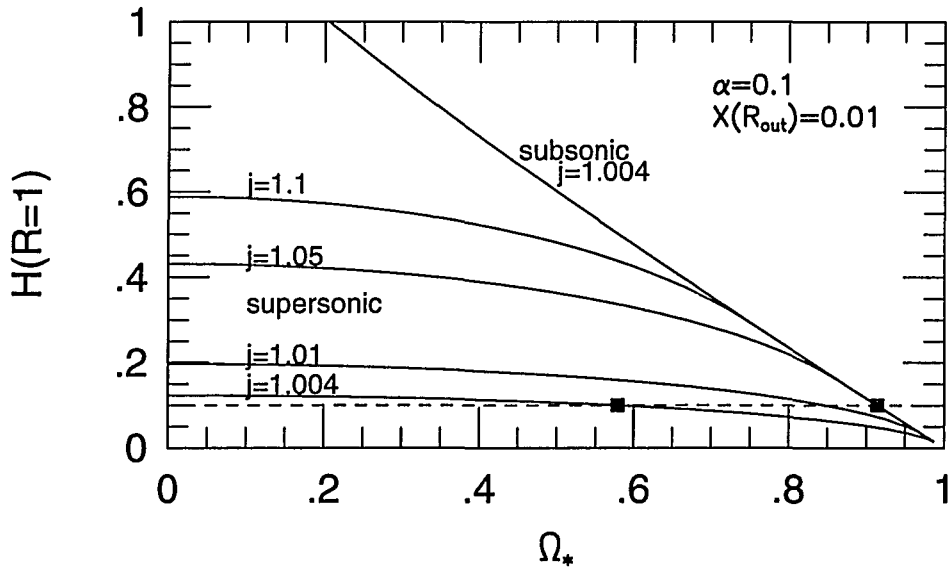

Fig. 5.4—Shows the disk height at the stellar surface $H(R = 1)$ as a function of the stellar rotation rate Ω_* for supersonic and subsonic solutions for $X = 0.01$, $\alpha = 0.1$, $R_{\rm out} = 100$, and various values of j. For $j > 1.0005$, both supersonic and subsonic branches of solutions exist; the two branches meet at a cusp point, which moves to lower Ω_* and higher disk height for larger values of j. For $j < 1.0005$, only subsonic solutions exist; the solutions corresponding to different j are very close together and are not resolved in this diagram.

5.3.2 *Spin History of an Accreting Star*

Figure 5.4 is similar to Figure 5.3, but shows the supersonic and subsonic branches for a range of values of j. Both branches exist for $j > 1.0005$, but only the subsonic branch is possible for $j < 1.0005$.

The dashed line in Figure 5.4 corresponds to our boundary condition, $H(R = 1) = 0.1$ (equation [18]). An accreting star that begins with no rotation traverses this line starting at $\Omega_* = 0$ and moving to the right. At each value of Ω_*, there is a unique value of j of the accretion disk, i.e. there is a unique rate at which

the star accretes angular momentum. The mapping between Ω_* and j is shown in Figure 5.5. For most of the range of Ω_*, the flow corresponds to the supersonic branch, and the value of j is relatively insensitive to Ω_*. However, when as a result of spin-up Ω_* exceeds 0.914, the solution switches from the supersonic to the subsonic branch. Immediately, the nature of the Ω_* vs. j mapping also changes dramatically. Now the curves corresponding to different j crowd together in Figure 5.4 and, consequently, a small increase in Ω_* causes a large decrease in j.

The fact that j plummets to large negative values as Ω_* approaches unity implies that any star will be able to continue accreting indefinitely without ever encountering an angular momentum barrier. Consider, for instance, the situation we mentioned in sect. 5.1, namely accretion on to an unmagnetized massive white dwarf. This is a case where the maximum angular momentum $J_{\max}$ of the star *decreases* as its mass M increases. This means that when such a star approaches the critical rotation it will require a disk with negative j in order to continue to accrete. From Hachisu's (1986) results we estimate that a white dwarf close to the Chandrasekhar limit may need $j \sim -1$. As we have shown above (Figure 5.5), subsonic solutions with negative j are available and the star can indeed continue accreting.

Figure 5.6 shows in detail the solution corresponding to $j = -10$. It will be noted that this solution is rather similar to the subsonic solution with $j = 1.004$ shown in Figure 5.2. Thus, the negative j solutions are not different or peculiar in any way. They are quite reasonable solutions which may be expected to occur whenever the conditions require them.

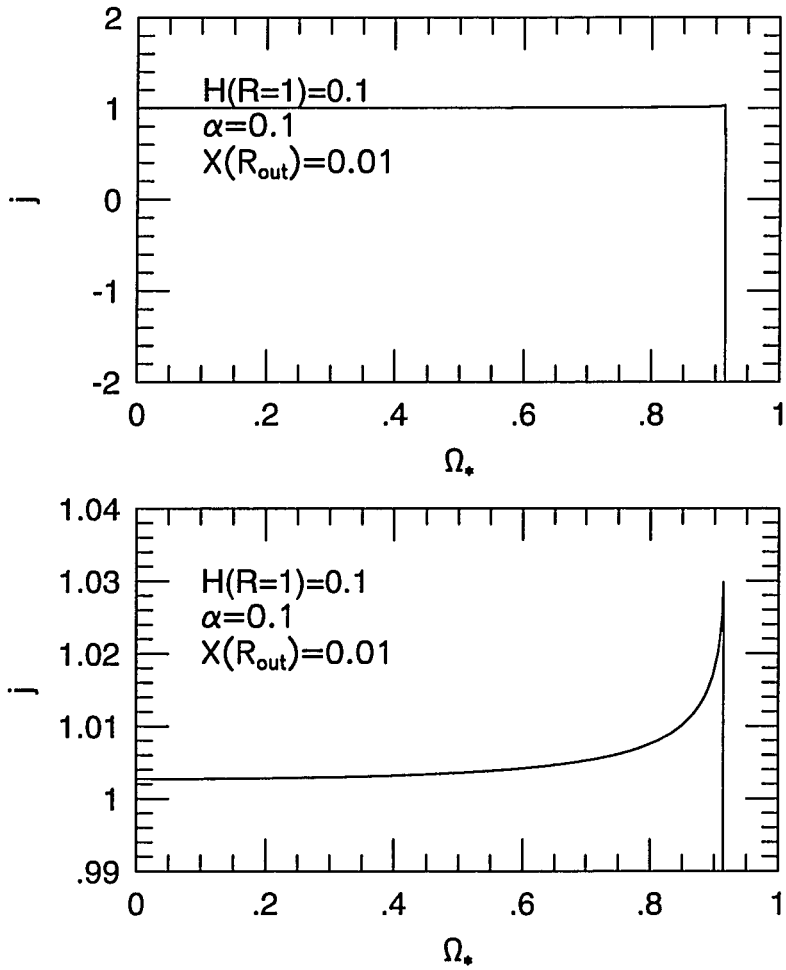

Fig. 5.5—Shows the variation of the specific angular momentum j with the stellar rotation rate Ω_* for $X = 0.01$, $\alpha = 0.1$, $R_{\rm out} = 100$, and our inner boundary condition, $H(R = 1) = 0.1$. The scale is expanded in the lower panel. For $\Omega_* < 0.914$, the solutions are supersonic and $j \sim 1$, as in the standard picture of a disk and boundary layer. The specific angular momentum is $j \cong 1.003$ at $\Omega_* = 0$, and increases very slowly with Ω_*, then more rapidly until it peaks at $j \simeq 1.03$ at $\Omega_* = 0.914$. The peak in j corresponds to the transition between supersonic and subsonic solutions. Note that these values are expressed in our dimensionless units; the physical j actually increases more rapidly with Ω_* due to rotational flattening of the star. For $\Omega_* > 0.914$, the solutions are subsonic, and j decreases very rapidly for only a slight increase in Ω_*.

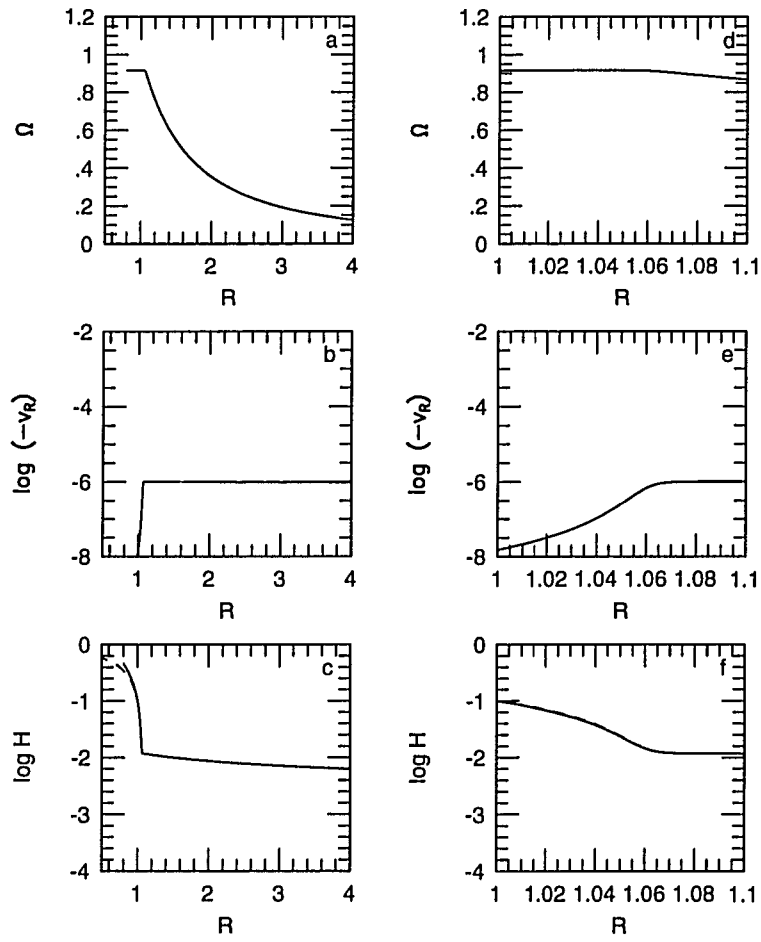

Fig. 5.6—Shows Ω, v_R, and H for a subsonic disk solution corresponding to $X = 0.01$, $\alpha = 0.1$, $R_{\rm out} = 100$, $j = -10$, and $\Omega_* = 0.915$. Note the close similarity to the solution of Fig. 5.2 which corresponds to a more standard angular momentum accretion rate of $j = 1.004$; as in Fig. 5.2, all quantities are continuous, and the dashed line shows H vs. R for a uniformly-rotating star in a point-mass potential with the same Ω_*.

5.3.3 *Location of the Stellar Edge*

A somewhat unsatisfactory feature of our analysis is that we are unable to identify uniquely the boundary between the star and the disk. Figures 5.1, 5.2 and 5.6 show that our particular choice (based on equation [18]) is not unreasonable since (i) $\Omega(R)$ is very nearly constant interior to our defined boundary at $R = 1$ and varies rapidly outside it, (ii) the vertical thickness of the fluid increases rapidly interior to $R = 1$ as it would in a star, and (iii) the infall velocity $|v_R|$ decreases rapidly for $R < 1$. All these criteria suggest that the "real" stellar edge is not very far from our defined edge.

In order to demonstrate that the fluid at $R < 1$ does represent the star fairly well, we show by dashed lines in Figures 5.1, 5.2, 5.6, and 5.7, the shape of a rigidly-rotating polytropic star in a point-mass potential with a rotation rate Ω_*. We see that the $H(R)$ profiles obtained from our solutions track those of the model stars reasonably well. (The small mismatch in Figure 5.1f occurs because the "star" in our solution spins faster in its outer layers.) Despite the satisfactory agreement between our solutions and the model stars, the smooth transition from disk to star makes it difficult to identify uniquely the radius of the star.

This uncertainty regarding the stellar radius in turn makes it difficult to answer the simple question: what is the ratio of the maximum or "equilibrium" rotation, $(\Omega_*)_{\rm max}$, achieved by an accreting star to its break-up rotation, $\Omega_{\rm max}$? We have expressed Ω_* in terms of the Keplerian Ω_K at the edge of the star, defined as the radius where $H/R = 0.1$. In these units, we see from Figure 5.6 that $(\Omega_*)_{\rm max} = 0.9157$ for a star that requires $j = -10$ at equilibrium. More normally, j is probably $\gtrsim 0$ at equilibrium and $(\Omega_*)_{\rm max} \simeq 0.9145$. An isolated uniformly rotating polytropic

star with $H = 0.1$ at $R = 1$ breaks up if $\Omega_* > 0.9141$. If we use this as our definition of $\Omega_{\rm max}$ (cf. Paczyński 1991), then we see that the cases with $j = -10$ and 0 mentioned above are both spinning faster than break-up. Of course, the stars do not actually break up because they spin more slowly on the outside.

5.3.4 *The Role of the Supersonic Solutions*

In the calculations reported above, we found a sudden change in the character of the solutions, as well as in the j vs Ω_* mapping, between the supersonic and subsonic branches. This might lead one to suspect that it is the existence of the supersonic branch that leads to the particular nature of the mapping. In fact, this turns out not to be the case.

Papaloizou & Stanley (1986) showed that supersonic flows occur in disk boundary layers only if the viscosity is high. By using a lower viscosity coefficient in the boundary layer, where the pressure scale height becomes smaller than the disk thickness, they could find completely subsonic flows even with slowly-rotating stars. Appendix B presents an analysis of our fluid equations in the region of the boundary layer which confirms this result. We find that for $\gamma = 2$, fully subsonic solutions should be possible if the following condition is satisfied, viz.

$$\alpha \lesssim CX^2, \tag{19}$$

where X is defined at $R_{\rm out} = 100$ (see eq. 5). The constant C is estimated to be $\sim$0.4 and may be up to a factor $\sim$2 smaller.

The calculations presented so far have used $X = 0.01$, $\alpha = 0.1$. Since these parameters violate the above constraint by a large factor, we obtained supersonic

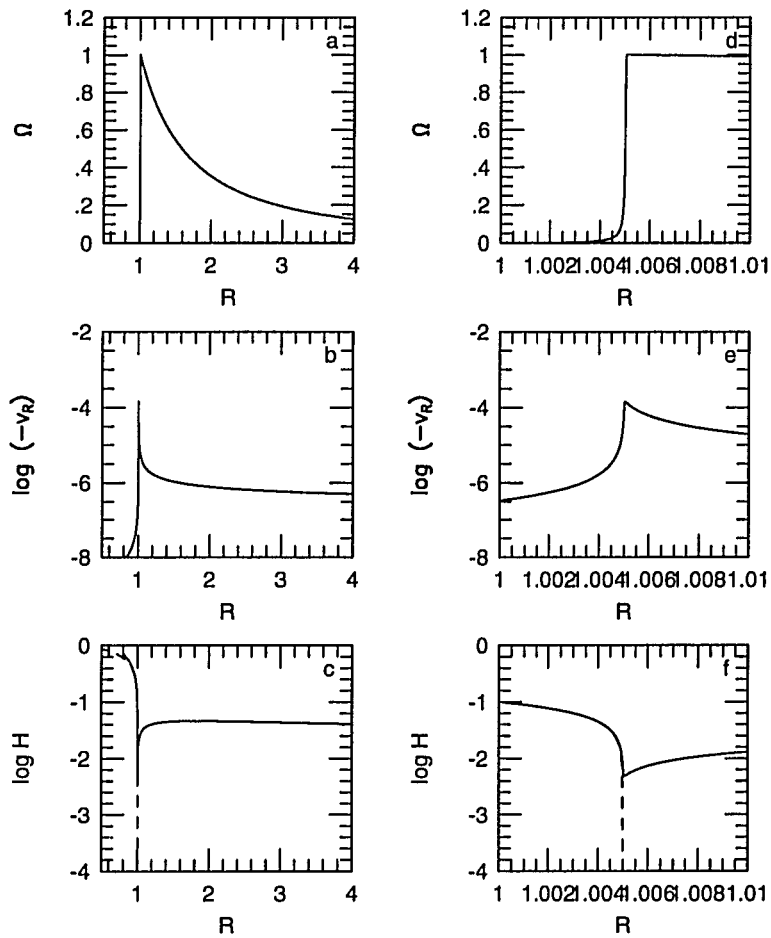

Fig. 5.7—Shows Ω, v_R, and H for a subsonic disk solution corresponding to $X = 0.1$, $\alpha = 0.0001$, $R_{\rm out} = 100$, $j = 1.0110$, and $\Omega_* = 0$. Note the broad similarity to the supersonic solution of Fig. 5.1, except that this solution does not have a sonic point or shock, and there are no discontinuities in the quantities or their derivatives. The dashed line shows H vs. R for a uniformly-rotating star in a point-mass potential with the same Ω_*.

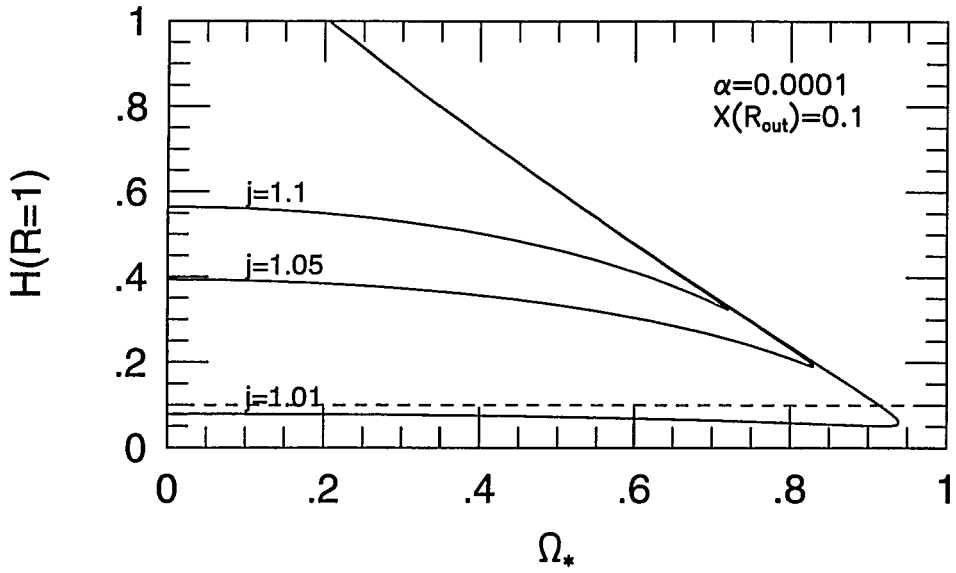

Fig. 5.8—Similar to Fig. 5.4, but for $X = 0.1$, $\alpha = 0.0001$, $R_{\rm out} = 100$. All the branches here are subsonic, in contrast to the case in Fig. 5.4, and the sharp cusps of Fig. 5.4 are rounded off here.

solutions for a wide range of Ω_*. To test this further, we have repeated our calculations for the parameter values, $X = 0.1$, $\alpha = 0.0001$, which satisfy the constraint in equation (19). For these parameters, we do find subsonic solutions for all Ω_*, as expected. Figure 5.7 shows the profiles of Ω, v_R and H of the solution corresponding to $\Omega_* = 0$. This solution looks rather similar to the supersonic solution of Figure 5.1, except that it is entirely subsonic. A plot of H/R vs Ω_* for various j is shown in Figure 5.8. Again, rather surprisingly, this looks quite similar to Figure 5.4, except that whereas there is a true cusp connecting the two branches in Figure 5.4, there is a rounded transition in Figure 5.8. The similarity between Figures 5.4 and 5.8 means that the mapping between j and Ω_* in the present case will be very

similar to the behavior shown in Figure 5.5. We thus conclude that the main results of this paper are valid for quite a wide range of the disk thickness parameter X and viscosity parameter α. The occurrence of supersonic solutions for astronomically relevant ranges of X and α is quite interesting, but is not crucial to the argument.

5.4 Discussion

The main result of this paper is that we have found a branch of accretion disk solutions that transfer little, no, or even negative amounts of, angular momentum to the accreting star. These fully subsonic disk configurations (e.g. Figures 5.2, 5.6) are available whenever the star spins at a rate near its "break-up" rate, $\Omega_{\rm max}$. Thus, by selecting the solution with the appropriate j, a rapidly-rotating star can continue to accrete without spinning up any further. The star thus achieves an "equilibrium" spin rate, $(\Omega_*)_{\rm max}$. This is possible even in the extreme case of an accreting massive white dwarf, which has to *lose* angular momentum in order to accrete mass.

We have not been able to calculate precisely the ratio of the maximum or "equilibrium" spin rate, $(\Omega_*)_{\rm max}$, to the "break-up" spin rate, $\Omega_{\rm max}$. This question is discussed in sect. 5.3.3. The problem is that $\Omega_{\rm max}$ can be estimated only if the outer edge of the star can be identified, and we have been unable to do this in a unique way. For most of the calculations, we have defined the edge of the star to be the point at which the vertical half-thickness of the fluid is a tenth of the radius. This arbitrary choice is quite adequate for most of the purposes of this paper, but it fails to provide an estimate of $\Omega_{\rm max}$. Using a polytropic stellar model

to define $\Omega_{\rm max}$, it could be argued that the "equilibrium" spin rate $(\Omega_*)_{\rm max}$ *exceeds* break-up. Of course, the star is saved from actually breaking up because it rotates differentially on the outside, where it merges with the disk. In the discussion below we ignore the question of whether $(\Omega_*)_{\rm max}$ is greater or less than $\Omega_{\rm max}$, and refer to the branch of solutions under discussion as merely being "near" break-up.

The wide range of j allowed in the solutions near break-up may seem paradoxical, but is actually easily understood. As shown by equation (9), at any R in the disk there is angular momentum flow in opposite directions due to different causes. Angular momentum is advected inwards by the accreting fluid, but at the same time angular momentum is also moved outwards by shear stresses. The net flow, $\dot{J} = j\dot{M}$, is the difference of these two quantities, and can, in principle, have either sign and a range of magnitudes. There is a constraint, however, if the central star is rotating slowly. In that case, $\Omega(R)$ must reach a maximum somewhere close to the stellar surface, so that $d\Omega/dR = 0$, and the shear stress vanishes (see Figures 5.1 and 5.7). Consequently, $\dot{J}$ is directly equal to the advected angular momentum at this radius and is constrained to be positive. Indeed, since the transition zone (the boundary layer) is usually narrow and occurs just outside the stellar surface, the value of j is constrained to have a value $\sim$1 (in our units). In contrast, the solutions that match on to a rapidly rotating star are very different. Here, $d\Omega/dR < 0$ at all R and so there is an outward shear-induced flow of angular momentum at every point. By adjusting $\Sigma(R)$ (or equivalently $v_R(R)$ through equation [3]), the outward angular momentum flow can be made larger or smaller than the advected flow, and so there is no constraint on either the magnitude or sign of $\dot{J}$.

An important feature of the solutions near break-up is that there is a smooth transition from a near-Keplerian thin disk to the rapidly-rotating star. Consequently, there is no separate entity such as a "boundary layer" separating the two; in particular, there is no component of additional luminosity from the boundary layer. It has been a long-standing problem that most cataclysmic variables show no evidence for the strong x-ray emission expected from the boundary layer (e.g. Ferland *et al.* 1982). It is tempting to speculate that most of these systems may be spinning near break-up and therefore no longer have distinct boundary layers.

In an earlier paper (Narayan & Popham 1989, Chapter 4) we had argued against the accretion-induced-collapse (AIC) scenario for the formation of binary neutron stars, on the grounds that a white dwarf that has been spun up close to break-up will be unable to accrete any further. As we have shown in the present paper, this argument is false, and AIC is not limited by any barrier due to angular momentum. Also, although the winds and outflows produced by protostars may arise in the boundary-layer region, there is no necessity for such winds because of any barrier to accretion, as proposed by Shu *et al.* (1988).

The second branch of solutions that we have discovered corresponds to slowly-rotating stars, with Ω_* ranging from zero to a little below break-up. These solutions agree more closely with the standard picture of thin accretion disks (see Figures 5.1 and 5.7). They have a narrow transition zone just outside the star where $\Omega(R)$ falls rapidly from nearly Keplerian to nearly the stellar rate Ω_*. A substantial fraction of the total luminosity of the system is produced in this boundary layer. In these solutions, the specific angular momentum accreted by the star corresponds

to $j \sim 1$, as in the standard picture, and this value is only weakly dependent on Ω_* (see Figure 5.5).

An interesting feature of this branch of solutions is that the flow may or may not become supersonic close to the star, depending on the parameters of the disk. If the inequality of equation (19) is satisfied, the flow remains entirely subsonic, but if it is violated the flow must become supersonic at least for some range of Ω_*.

Standard disk parameters corresponding to cataclysmic variables, viz. relative disk thickness $X \sim 0.01$, viscosity parameter $\alpha \sim 0.1$, violate the condition (19) by a large factor and so supersonic flow is indicated in these systems. We note that Kley (1989) also obtained supersonic flow in a two-dimensional calculation of a boundary layer including radiation processes. Rather surprisingly, the character of the mapping between j and Ω_* does not seem to depend on whether the flow is subsonic or supersonic (see sect. 5.3.4). In those cases where there is supersonic flow, there is also a radial shock where most of the kinetic energy of free-fall is thermalized. The existence of this shock may possibly be identified observationally, thus providing a diagnostic to distinguish between subsonic and supersonic boundary layers.

We must mention, however, a potentially serious problem with the supersonic solutions. Since the supersonic zone between R_s and R_{sh} in these solutions acts like an isolating element between the star and the disk, no sound waves can travel back to the disk across the supersonic zone to convey information about the accreting star, and one wonders how the disk will know what j to choose in order to match the inner boundary condition. A resolution of this question is beyond the scope of the present analysis. However, we note that, within the assumptions of our analysis, and for reasonable choices of X and α and a wide range of stellar rotation rates

Ω_*, the supersonic solutions are the only ones that are allowed — there just are no other solutions that can match all the boundary conditions.

As we saw in sect. 5.3.4, the supersonic solutions can be avoided by reducing α significantly and using a large value of X. We do not consider this alternative particularly attractive since our choice of these parameters is quite reasonable according to standard disk models (though Papaloizou & Stanley [1986] make the plausible argument that the boundary layer is likely to have a much smaller effective α than the rest of the disk.) Another possibility is that the disk may violate either the steady-state or axisymmetric assumptions. It is conceivable that a time-variable or non-axisymmetric (e.g. spiral shocks, cf. Spruit 1987) solution may contrive to match the boundary conditions while at the same time remaining radially subsonic. Any such solution will, in a time/azimuthally-averaged sense, probably be similar to our supersonic solutions.

It seems likely that the spectra of accretion disks around rapidly-rotating stars, particularly disks with negative j, will be different from the spectra of standard models of thin disks. In order to calculate realistic spectra for comparison with observations one should solve a more complete set of equations than we have done here, including an energy equation and radiative transfer. We are currently working on this.

6. SUPERSONIC INFALL AND CAUSALITY IN ACCRETION DISK BOUNDARY LAYERS

Abstract

Previous studies of accretion disk boundary layers have indicated the presence of supersonic radial inflows. Such flows are troubling since they would presumably break causal contact between the accreting central star and the disk, thus calling into question the physical self-consistency of the solutions. We identify certain non-physical aspects of the standard α-viscosity prescription as the cause of this paradoxical behavior. We attempt to come up with a more physically realistic description of viscosity by making modifications to the α-prescription, and check to see whether these modifications eliminate the non-causal behavior. We first modify the viscosity coefficient to account for the reduced radial pressure scale height in the boundary layer. This reduces the radial velocities but, as noted by previous workers, does not eliminate supersonic infall for large values of α. We then include a second factor to allow for the fact that the viscosity coefficient must vanish when the steady-state radial velocity of the flow reaches the maximum speed of the diffusive particles (in this case, turbulent fluid blobs) that produce the viscosity. When this modification is used, we find causally connected, physically self-consistent solutions for all choices of parameters. We thus conclude that information flow between the star and the disk can be maintained in all accreting systems in steady-state.

6.1 Introduction

The boundary layer, where an accretion disk meets the central accreting object, is important to observations of accreting systems, since up to half the accretion luminosity can be released there. This vital region presents a substantial challenge to modelers of accretion flows, since the standard approximations used in the disk break down. The angular velocity Ω generally reaches its peak value in the boundary layer, and subsequently drops from a near-Keplerian value to match the stellar angular velocity Ω_*. In the process, pressure gradient replaces centrifugal force as the primary means of radial support for the accreting material. The radial velocity also generally reaches its maximum value in this region, making it the most likely location for the occurrence of supersonic radial infall.

The question of whether the radial velocities will be supersonic in the boundary layer has been the subject of some discussion. Pringle (1977) argued on physical grounds that a supersonic region cannot exist because information from the central star will not be able to cross such a region and reach the disk. Such information transfer is vital for the self-consistency of accretion disk flows since the amount of angular momentum that a steady-state disk transfers inwards depends on the properties of the central star (Pringle 1981, Popham & Narayan 1991). It is difficult to understand how a disk will be able to select the appropriate amount of angular momentum to transfer without any feedback from the star.

Despite Pringle's persuasive argument, several numerical studies of the boundary layer have found that supersonic flows can occur, particularly when the viscosity coefficient is large enough. Papaloizou & Stanley (1986) modeled the boundary layer using a simple polytropic equation of state and reduced the viscosity coefficient by

modifying the standard α-prescription of Shakura & Sunyaev (1973) to include the influence of the radial pressure gradient. Despite this modification, they found that supersonic radial infall still occurred in some of their models. Kley (1989) constructed a more sophisticated two-dimensional model and included radiative transfer, but used a fairly large constant value for the viscosity coefficient. He too found radial velocities in excess of the sound speed.

In our previous paper (Popham & Narayan 1991, Chapter 5), we constructed a simple model which treated the disk, boundary layer and star as a single two-dimensional fluid system governed by a polytropic equation of state. We used the standard α-viscosity prescription with $\alpha = 0.1$, and found solutions which attained supersonic radial velocities in the boundary layer. From an analysis of the flow equations, we derived an approximate condition which showed that either a very small value of α or a large relative disk thickness was required for subsonic radial infall. Disk models which satisfied this condition were indeed fully subsonic; however, for normal thin disk parameters, the value of α required, $\alpha \sim 10^{-4}$, was unacceptably small. Paczyński (1991) used a model similar to that in Chapter 5, but assumed subsonic radial flow by making an effective hydrostatic approximation. He found that this assumption would be violated for some of his solutions unless α was very small.

All of these results suggest that we may be missing some important ingredient in our understanding of accretion disks. Pringle's argument is simple and compelling, and yet most efforts to model the boundary layer have resulted in solutions which violate his consistency requirement. The purpose of this paper is to resolve this paradoxical situation.

We begin by making an important qualitative point. A steady-state axisymmetric thin disk has motions that are essentially two-dimensional and therefore has two components to the equation of motion. The pressure gradient contributes to the radial equation and therefore this equation is strongly influenced by sound waves. On the other hand, the azimuthal, or tangential, equation of motion is dominated by viscosity, which is a diffusive process. The viscous transport of angular momentum is usually modeled through the standard diffusion equation, which implicitly propagates information at infinite speed (cf. Narayan 1992 for a discussion of this point). Therefore, even when the radial flow is supersonic in the boundary layer, the tangential motions in the disk could still be coupled to the star through the viscous interaction. One could thus circumvent Pringle's consistency condition by saying that there is viscous communication even across supersonic regions, so that the supersonic solutions are formally self-consistent.

This, however, is a very unsatisfactory resolution of the paradox because it depends on an unphysical feature in the mathematical modeling of viscous transport. In real fluids, particularly those with turbulent diffusion, transport is mediated by blobs of fluid, and it is likely that diffusive information transfer will be limited to some speed comparable to the sound speed. In such a situation, will an accreting star be able to maintain causal contact with the surrounding disk? The calculations we report here provide an answer to this question.

In the following sections, we attempt to describe the viscosity in a more realistic way by making two modifications to the α-viscosity prescription. We then perform calculations using the model of Chapter 5 to examine the effects of these modifications on the radial velocity in the boundary layer. First, we introduce a

prescription similar to the one used by Papaloizou & Stanley (1986) to account for the reduced mean free path in regions where the pressure scale height in the radial direction is substantially smaller than that in the vertical direction. We confirm Papaloizou and Stanley's result that this modification alone cannot eliminate supersonic flows under all conditions. Next, we invoke the concept of a causally limited viscosity as described by Narayan (1992). This involves introducing a factor which reduces the viscosity coefficient as the radial velocity approaches the maximum speed of the diffusive particles. With this change, we find causally connected solutions for all reasonable choices of parameters, thus resolving the paradox.

The remainder of the paper is divided into three sections. Section 6.2 summarizes our simple disk model and discusses the modifications to the viscosity prescription. Section 6.3 presents the results of our calculations and illustrates the effects of the modifications discussed in sect. 6.2. Section 6.4 discusses the implications of the results and possible improvements to the model.

6.2 Theory

6.2.1 *The Role of Viscosity*

Standard theory (Shakura & Sunyaev 1973, Pringle 1981) shows that the outward appearance of an accretion disk does not depend strongly on the magnitude of the viscosity coefficient ν. As long as ν is large enough to prevent the self-gravity of the disk from becoming important, the surface density Σ of the disk will adjust itself to provide the appropriate mass accretion rate $\dot{M}$, so that the energy dissipated per unit area will be independent of viscosity.

Viscosity plays a more important role in models of accretion disks. Assuming a steady-state disk, the rate of angular momentum flow $\dot{J}$ through any radius R in the disk is given by

$$\dot{J} = \dot{M}\Omega R^2 + 2\pi R^2 \nu \Sigma R \frac{d\Omega}{dR}, \tag{1}$$

where Ω is the angular velocity of the fluid. Equation (1) can be rearranged to give

$$\frac{d\Omega}{dR} = \frac{v_R}{\nu}\left(\Omega - \frac{j}{R^2}\right), \tag{2}$$

where we have used $\dot{M} = -2\pi R v_R \Sigma$, so that the radial velocity v_R is negative for accretion, and have defined $j = \dot{J}/\dot{M}$. In the boundary layer, we expect $d\Omega/dR$ to be large, so that a large value of ν will require a large value of v_R.

To know whether the radial velocity becomes supersonic in the boundary layer, we must examine the radial equation of motion,

$$v_R \frac{dv_R}{dR} = (\Omega^2 - \Omega_K^2)R - \frac{1}{\Sigma}\frac{dP}{dR}, \tag{3}$$

where $\Omega_K = (GM/R^3)^{1/2}$ is the Keplerian angular frequency. We use units in which the radius of the star, R_*, is the unit of length and $\Omega_K(R_*)$ is the unit of frequency. Using a polytropic equation of state, $P = K\Sigma^\gamma$, for the height-integrated pressure and defining the sound speed c_s by the relation $c_s^2 = dP/d\Sigma$, we can rewrite (3) in the form

$$\frac{dv_R}{dR} = \frac{v_R[(\Omega_K^2 - \Omega^2)R^2 - c_s^2]}{R(c_s^2 - v_R^2)}. \tag{4}$$

Equations (2) and (4) are identical to those used in Chapter 5, which also gives more details about the disk model. Combining the two equations, we find

$$\frac{dv_R}{d\Omega} = \frac{\nu[(\Omega_K^2 - \Omega^2)R^2 - c_s^2]}{R(c_s^2 - v_R^2)(\Omega - j/R^2)}. \tag{5}$$

For a slowly rotating star, Ω drops from $\Omega_K(R_*)$ to ~ 0 in the boundary layer. From (5) we see that the corresponding change in v_R is proportional to ν. Hence, if ν is large enough, the flow is bound to become supersonic.

6.2.2 *Viscosity Prescriptions*

6.2.2.1 *Alpha Viscosity*

Viscosity is fundamentally a diffusive process which redistributes transverse momentum in a shearing medium, or angular momentum in a differentially rotating flow. The viscosity coefficient ν serves as the diffusion constant, and is given by the product of the velocity and the mean free path of the diffusing elements. The viscosity coefficient in accretion disks is generally taken to be $\nu = \alpha c_s H$, where $H \sim c_s/\Omega_K$ is the vertical pressure scale height. This assumes that the diffusion is produced by turbulence in the disk, so the diffusing elements are turbulent blobs of fluid.. The turbulent velocity is taken to be less than or approximately equal to the sound speed c_s, since it is generally assumed that any supersonic motions will quickly be slowed by shocks. The mean free path for turbulent motions is taken to be less than or equal to the vertical pressure scale height H, since this is probably the maximum size of a turbulent eddy in the disk. The factor α simply allows us to combine our uncertainties into a single number.

6.2.2.2 *Viscosity Incorporating Radial Pressure Scale Height*

Like several of the other assumptions used in accretion disk theory, the assumption that the mean free path for turbulence is limited only by the vertical pressure scale height of the disk breaks down in the boundary layer region. Rather,

one would expect that the length scale for turbulence in the radial direction would be given by the radial pressure scale height, which becomes smaller than the vertical pressure scale height as the flow makes the transition from centrifugal to pressure support. This was noted by Papaloizou & Stanley (1986), who used a viscosity coefficient given by

$$\nu = \frac{\alpha c_s}{1/H + 1/H_p}, \tag{6}$$

where H_p is the radial pressure scale height. This prescription essentially allows ν to be determined by the smaller of H and H_p, yielding values of ν which are close to those given by the usual α-prescription in the disk, but are substantially reduced in the boundary layer due to the small radial pressure scale height. We adopt this basic form for the viscosity coefficient, but write the radial pressure scale height as

$$H_p = \frac{P}{|dP/dR|} = \left|\gamma\left(\frac{1}{R} + \frac{1}{v_R}\frac{dv_R}{dR}\right)\right|^{-1}, \tag{7}$$

which differs slightly from the expression used by Papaloizou & Stanley (1986). This yields a viscosity coefficient

$$\nu = \frac{\alpha c_s}{\frac{\Omega_K}{c_s} + \left|\gamma\left(\frac{1}{R} + \frac{[(\Omega_K^2-\Omega^2)R^2-c_s^2]}{R(c_s^2-v_R^2)}\right)\right|} = \frac{\alpha c_s^2}{\Omega_K + \left|\gamma\frac{c_s[(\Omega_K^2-\Omega^2)R^2-v_R^2]}{R(c_s^2-v_R^2)}\right|}. \tag{8}$$

6.2.2.3 *Causally Limited Viscosity*

The turbulent diffusive motions assumed to be occurring in accretion disks are presumably limited to some maximum velocity v_t which is expected to be $\sim c_s$. Diffusive motions in the radial direction redistribute angular momentum, but it is important to remember that at the same time the disk material is also flowing inward with a velocity v_R. For a small flow velocity $v_R \ll v_t$ one expects that the

bulk flow does not affect the efficiency of diffusion. However, if the flow reaches a velocity approaching v_t, diffusion in the upstream direction ought to be suppressed, shutting off completely for $v_R > v_t$. Thus one would expect the viscosity coefficient ν to depend on v_R and to vanish if v_R exceeds the turbulent velocity v_t. Narayan (1992) has developed a model for viscosity in the presence of bulk flows, using an approach analogous to the flux-limited diffusion theory of Levermore & Pomraning (1981). The basic result of this analysis is that the viscosity coefficient is reduced by a factor given approximately by $(1 - v_R^2/v_t^2)^n$, where n is an integer whose value depends on what one assumes for the scattering properties of the diffusive elements. For reasonable assumptions, one obtains $n = 2$ (see Narayan 1992), which we adopt in this paper. Let us write the maximum turbulent velocity as $v_t = \beta c_s$, where we expect β to be of order unity. This yields a modified viscosity coefficient

$$\nu = \frac{\alpha c_s^2}{\Omega_K}\left(1 - \frac{v_R^2}{\beta^2 c_s^2}\right)^2. \tag{9}$$

Combining this prescription with the radial pressure scale height prescription in equation (8) gives

$$\nu = \frac{\alpha c_s^2 (1 - v_R^2/\beta^2 c_s^2)^2}{\Omega_K + \left|\gamma \frac{c_s[(\Omega_K^2 - \Omega^2)R^2 - v_R^2]}{R(c_s^2 - v_R^2)}\right|}. \tag{10}$$

6.3 Results

6.3.1 *Calculations*

The calculation method is similar to that used in Chapter 5. We numerically solved equations (2) and (4) using a relaxation method and a polytropic index $\gamma = 2$. The outer edge of the disk was fixed at 100 stellar radii; the ratio of the sound speed to the Keplerian velocity at the outer edge was taken to be 0.01, and the angular velocity at the outer edge was assumed to be Keplerian. At the inner edge, we defined $R = 1$ as the radius where the disk height reaches $0.1R$. We also specified that the angular velocity at $R = 1$ equals the stellar angular velocity Ω_*. Chapter 5 gives more details about how the boundary conditions were set.

6.3.2 *Alpha-Viscosity*

As Chapter 5 demonstrated, disk solutions using alpha-viscosity and $\alpha = 0.1$ have a supersonic boundary layer unless the star is rotating near breakup speed. Solution a in Figure 6.1 shows such a solution for the case where the star is rotating quite slowly. The flow reaches a large Mach number before being slowed by a radial standing shock and settling onto the star. The angular velocity drops rapidly as the flow accelerates and is continuous across the shock. It drops much more slowly in the post-shock region, however, since the viscosity rises rapidly with the increasing sound speed and height of the disk.

Solution a in Figure 6.1 is an example of a case where the inner boundary conditions are apparently communicated to the outer disk despite the presence of an intervening supersonic zone. This communication is seen explicitly through the

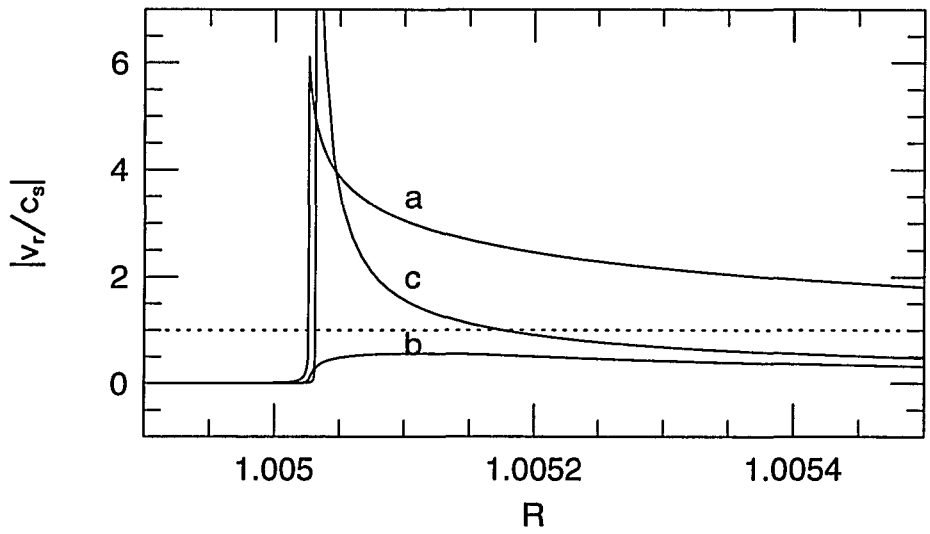

Fig. 6.1—The Mach number, $|v_R/c_s|$, in the boundary layer region for two different forms of the viscosity coefficient ν. Solution a uses the standard α-viscosity prescription $\nu = \alpha c_s H$ with $\alpha = 0.1$. The Mach number rises to about 15 before the infalling matter encounters a shock and settles onto the star. Solutions b and c use a modified viscosity coefficient (eq. 8) based on the reduced radial pressure scale height in the boundary layer; Solution b has $\alpha = 0.1$, and Solution c has $\alpha = 1$. Solution b remains subsonic, but Solution c becomes supersonic and achieves a Mach number of about 6 before reaching a shock. All three solutions correspond to a slowly rotating star; the angular velocity Ω drops rapidly from ~ 1 to ~ 0 in the boundary layer.

presence of the global eigenvalue j, or equivalently the global angular momentum flux $\dot{J}$, in the solution. The accretion disk transfers the exact amount of angular momentum appropriate to the boundary conditions; in other words, it selects the value of $\dot{J}$ which permits it to match the radius R_* and rotation rate Ω_* of the star. If R_* or Ω_* changes, the disk will presumably find a new value of $\dot{J}$ to match the new boundary conditions. How is this possible if there is a supersonic zone isolating the disk from the star? This is the basic paradox we are attempting to resolve.

6.3.3 *Viscosity Modified by the Reduction in Radial Pressure Scale Height*

The radial pressure scale height becomes small when the angular velocity drops substantially below Keplerian. We have computed solutions using a viscosity coefficient of the form given in equation (8), i.e. taking account of the reduction in radial pressure scale height but not including any causal limiting factor. Solution b of Figure 6.1 shows such a solution for $\alpha = 0.1$ and a slowly rotating star. The viscosity coefficient drops substantially below the value derived from the normal alpha-prescription; in fact, this reduction is sufficient to prevent the flow from exceeding the sound speed. Unfortunately, this modification is not sufficient to prevent supersonic flows for all reasonable values of α. Solution c of Figure 6.1 uses this same form of the viscosity, again for a slowly rotating star, but with $\alpha = 1$. The flow now becomes supersonic, and we are once again left with the original problem of how the inner boundary conditions can be communicated to the disk.

6.3.4 *Causally-Limited Viscosity*

We next include the effect of causality in the viscosity prescription by calculating disk solutions using the viscosity coefficient given in equation (10). We note that there are now two critical velocities in the problem: c_s, which represents the speed at which pressure fluctuations are transmitted, and v_t, which measures the maximum speed for the turbulent motions which transport angular momentum. In order to clearly demonstrate the role of these two velocities, we have carried out calculations for two separate cases, one with $v_t < c_s$ and the other with $v_t > c_s$.

Solution a of Figure 6.2 shows the boundary layer around a slowly rotating star, using the causally limited viscosity coefficient with $\alpha = 1$ and $v_t = 0.8c_s$. As

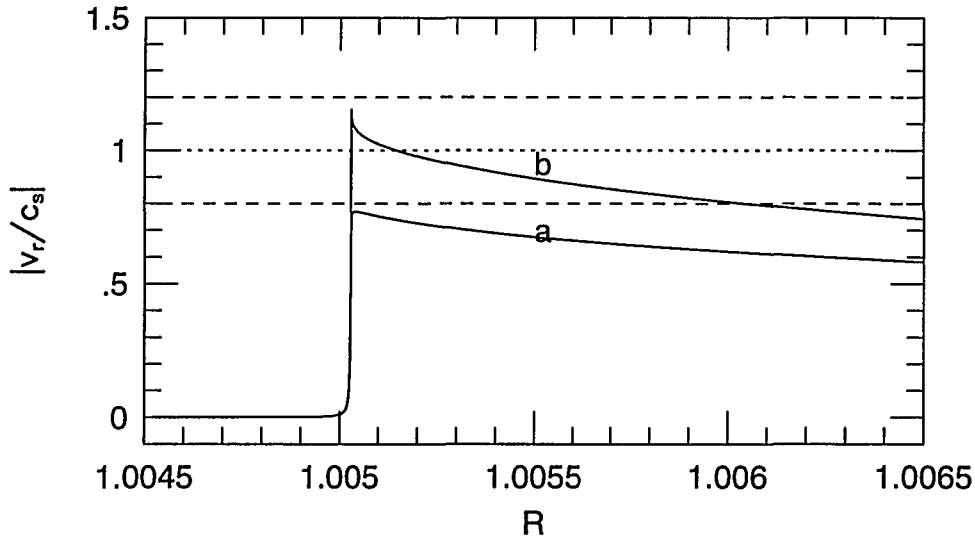

Fig. 6.2—The Mach number in the boundary layer region for disk solutions using a causally limited viscosity prescription (eq. 10). Solution a sets the maximum velocity of turbulent motions $v_t = 0.8c_s$, while Solution b uses $v_t = 1.2c_s$. Solution b briefly becomes supersonic, but neither solution ever has radial velocity in excess of v_t, so the star and disk are in causal contact in both solutions. Like the solutions shown in Fig. 6.1, these solutions correspond to a slowly rotating star.

the flow velocity v_R approaches the maximum turbulent velocity v_t, the viscosity coefficient drops dramatically, as seen in Figure 6.3. This in turn allows the angular velocity to drop very rapidly down to match the slowly rotating star. The flow velocity never exceeds the maximum turbulent velocity, and, because $v_t < c_s$, the flow remains fully subsonic. This is a case where the star is clearly in complete communication with the disk.

As a second example, we examine the effect of setting the maximum velocity of turbulent motion to be $v_t = 1.2c_s$. In this case, again using $\alpha = 1$ and a slowly rotating star, we obtain Solution b shown in Figure 6.2. Figure 6.3 shows

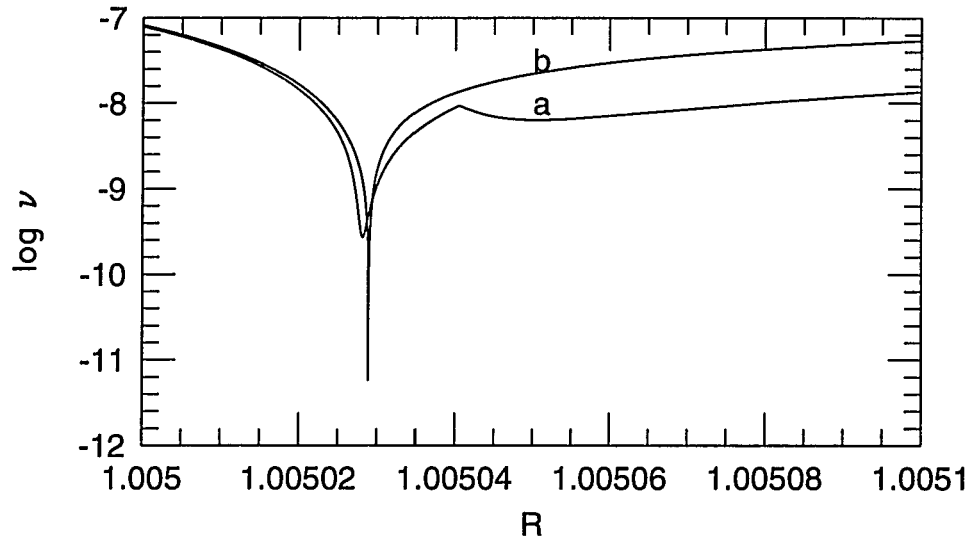

Fig. 6.3—The viscosity coefficient ν in the boundary layer region for the solutions shown in Fig. 6.2. The viscosity coefficient drops dramatically in the boundary layer in both solutions as the radial pressure scale height drops and the radial velocity approaches the maximum velocity of turbulent motions v_t. The local maximum in the viscosity coefficient for Solution a at $R = 1.00504$ corresponds to the point where the radial velocity reaches its maximum value. This results in a relatively large radial pressure scale height since the velocity gradient is zero at that point (cf. eq. 7).

that the viscosity drops to a very small value as the radial velocity approaches v_t. Although the solution does have a supersonic zone, nonetheless v_R never exceeds v_t. This is therefore a very interesting case where the star is in *partial* contact with the disk. There is viscous communication which enables the disk to select the value of $\dot{J}$ appropriate to the stellar boundary conditions. However, there is no pressure communication because of the supersonic zone, resulting in a shock where the infalling supersonic material hits the star.

6.3.5 *The j vs. Ω_* Relation*

Chapter 5 showed that the value of $j = \dot{J}/\dot{M}$ required to match the stellar boundary conditions is fairly insensitive to the stellar rotation rate Ω_* as long as Ω_* is less than the breakup rotation rate. However, once the star is at breakup, j becomes very sensitive to Ω_*, dropping rapidly as Ω_* increases. Similar results were found by Paczyński (1991). The solutions in Figures 6.1-6.3 correspond to a slowly rotating star, since these are the solutions which attain the largest radial velocities. For each form of the viscosity we have also performed calculations for a range of values of Ω_* in order to see whether the form of the j *vs.* Ω_* relation changes in any substantial way when modifications are made to the viscosity prescription. We find that the basic form of the relation is essentially unchanged, and the actual numerical values of j vary only slightly as the viscosity prescription changes.

Figure 6.4 shows the j *vs.* Ω_* curve for a series of solutions calculated using the viscosity of equation (10) with $v_t = 0.8c_s$, which includes Solution a in Figure 6.2. The basic form of the curve is identical, with j increasing slowly from about 1.003 to 1.03 as Ω_* increases from zero to about the breakup value, then falling very rapidly as Ω_* is increased farther. The j values do appear to be slightly smaller here than they were for the case calculated in Chapter 5; this is probably a result of the change in α rather than the change in the form of the viscosity. This weak dependence on α can also be seen in Figure 5.7, where for $\alpha = 10^{-4}$ we found $j = 1.011$ for $\Omega_* = 0$.

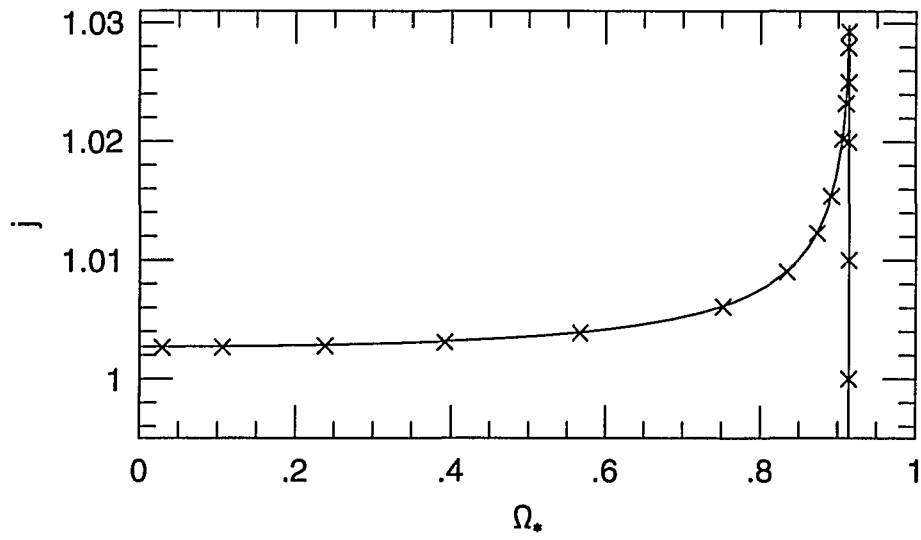

Fig. 6.4—The angular momentum per unit mass accreted by the central star, j, as a function of the stellar rotation rate Ω_*. The solid line is the $j(\Omega_*)$ relation from Chapter 5 (Fig. 5.5). The points correspond to values of $j(\Omega_*)$ calculated for a series of solutions using causally limited viscosity with $v_t = 0.8c_s$. Solution a of Fig. 6.2 corresponds to the point at $j = 1.0026, \Omega_* \simeq 0.03$.

6.4 Discussion

The basic conclusion of this paper is that the problem of having apparently non-causal radial velocities in the boundary layer region can be overcome by making simple, physically justifiable modifications to the alpha viscosity prescription. The required modifications fit naturally into the framework of diffusive transport of angular momentum by turbulent motions. It seems clear that the α-prescription substantially overestimates the value of the viscosity coefficient in the boundary layer region, both by assuming that there is no limit to the speed at which viscous angular momentum transport can occur, and by using the vertical pressure scale

height of the disk to represent the radial mean free path. Our modified viscosity prescription corrects these problems by imposing a reasonable limit on the velocity of viscous transport, and by including the radial pressure scale height in estimating the mean free path of turbulent motions. These modifications serve to generalize the basic α-prescription to make it applicable over a wider range of physical conditions, including those in the boundary-layer region, where the unmodified α-prescription produces unphysical behavior.

Radial velocities in disk solutions found using this modified viscosity never exceed the maximum velocity of the diffusive elements which transfer angular momentum. Thus the disk remains in viscous communication with the star whether or not the radial velocity becomes supersonic, as demonstrated by Solutions a and b shown in Figure 6.2. This result validates the assumption that a global eigenvalue j can exist for the whole fluid system. The disk is always causally connected to the star and should be able to match changes in the stellar radius R_* and the stellar rotation rate Ω_* by adjusting the angular momentum accretion rate $\dot{J}$. Such changes are an inevitable result of the accretion process, due to the addition of mass and angular momentum to the central accreting object. Thus one might expect the time evolution of an accreting system essentially to follow a series of steady-state solutions in which changes in the stellar boundary conditions reflect variations in the mass, radius, and rotation rate of the central star. Of course, the existence of such a series of solutions does not ensure that the evolution of the system will necessarily follow this course, but the fact that the present solutions allow the star to communicate with the disk makes it a viable scenario.

The results obtained in this paper lead to a generalization of the usual picture of information transfer in moving fluids. In a steady, one-dimensional flow, sound waves transmit information both upstream and downstream. However, if the flow velocity exceeds the sound speed, sound waves which travel upstream in the frame of the fluid are moving downstream in the observer's frame. This leads to the standard conclusion that sound waves cannot transfer information in the upstream direction against a supersonic flow. Since the fluid is unaware of anything lying downstream, the supersonic zone is terminated by a shock when the flow encounters any kind of a barrier, such as a slower-moving region of fluid.

When we consider a two-dimensional shearing flow like that in the boundary layer, the situation is slightly more complicated. Now there are two kinds of motions, and each has its own mode of coupling to the fluid. Longitudinal motions are coupled by sound waves, so for them communication is still limited by the sound speed c_s. However, transverse motions interact through viscosity, and viscous communication could in principle be limited by a different speed, which we have called v_t. The longitudinal flow velocity, which corresponds to the radial velocity v_R in an accretion disk, may be less than both v_t and c_s, in which case there will be full communication between the disk and the star. If v_R exceeds one of the two limiting velocities but not the other, there will still be partial communication, but if it exceeds both, communication will be cut off completely.

In the case of the accretion disk boundary layer, we have shown in this paper that the flow velocity v_R always stays below the viscous limiting speed v_t. This is exactly what we need to resolve the paradox we started with. We recall that the paradox had to do with the fact that the disk needs to be told how much angular

momentum the star is willing to accept. Since angular momentum is associated with the transverse degree of freedom of the fluid, this information is transmitted through viscosity, and therefore communication can be maintained so long as v_R does not exceed v_t. A shock can still be present if v_R exceeds c_s. The key point is that even when there is a shock, there is only partial blockage of information flow since the viscous coupling continues to operate in the upstream direction.

Another result of this work is that the j *vs.* Ω_* relation, i.e. the mapping between the specific angular momentum added to the star and the stellar rotation rate, is essentially independent of the form of the viscosity. This means that the time evolution of an accreting star should follow the course outlined in Chapter 5. An initially non-rotating star will be spun up by accretion, with $\dot{J} \sim \dot{M}\Omega_K(R_*)R_*^2$, until Ω_* reaches the nominal breakup value. Past this point j falls rapidly with increasing Ω_*, so the system finds an equilibrium value of Ω_* which will permit further accretion without spin-up. This final state will be a stable situation; if the star spins faster, j decreases and the star is spun down and vice versa. The equilibrium value of Ω_* will be the one which corresponds to $j \sim 0$ if the moment of inertia of the star is not sensitive to the mass added by accretion; however, for a white dwarf near the Chandrasekhar limit, adding mass decreases the moment of inertia, and negative values of j will be required.

We should, however, point out some weaknesses of the model used to derive our results. We neglect bulk viscosity and the accompanying radial viscous force in our calculations. The radial acceleration due to this term should be of order $\nu d^2 v_R/dR^2$, so one would expect it to be most important in the boundary layer region where the velocity gradients are large. On the other hand, the viscosity also

becomes small in this region according to the modifications we have made to the α-prescription. We have calculated the magnitude of the radial viscous term and compared it to the other terms in equation (3). We find that this term becomes comparable to the dominant terms only under the most extreme conditions, so we expect that the inclusion of bulk viscosity would have only a minor effect on the solutions.

Our model also makes the simplifying assumption that the disk is in a steady state. Without doing a time-dependent calculation, it is impossible to know whether or not the evolution of an accreting system will simply look like a series of steady-state solutions. In particular, the large gradients and small radial extent of the boundary layer suggest that it may be prone to instabilities. Such instabilities might provide a natural explanation for the time-variable "flicker" and quasi-periodic oscillations observed in accreting systems.

Finally, by using the polytropic assumption in place of an energy equation, we have ignored the difficulties of energy generation and radiative transfer. A more complete treatment would make it possible to generate spectra of the accretion disk and boundary layer as a single system rather than treating the boundary layer as a separate, independent component. It would also allow an examination of the dependence of the spectrum on the stellar rotation rate and on the presence of a supersonic zone and shock. We are currently working on such a model.

7. SELF-CONSISTENT ACCRETION DISKS AROUND BLACK HOLES

7.1 Introduction

Shakura & Sunyaev (1973, hereafter SS), in a classic paper, established the foundations of the theory of thin accretion disks. They introduced the now-standard α-prescription for the viscosity and found analytic solutions for disks around black holes. These solutions extend from the inner edge of the disk, near the black hole horizon, out to large radii, and have been the basis of numerous investigations of disks in a variety of astrophysical systems (e.g. Frank, King & Raine 1985).

The SS formulation of the basic disk equations involves several approximations, the most serious of which (for the purpose of this paper) is the neglect of pressure gradients and acceleration in the radial momentum equation. This simplification is reasonable in the outer regions of the disk, where a nearly perfect balance exists between gravity and centrifugal force. However, in the inner regions of the disk, especially in the vicinity of the sonic point, the approximations made by SS are no longer valid.

Starting with the early work of Paczyński & Bisnovatyi-Kogan (1981) and Muchotrzeb & Paczyński (1982), various authors have attempted to obtain self-consistent solutions of accretion disks around black holes using a more complete set of disk equations. However, these investigations have met with only limited success. Muchotrzeb & Paczyński (1982) found numerical solutions for very small values

of the α-parameter in the viscosity prescription, but were unable to find steady-state solutions for values of $\alpha > 0.03$ (Muchotrzeb 1983). This has led to several discussions on possible peculiarities in the nature of the sonic point (Matsumoto et al. 1984, Muchotrzeb-Czerny 1986, Abramowicz & Kato 1989), as well as to suggestions that disks with large values of α around black holes may have to be time-dependent (Muchotrzeb-Czerny 1986, Paczyński 1987).

In our view, the lack of self-consistent solutions of accretion disks around black holes for physically reasonable parameters represents a major gap in current disk theory. We wish to report some progress on this problem. We show that, with a modified form of α-viscosity which we introduced in an earlier study of disk boundary layers, we can find physically reasonable and self-consistent disk solutions for any value of α up to the maximum of $\alpha = 1$. We introduce the basic equations of a polytropic thin disk in sec. 7.2, introduce our modified viscosity prescription and describe our results in sec. 7.3, and conclude with a discussion in sec. 7.4.

7.2 The Basic Disk Equations

Following SS, we consider an axisymmetric time-independent vertically-averaged system, so that all quantities are functions only of the radius R. For a steady mass accretion rate $\dot{M}$, mass conservation gives

$$\dot{M} = -2\pi R v_R \Sigma, \tag{1}$$

where v_R is the radial velocity, taken to be negative for accretion, and Σ is the surface mass density.

As in an earlier work on the dynamics of disks (Popham & Narayan 1991), we simplify the problem by considering a polytropic fluid. The height-integrated pressure P and the sound speed c_s then satisfy

$$P = K\Sigma^\gamma, \quad c_s^2 = dP/d\Sigma = K\gamma\Sigma^{\gamma-1}, \tag{2}$$

where K and γ are constants. By using this equation of state, we avoid all the complications associated with energy generation and transport without sacrificing any of the physics associated with the hydrodynamics of the flow. As in our previous work, we set $\gamma = 2$, which gives the closest analogy to the standard disk equations of SS.

We model the gravitational influence of the black hole by means of the pseudo-Newtonian potential introduced by Paczyński & Wiita (1980),

$$\Phi_G(R) = -\frac{GM}{(R - R_g)}, \tag{3}$$

where M is the mass of the hole, and $R_g = 2GM/c^2$ is the radius of the event horizon. This potential mimics most of the important features of the Schwarzschild metric, without introducing any unphysical features. It would be straightforward to carry out the calculations with the full general relativistic dynamical equations, but we prefer to use (3) in order to facilitate comparison with previous work on this problem. We choose our units of length and time such that $GM = c = 1$.

The radial equation of motion of the disk is given by

$$v_R \frac{dv_R}{dR} - \Omega^2 R + \Omega_K^2 R + \frac{1}{\Sigma}\frac{dP}{dR} = 0, \tag{4}$$

where $\Omega(R)$ is the angular velocity of the fluid and $\Omega_K(R)$ is the local 'Keplerian' angular velocity, given by

$$\Omega_K(R) = \left(-\frac{1}{R}\frac{d\Phi_G}{dR}\right)^{1/2} = \frac{1}{R^{1/2}(R-R_g)}. \tag{5}$$

In steady state, the azimuthal component of the momentum equation gives

$$\dot{M}\Omega R^2 - 2\pi R^2 \tau_\phi(R) = \dot{M}j, \tag{6}$$

where j is a constant which represents the net inward flux of angular momentum per unit mass. The first term on the left describes the direct advection of angular momentum by the accretion flow, while the second gives the angular momentum flux due to viscous stresses. In the original SS formulation the viscous stress was written in terms of the pressure as

$$\tau_\phi(R) = \alpha P, \tag{7}$$

where α is a dimensionless constant, which is expected on physical grounds to satisfy $\alpha \lesssim 1$. The parameter α is designed to absorb all of the uncertainties in the nature of the viscosity. A somewhat improved form of this expression explicitly includes the dependence of the viscous stress on the angular velocity gradient,

$$\tau_\phi(R) = -\nu\Sigma R\frac{d\Omega}{dR}, \tag{8}$$

where the kinematic shear viscosity coefficient ν is again written in terms of an α parameter,

$$\nu = \alpha c_s^2/\Omega_K. \tag{9}$$

In the standard disk equations employed by SS, the two terms in eq. (4) which involve radial derivatives are neglected, so that $\Omega(R) = \Omega_K(R)$. The inner edge of the disk is assumed to be located at the marginally stable orbit at $R_{in} = 3R_g$, where the Keplerian angular momentum reaches a minimum. Assuming further that the viscous torque vanishes at $R = R_{in}$, eq. (6) provides the boundary condition $j = (\Omega R^2)_{R=R_{in}} = \Omega_K(R_{in})(R_{in})^2$. Once j is determined through this condition, eq. (6) can be solved for other quantities of interest such as $\Sigma(R), v_R(R)$, etc. Of course, the SS formulation also included equations to describe energy generation and transport which led to solutions for the temperature, radiation flux, etc. These additional variables do not figure in our polytropic version of disk theory.

7.3 Improved Dynamical Equations with Modified Viscosity

One major limitation of the SS theory is that it does not solve the full dynamical equations (4) and (6), but instead assumes $\Omega = \Omega_K$. The full dynamical equation allows the possibility of sonic transitions; in fact, in the case of black hole accretion, the fluid free-falls into the horizon, so we are guaranteed that all solutions will have a sonic point. We therefore identify the inner edge of the disk R_{in} with the sonic point, where two regularity conditions must be satisfied (cf. Popham & Narayan 1991), viz.

$$v_R = c_s, \quad \Omega_K^2 = \Omega^2 + c_s^2/R^2, \text{ at R} = \text{R}_{\text{in}}. \tag{10}$$

Another difficulty with the standard disk equations is that the formulation of viscosity through the shear stress (8) does not satisfy causality. This is a defect

which is common to all diffusion problems, but is usually not serious. However, it appears that in modeling viscous accretion disks, this unphysical feature of the model leads to unexpected and serious consequences.

In our previous work on boundary layers in accretion disks around regular stars we noticed certain paradoxical features in the solutions (Popham & Narayan 1991, 1992) which we finally traced to the non-causality of our viscosity model. Motivated by this, we proposed a modified form of the viscosity coefficient (9) of the form (Narayan 1992)

$$\begin{aligned} \nu &= \frac{\alpha c_s^2}{\Omega_K}\left[1-\left(\frac{v_R}{\beta c_s}\right)^2\right]^2, \quad v_R \le \beta c_s, \\ &= 0, \qquad\qquad\qquad\quad v_R > \beta c_s. \end{aligned} \tag{11}$$

where β is a constant ~ 1. The key feature of this formula is that it explicitly cuts off the viscous stress as soon as the radial velocity of the flow exceeds a critical speed equal to βc_s. This is the maximum speed of the particles which mediate viscous interactions, which limits the speed at which the influence of shear can propagate. The model is highly simplified and is valid only in steady state, but it does explicitly guarantee causality.

When the modified viscosity prescription given in eq. (11) was used in place of the standard α-prescription (eq. (9)) in the boundary layer problem, the paradoxical behavior disappeared completely (Popham & Narayan 1992), showing that the violation of causality was indeed at the root of our earlier difficulties. Because of this, we have used this modified viscosity in the present study of black hole disks. In general, it seems reasonable to select $\beta = 1$ and we do so in this paper.

In order to find a numerical solution, we have to solve two differential equations, eqs. (4) and (6), using the shear stress given by eqs. (8) and (11). At the same time, we also have to solve self-consistently for the two unknown parameters R_{in} and j. We thus need a total of four boundary conditions. Eq. (10) provides two boundary conditions at $R = R_{in}$. Another boundary condition is that $\Omega = \Omega_K$ at some outer radius R_{out} of the disk, which we usually take to be 100 R_{in}. The final boundary condition is a 'no-torque' condition at the point where the viscosity vanishes, which is the sonic point when $\beta = 1$. This gives

$$j = \Omega R^2, \qquad R = R_{in}, \tag{12}$$

which is essentially a regularity condition on the azimuthal equation (6). To apply this condition we integrate eqs. (4) and (6) from R_{in} inward to near R_g.

The solutions have an additional degree of freedom whereby, for each choice of α, there is a one-parameter family of polytropic solutions. These solutions are parametrized by a quantity X (see Popham & Narayan 1991), which measures the vertical height of the disk at some fiducial radius, usually R_{out}. X is a free parameter given by a particular combination of $\dot{M}$ and K. If we had included an energy equation instead of the polytropic equation of state, X would have been replaced by another parameter, $\dot{M}/\dot{M}_{crit}$, where $\dot{M}_{crit}$ is the critical value of $\dot{M}$ at which the luminosity is equal to the Eddington limit.

Once a solution has been obtained numerically between $R = R_{in}$ and $R = R_{out}$, it is necessary to integrate the equations from $R = R_{in}$ to $R = R_g$ to check whether the flow can reach the horizon smoothly. Since the viscous stress vanishes

for $R < R_{in}$, eq. (6) gives $j = \Omega R^2$, and substituting this in eq. (6) we find another conserved quantity

$$\frac{1}{2}v_R^2 + \frac{1}{2}\Omega^2 R^2 + (\gamma - 1)c_s^2 - \Phi_G(R) = \text{constant}. \tag{13}$$

Consistency of the solution merely requires $v_R > c_s$ for all $R_g < R < R_{in}$, which is easy to check.

With the above formulation of the black hole disk problem, and using the modified viscosity prescription (11), we have been able to find steady state solutions for all reasonable values of α up to $\alpha = 1$, using values of X from ~ 0 to 1. We did not use values of $\alpha > 1$ since these are not considered physical, and we did not consider $X > 1$ since this corresponds to thick disks which are not likely to be represented well by our height-integrated equations. These represent the first black hole solutions for reasonable values of α.

Figures 7.1 and 7.2 show some typical solutions that we have obtained for polytropic disks around black holes. Four velocities are plotted as a function of the radius for each solution; these include the radial velocity v_R, the sound speed c_s, the rotational velocity ΩR, and the 'Keplerian' rotational velocity $\Omega_K R$, where Ω_K is defined in eq. (5). Figure 7.1 shows two solutions with $\alpha = 0.1$; one of the solutions has $X = 0.1$, and the other has $X = 1.0$. The two solutions are basically quite similar. In both, $v_R \ll c_s$ throughout most of the disk, but as the gas approaches the last stable orbit at $R = 3R_g$ ($\log(R/R_g) = 0.477$), v_R increases rapidly, and reaches the sonic point just inside of $R = 3R_g$. After it exceeds the sonic speed, the infalling gas continues to accelerate until it reaches the event horizon at $R = R_g$ ($\log(R/R_g) = 0$). The rotational velocity is very nearly 'Keplerian' until

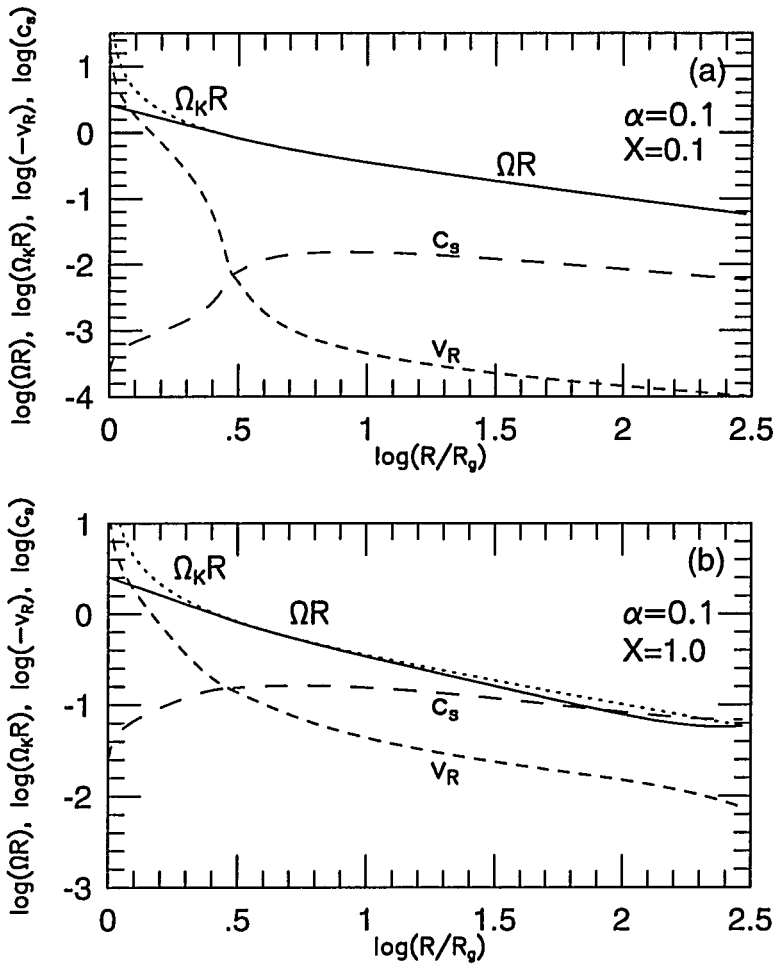

Fig. 7.1—(a) The radial velocity v_R (short-dashed line), the sound speed c_s (long-dashed line), the rotational velocity ΩR (solid line), and the 'Keplerian' rotational velocity $\Omega_K R$ (dotted line) for a disk solution around a black hole with $\alpha = 0.1$, $X = 0.1$. (b) Similar to (a), but for a solution with $\alpha = 0.1$, $X = 1.0$.

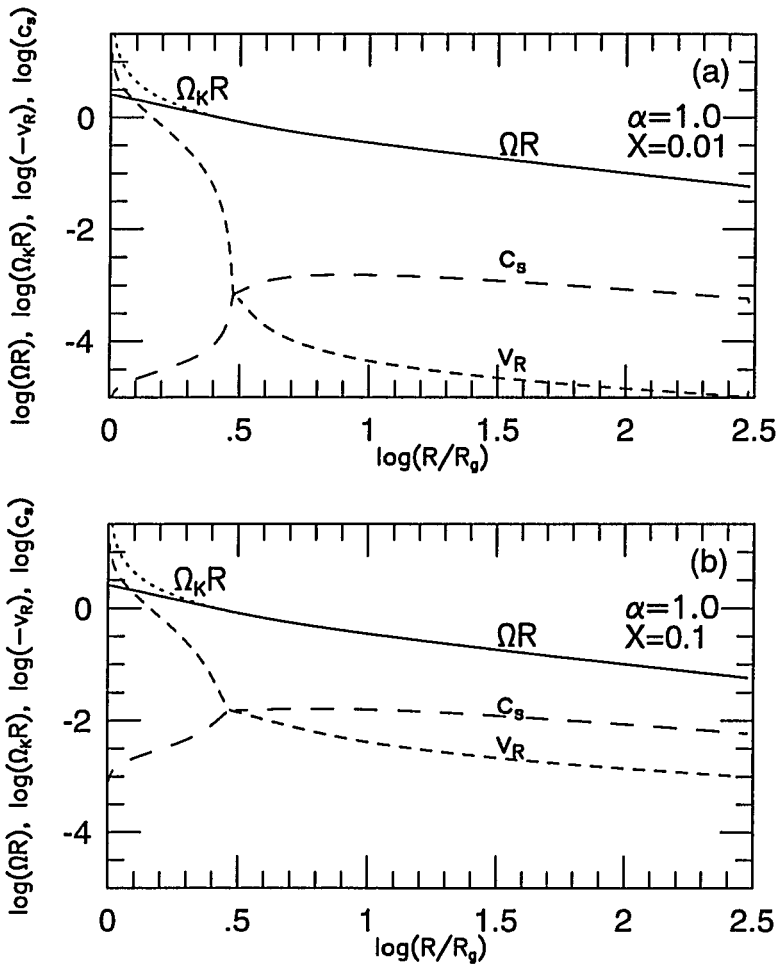

Fig. 7.2—(a) Similar to Figure 1, but for a solution with $\alpha = 1.0$, $X = 0.01$. (b) Similar to (a), but for a solution with $\alpha = 1.0$, $X = 0.1$.

the gas reaches the sonic point; inside the sonic point, it does not increase as rapidly as the 'Keplerian' rotational velocity, which becomes infinite at the event horizon. Instead, the gas conserves angular momentum, so that $\Omega \propto R^{-2}$. Figure 7.2 shows two solutions with $\alpha = 1.0$, one with $X = 0.01$ and one with $X = 0.1$. The solutions are quite similar to those shown in Figure 7.1. One qualitative difference is that because the viscosity coefficient is larger, the transition between the viscous, subsonic region and the non-viscous, supersonic region is more abrupt. Nonetheless, all of the quantities vary smoothly through the sonic point.

7.4 Discussion

The main result of this paper is that we have obtained the first self-consistent solutions of accretion disks around black holes for the entire physical range of the viscosity parameter α. For simplicity, we used a polytropic fluid, which eliminates the need for any description of the thermal structure of the disk. This is, of course, a major simplification, and it is now necessary to show that we can obtain similar solutions even when equations describing energy generation and transport are included. We do not anticipate any conceptual difficulties in this step, although it will almost certainly be more complex than the problem we have solved here.

The important difference in the present analysis, compared to previous unsuccessful attempts, is that we have used a modified version of the α-viscosity prescription which is designed to satisfy causality. The standard α-prescription allows viscous shear signals to propagate at infinite speed whereas our modified formulation explicitly limits the speed to a finite value, which we have set equal

to the sound speed. We stress that the modification we have introduced is not an arbitrary one designed just for the present study. We have already demonstrated the usefulness of this prescription in an earlier study of disk boundary layers where the standard α-prescription produced paradoxical results. The same modification which enabled us to solve that problem also seems to solve the black hole disk case.

In combination with our previous work, the present paper highlights the importance of using a physically consistent description of viscosity which can model the finite speed of propagation of viscous signals. The prescription we have used is an approximate one, which was derived under several simplifying assumptions; moreover, it is valid only in steady state situations. In view of the apparent importance of this issue for a self-consistent description of accretion disks, we feel that it is worthwhile to find a more general description of viscous interactions which can introduce causality naturally even into time-dependent flows.

8. HARD X-RAYS FROM ACCRETION DISK BOUNDARY LAYERS

8.1 Introduction

Accretion disks (Shakura & Sunyaev 1973, Pringle 1981) are found in a wide variety of objects in astrophysics, ranging from newly-formed stars to mass-transferring binaries to quasars and other active galactic nuclei (AGN). Detailed modeling of these systems has long been handicapped by a lack of understanding of the boundary layer, which is the interface between the disk and the star where up to half the accretion luminosity may be liberated. Until now there has been no satisfactory description of the flow and thermal structure of the boundary layer, resulting in serious incompleteness in models of disk spectra. We have calculated numerical solutions of thin accretion disks around a central white dwarf of mass $M_* = 1\,\mathrm{M}_\odot$ and radius $R_* = 5 \times 10^8$ cm, which include for the first time a self-consistent description of the boundary layer. We find a bifurcation in the nature of the solutions as a function of the mass accretion rate $\dot{M}$. At high rates, $\dot{M} \gtrsim 10^{-9}\,\mathrm{M}_\odot\ \mathrm{yr}^{-1}$, we obtain optically thick boundary layers whose radial width ΔR_{BL} and maximum temperature T_{BL} decrease with decreasing $\dot{M}$. However, for $\dot{M} \lesssim 10^{-9}\,\mathrm{M}_\odot\ \mathrm{yr}^{-1}$, the boundary layer becomes optically thin and ΔR_{BL} and T_{BL} increase dramatically with decreasing $\dot{M}$. For sufficiently low $\dot{M}$, ΔR_{BL} becomes comparable to R_*, and the temperature exceeds $10^8 K$. These results explain the hard X-rays that are observed (Patterson & Raymond 1985a) in cataclysmic variables (CVs), especially at low $\dot{M}$. The techniques developed here should permit us to construct self-consistent

models of other accretion disks in astrophysics, such as disks around neutron stars, black holes (both stellar-mass and supermassive), and newly-formed stars.

8.2 Disk and Boundary Layer Model

The solutions described here were obtained by numerically solving a set of coupled differential equations which describe the hydrodynamical and thermal structure of a steady state thin accretion disk as a function of radius R. The radial and tangential components of the momentum equation give (Popham & Narayan 1991, Paczyński 1991)

$$v\frac{dv}{dR} - \left(\Omega^2 - \Omega_K^2\right) R + \frac{1}{\rho}\frac{dP}{dR} = 0, \qquad \Omega_K(R) = \left(\frac{GM_*}{R^3}\right)^{1/2}, \tag{1}$$

$$\nu\frac{d\Omega}{dR} - v\left(\Omega - \frac{J}{R^2}\right) = 0, \tag{2}$$

where v is the radial velocity at radius R, Ω is the angular velocity, Ω_K is the Keplerian value of Ω, ρ is the density, P is the pressure, ν is the coefficient of shear viscosity, and J is an eigenvalue describing the inward flux of angular momentum per unit mass. We employ a modified prescription (Narayan 1992, Popham & Narayan 1992) for ν, which is an extension of the usual α -prescription of Shakura & Sunyaev (1973), designed to satisfy causality. We set $\alpha = 0.1$.

A crucial feature of this work is the inclusion of an energy equation (Paczyński & Bisnovatyi-Kogan 1981, Muchotrzeb & Paczyński 1982, Abramowicz *et al.* 1988),

$$\dot{M}T\frac{dS}{dR} - \dot{M}\frac{\nu}{v}\left(R\frac{d\Omega}{dR}\right)^2 - \frac{d}{dR}(4\pi RHF_R) - 4\pi RF_V = 0, \tag{3}$$

where the four terms correspond to entropy advection, viscous energy generation, divergence of radial radiative flux F_R, and energy loss via vertical flux F_V through

the top and bottom of the disk; H is the half-thickness of the disk, such that $\dot{M} = 4\pi RH\rho|v|$. We assume an ideal equation of state, corresponding to a perfect gas mixed with radiation.

For the vertical flux F_V we use approximate solutions (Hubeny 1990) relating the effective temperature T_{eff}, defined by $F_V \equiv \sigma T_{eff}^4$, to the central temperature T. We use a simple gray opacity which includes Kramers free-free absorption and electron scattering. For the radial flux F_R, we employ a "two-stream" model of radiative transfer, which leads to two differential equations for the radiation density U and radial flux F_R. We thus have a total of five first-order ordinary differential equations. We solve these numerically with three inner boundary conditions at $R = R_*$, viz. $\Omega = \Omega_*$, $P = P_*$, $F_R = \sigma(T_*)_{eff}^4$, where we arbitrarily assume $(T_*)_{eff} = 2 \times 10^4 K$, and two outer boundary conditions at $R = R_{out} = 100R_*$, viz. $\Omega = \Omega_K$, $U = aT^4$. We use a relaxation method to compute the solutions, taking care to maintain sufficient resolution in the difficult boundary layer region.

8.3 Results

Figure 8.1 shows typical solutions at high $\dot{M}$ for a star rotating with angular frequency $\Omega_* = 0.5\ \Omega_b$, where $\Omega_b \simeq \Omega_K(R_*)$ is the "break-up limit" on the spin of the star. The boundary layers in these solutions are optically thick. Note that there are two distinct widths. The dynamical width over which Ω changes from Ω_K to Ω_* is quite narrow, less than $0.01R_*$, while the thermal width over which the boundary layer luminosity is radiated is somewhat larger, $\sim 0.1R_*$. Both widths decrease monotonically with decreasing $\dot{M}$, and so do the central temperature T

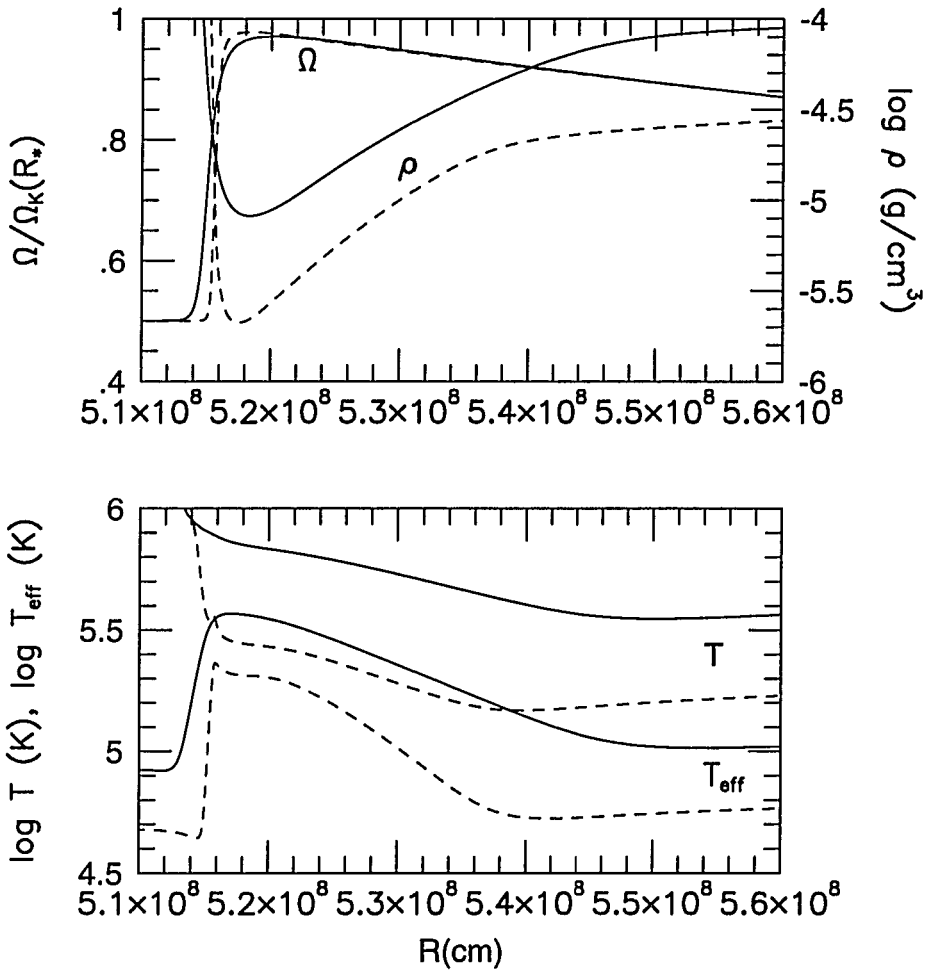

Fig. 8.1—The optically thick boundary layer region for two solutions with high mass accretion rates $\dot{M}$; the solid lines correspond to $\dot{M} = 10^{-7.5}\,\mathrm{M}_\odot\,\mathrm{yr}^{-1}$, and the dashed lines to $\dot{M} = 10^{-8.5}\,\mathrm{M}_\odot\,\mathrm{yr}^{-1}$. The accreting material flows from right to left, and meets the stellar surface at $R \sim 5 \times 10^8$ cm. The top panel shows the angular velocity of the accreting material Ω, and the density ρ. Ω is nearly Keplerian in the disk, but drops abruptly to the stellar rotation rate $\Omega_* = 0.5\Omega_K(R_*)$ in the boundary layer. The bottom panel shows the central temperature T and the effective temperature T_{eff}. T rises gradually through the boundary layer and more rapidly as the material settles onto the star. T_{eff} peaks in the boundary layer, but is large over a fairly wide region, so that the boundary layer luminosity is radiated from an area larger than that of the boundary layer itself.

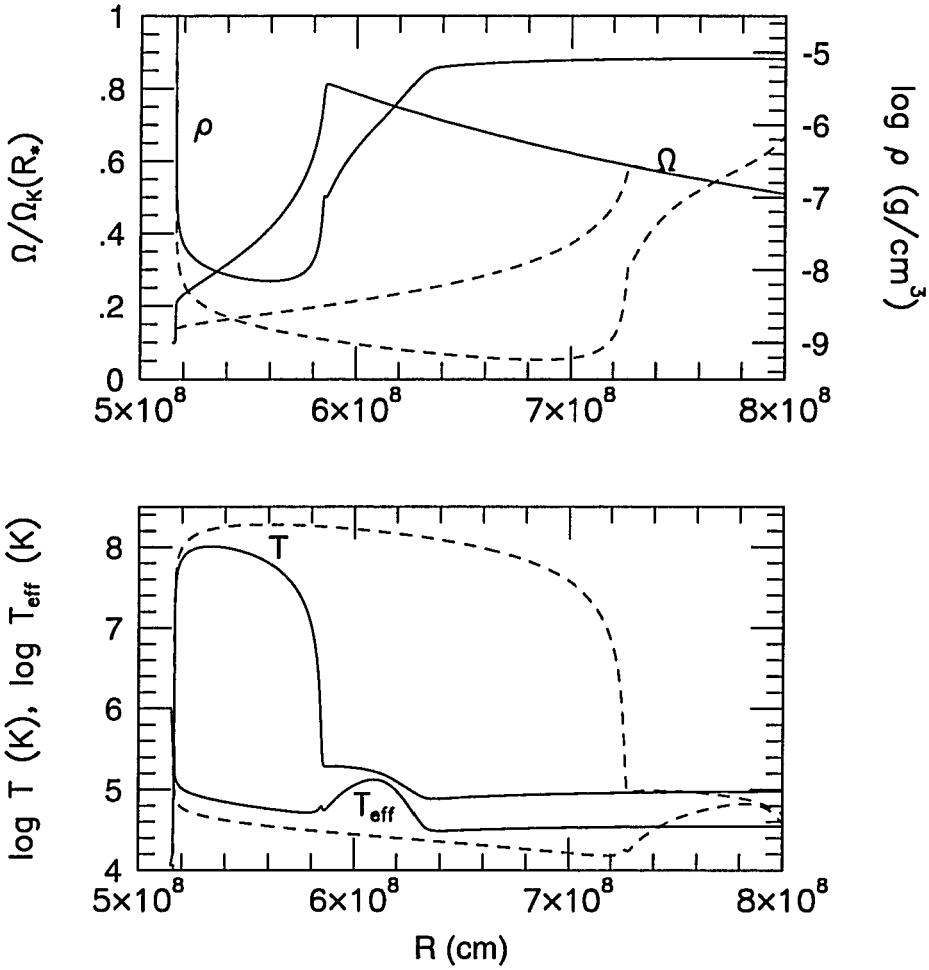

Fig. 8.2—The optically thin boundary layer region for two solutions with low mass accretion rates $\dot{M}$ and with a stellar rotation rate $\Omega_* = 0.1\Omega_K(R_*)$; the solid lines correspond to $\dot{M} = 10^{-9.5}\,\mathrm{M}_\odot\ \mathrm{yr}^{-1}$, and the dashed lines to $\dot{M} = 10^{-10.5}\,\mathrm{M}_\odot\ \mathrm{yr}^{-1}$. The boundary layers in these solutions are much wider than in the optically thick solutions shown in Figure 8.1. The width increases rapidly with decreasing $\dot{M}$. The drop in density in the boundary layer is far more pronounced than in the optically thick solutions, and the central temperature jumps dramatically, exceeding $10^8 K$ before falling suddenly when the accreting material reaches the star. The effective temperature is relatively low in the boundary layer because of the low optical depth, but is larger in a narrow spike at the inner edge of the boundary layer and in a small region just outside the boundary layer, where the optical depth is larger.

and effective temperature T_{eff}. Further, the boundary layer luminosity decreases as Ω_* is increased, vanishing when the star reaches break-up ($\Omega_* = \Omega_b$). None of these results is surprising, but we emphasize that this is the first time that self-consistent solutions have been actually calculated of this region of a disk.

Figure 8.2 shows some of our solutions at low accretion rates, where the boundary layer is optically thin. We see immediately very different behavior than in Fig. 8.1. Now, as $\dot{M}$ decreases, both the width and the temperature of the boundary layer increase very rapidly. Indeed, for $\dot{M} = 10^{-10.5}\,\mathrm{M}_\odot\ \mathrm{yr}^{-1}$ and $\Omega_* = 0.1\Omega_b$, the width ΔR_{BL} is comparable to the stellar radius R_* and the maximum temperature T_{BL} is well in excess of $10^8 K$. Both ΔR_{BL} and T_{BL} increase even further for lower $\dot{M}$, but decrease as Ω_* increases. Further, the results are quite sensitive to the choice of α. For $\dot{M} = 10^{-9.5}\,\mathrm{M}_\odot\ \mathrm{yr}^{-1}$ and $\Omega_* = 0.1\Omega_b$, as we increase α from 0.1 to 0.4, we find that ΔR_{BL} increases from $0.13R_*$ to $0.43R_*$ and T_{BL} goes from $10^8 K$ to $2 \times 10^8 K$. At these extreme temperatures the disk is no longer very thin; nevertheless, we expect the models to be reasonably realistic.

8.4 Discussion

8.4.1 *Thermal Instability*

The surprising behavior of the boundary layer at low $\dot{M}$ can be explained in terms of a thermal instability (Tylenda 1981, Patterson & Raymond 1985a). The accreting gas cannot cool efficiently due to the decreased density in the optically thin boundary layer. This forces the disk to store most of the viscously generated energy in the form of entropy, heating the boundary layer gas rapidly. The gas then

expands vertically, which serves to further decrease its density. Thus, in much of the boundary layer region, we do not have a balance between viscous heating and locally radiated vertical flux (the second and fourth terms in eq. 3), as in the rest of the disk. Instead, viscous heating is balanced primarily by entropy advection, the first term in eq. (3), while the two radiative flux terms play a relatively insignificant role. When the superheated material in the boundary layer finally reaches the star, the thermal instability works in reverse. The fluid now becomes optically thick and cools abruptly. Although there is no hydrodynamic shock at this point (Popham & Narayan 1992), the cooling instability sets in very suddenly and shows some features of a radiative shock. Previous approximate treatments of the boundary layer (Tylenda 1981, Regev 1983) included elements of the thermal instability but missed the importance of the advected entropy and the sudden cooling.

8.4.2 *Comparison to Observations of Cataclysmic Variables*

It is known that CVs radiate in hard X-rays, with spectra which appear to be consistent with a thermal bremsstrahlung spectrum with kT_{brems} of a few to tens of keV. As the accretion rates of CVs decrease, and especially when they drop below $\dot{M} \lesssim 10^{-9.5}\,\mathrm{M}_\odot\ \mathrm{yr}^{-1}$, their hard X-ray luminosity becomes a substantial fraction of the total flux (Patterson & Raymond 1985a). Our results are consistent with these observations. The high temperature ($\sim 10^8 K$), optically thin boundary layers which we find for low values of $\dot{M}$ should produce abundant X-rays with $kT_{brems} \sim 10$ keV. The optically thick boundary layers at higher values of $\dot{M}$ will emit a far smaller fraction of their total luminosity in X-rays. Since ΔR_{BL} and T_{BL} both depend on $\dot{M}$, M_*, R_*, Ω_* and α, we should be able to compare our

self-consistent solutions with observations and thus to constrain the parameters of the accreting white dwarfs.

A possible difficulty in comparing our results with observations is that the hard X-ray emission is often variable (perhaps due to time-dependent features of the thermal instability), which we cannot fit with our steady-state models. We must also caution that the radiative transfer we have used is somewhat simplistic. We have not for instance considered the scattering of horizontal to vertical flux (or vice versa) due to electron scattering, or energy transport through conduction. It is straightforward to include these effects, which will introduce modest changes, particularly in the thermal width of the boundary layer. We also intend to carry out more detailed vertical radiative transfer in order to compute realistic continuum spectra. We will then be in a position to make direct comparisons between observed spectra and model predictions. We should be able to understand, for instance, why so few cataclysmic variables have been detected in soft X-rays, as might be expected from an optically thick boundary layer (Patterson & Raymond 1985b).

8.4.3 *Future Applications*

Although the models we have presented here are for CVs, we may be able to use the same techniques to construct models of other accretion disk systems. One interesting application is to accreting neutron stars and black holes, which are similar to CVs in many respects but differ by being radiation-dominated in the boundary layer region (Shakura & Sunyaev 1973, Pringle 1981). In analogy with the present results, we might expect these systems to have cooler narrower boundary layers at high $\dot{M}$ and hotter wider boundary layers at low $\dot{M}$. There is

indeed evidence for this behavior, with some Galactic binary black hole candidates (Sunyaev & Trumper 1979, McClintock 1991) as well as a few neutron star systems showing transitions from a soft spectrum at higher luminosities (high $\dot{M}$) to a hard spectrum at lower luminosities.

A potentially important difference between neutron stars and black holes is in the nature of the inner boundary condition. Accretion on to an unmagnetized neutron star is similar to the white dwarf case considered here, with Ω changing from Ω_K to Ω_* within the boundary layer and v decelerating significantly when the material reaches the star. In contrast, a black hole has a "soft" inner boundary, so that Ω is nearly equal to Ω_K down to the inner edge of the disk and then nearly constant to the horizon. Also, the radial velocity v increases monotonically inwards, passing through a sonic point (Abramowicz *et al.* 1988). (A neutron star too can show similar behavior if its radius is smaller than the radius of the last stable orbit, but this needs a soft equation of state and a slowly rotating star.) This difference must lead to distinct signatures in the spectra, which we hope to discover using the techniques developed in this paper.

Many models of AGN postulate the presence of a supermassive black hole that creates a hot pair plasma (Rees 1984), but the mechanism by which the central engine maintains the required high temperatures has been unclear. By simply scaling from the white dwarf solutions presented here, we would expect optically thin boundary layers around black holes or neutron stars to produce temperatures as high as $10^{10} - 10^{11} K$ by steady low-$\dot{M}$ accretion. This is hot enough for the creation of e^+e^- pairs and could be relevant to pair production in AGN. However, our model does not include some effects which could be quite important at such high

temperatures. For instance, the boundary layer would be cooled both by Compton scattering of soft radiation from elsewhere in the disk (Shapiro *et al.* 1976), and by conduction. This will limit the maximum temperature that can be attained in these systems and should be included self-consistently in the models.

Finally, this work may also be applicable to accreting young stellar objects. Among this class of stars, the FU Orionis systems with high $\dot{M} \sim 10^{-4}$ $M_\odot$ yr^{-1} certainly have optically thick boundary layers, while T Tauri stars with $\dot{M} \lesssim 10^{-7}$ $M_\odot$ yr^{-1} may have optically thick or thin boundary layers (Bertout *et al.* 1988, Hartigan *et al.* 1991). There is a good deal of observational data on the disks and boundary layers of these systems which could be exploited by computing self-consistent models. An interesting point is that in a few T Tauri stars there is evidence that the accretion disk appears to terminate at a few stellar radii. We speculate that this may in some cases result from an optically thin boundary layer that happens to be several stellar radii wide. Such wide boundary layers are possible if $\alpha \gtrsim 1$ and if the central star spins much below break-up as observed.

9. OPTICALLY THICK BOUNDARY LAYERS IN CATACLYSMIC VARIABLES

9.1 Introduction

In Chapter 8, we presented boundary layer solutions for cataclysmic variables (CVs) as a function of the mass accretion rate $\dot{M}$. For CVs with high accretion rates, $\dot{M} \gtrsim 10^{-9}\,M_\odot\ yr^{-1}$, we found that the boundary layer region is optically thick. This chapter examines optically thick boundary layers in more detail. The solutions presented in this chapter were found using the same set of equations as described in Chapter 8. However, the results in this chapter are still preliminary and have not been published yet.

In Chapter 8, we concentrated on presenting a basic set of solutions for four accretion rates, using the same stellar parameters for each solution. In Section 9.2, we examine the variation in the structure and characteristics of the boundary layer as a function of the stellar mass and radius. Since we are assuming that the accreting star is a white dwarf, the radius is specified by the mass, so that the mass and radius taken together represent a single parameter. We also examine how the boundary layer changes for various values of the stellar rotation rate. Note that we have used a very approximate mass-radius relation in this work, and that we have not included the effects of the rotation rate on the equatorial radius of the white dwarf. In the near future, we plan to include these effects in our work by using the results derived by Hachisu (1986), who computed a grid of rotating white dwarfs.

Another issue which was not addressed in Chapter 8 was the "breakup branch" of boundary layer solutions, which were discovered in the work presented in Chapter 5, using a polytropic equation of state. The existence of these solutions suggested that accretion would continue even after the accreting star had spun up to breakup; however, it has not been demonstrated that these solutions exist when the more realistic equation of state and energy equation are used, as in the solutions in Chapter 8. In Section 9.3, we demonstrate that these solutions do indeed exist, and that they are quite similar to the breakup solutions presented in Chapter 5. In particular, we find solutions which transfer mass to the accreting star while transferring no angular momentum to the star, or even removing angular momentum from it. We examine these solutions in detail, and show how their boundary layer angular velocities, radial velocities, and temperatures differ from those of solutions on the normal "slow rotator branch".

Section 9.4 addresses the energetics of optically thick boundary layers. We examine the balance between various terms of the energy equation which characterize the various zones within the disk, boundary layer, and star. We also derive an expression for the total luminosity of the boundary layer and disk, and compare the luminosities generated in our models to those predicted by this expression.

9.2 Variations in the Boundary Layer as a Function of the Parameters of the Accreting White Dwarf

9.2.1 *Variations in the White Dwarf Mass and Radius*

We have calculated boundary layer solutions around accreting white dwarfs ranging in mass from 0.6 to 1.0 $M_\odot$. The mass of the central star is particularly important in the case of accretion disks around white dwarfs because for white dwarfs, the radius decreases as the mass increases. Thus, the accretion luminosity $L_{acc} \equiv GM_{WD}\dot{M}/R_{WD}$, where M_{WD} and R_{WD} are the mass and radius of the white dwarf, changes rapidly as the mass of the white dwarf changes.

The masses of white dwarfs in the field are highly concentrated around $M_{WD} \simeq 0.6\,M_\odot$ (Bergeron *et al.* 1992). On the other hand, estimates for the masses of white dwarfs in CVs have varied widely, but have averaged more than $0.6\,M_\odot$. Webbink (1990) found an average white dwarf mass of $0.74\,M_\odot$ in 84 CVs. We have calculated solutions for a range of masses in order to examine the variation of the boundary layer structure with stellar mass and radius.

Figures 9.1 and 9.2 show five boundary layer solutions with the same accretion rate, $\dot{M} = 10^{-7.5}\,M_\odot\ \mathrm{yr}^{-1}$, around white dwarfs with masses of 0.6, 0.7, 0.8, 0.9, and 1.0 $M_\odot$, and radii of 9×10^8, 8×10^8, 7×10^8, 6×10^8, and 5×10^8 cm, respectively. The 1.0 $M_\odot$, 5×10^8 cm solution is the same solution as presented in Chapter 8; it has a stellar rotation rate $\Omega_{WD} = 0.5\mathrm{s}^{-1}$. The other solutions have rotation rates which have been adjusted in order to keep the ratio of Ω_{WD} to the breakup rotation rate $\Omega_{breakup}$ the same in all five solutions.

Figure 9.1 shows the variation of the angular velocity Ω and the radial velocity v_R in the boundary layer region for these solutions. Although both the angular and radial velocities decrease as the white dwarf mass decreases, the velocity profiles are quite similar for all five solutions. The angular velocity falls from nearly Keplerian to the stellar rotation rate quite rapidly, in a dynamical boundary layer with a width of only one or two percent of the white dwarf radius. The radial velocity (negative for accretion) rises dramatically and reaches a peak in the boundary layer, then falls just as dramatically as the flow approaches the stellar surface. Figure 9.2 shows the central temperature T_c, the effective temperature T_{eff}, and the combined spectrum of the boundary layer and disk for each of these solutions. As the white dwarf mass decreases and the radius increases, both the central and effective temperatures steadily decrease. The peak effective temperature in the boundary layer reaches about 400,000 K in the $M_{WD} = 1\,\mathrm{M}_\odot$ solution, but only reaches about 200,000 K in the $M_{WD} = 0.6\,\mathrm{M}_\odot$ solution. Nonetheless, as with the velocities, the temperature profiles are quite similar in all five solutions. The spectra of the solutions for the more massive white dwarfs extend into the soft X-ray band, whereas those with less massive white dwarfs would produce far fewer X-rays. Nevertheless, the spectra are quite similar in shape. Thus we can conclude that, at least for this accretion rate, the mass and radius of the accreting white dwarf make a quantitative rather than a qualitative difference in the boundary layer characteristics.

9.2.2 *Variation in the White Dwarf Rotation Rate*

The stellar rotation rate Ω_* is particularly important to the boundary layer because it determines how much rotational kinetic energy the accreting material will

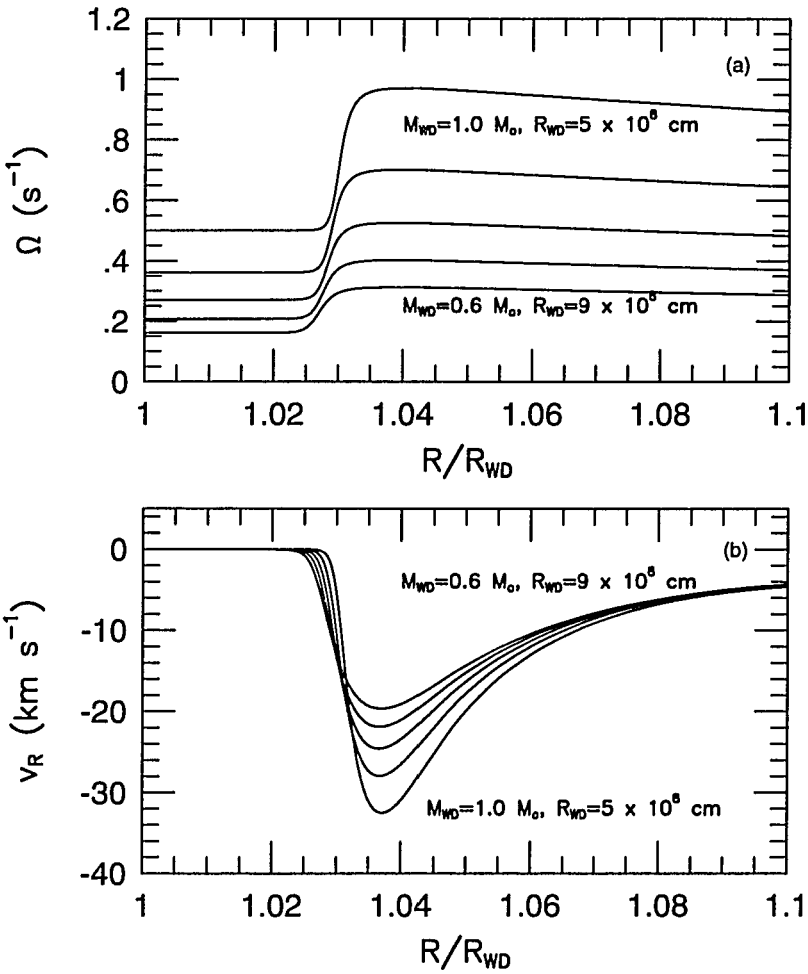

Fig. 9.1—Variation of (a) the angular velocity Ω and (b) the radial velocity v_R in the boundary layer as a function of the white dwarf mass and radius. The five solutions shown have white dwarf masses of 0.6, 0.7, 0.8, 0.9, and 1.0 $M_\odot$, and radii of 9×10^8, 8×10^8, 7×10^8, 6×10^8, and 5×10^8 cm, respectively. All of the solutions have a mass accretion rate of $10^{-7.5}\,M_\odot\ yr^{-1}$ and an angular momentum accretion rate of 1.02 times the Keplerian rate. The stellar rotation rate is chosen to be the same fraction of the breakup rotation rate in each case; it is about half of the breakup rate.

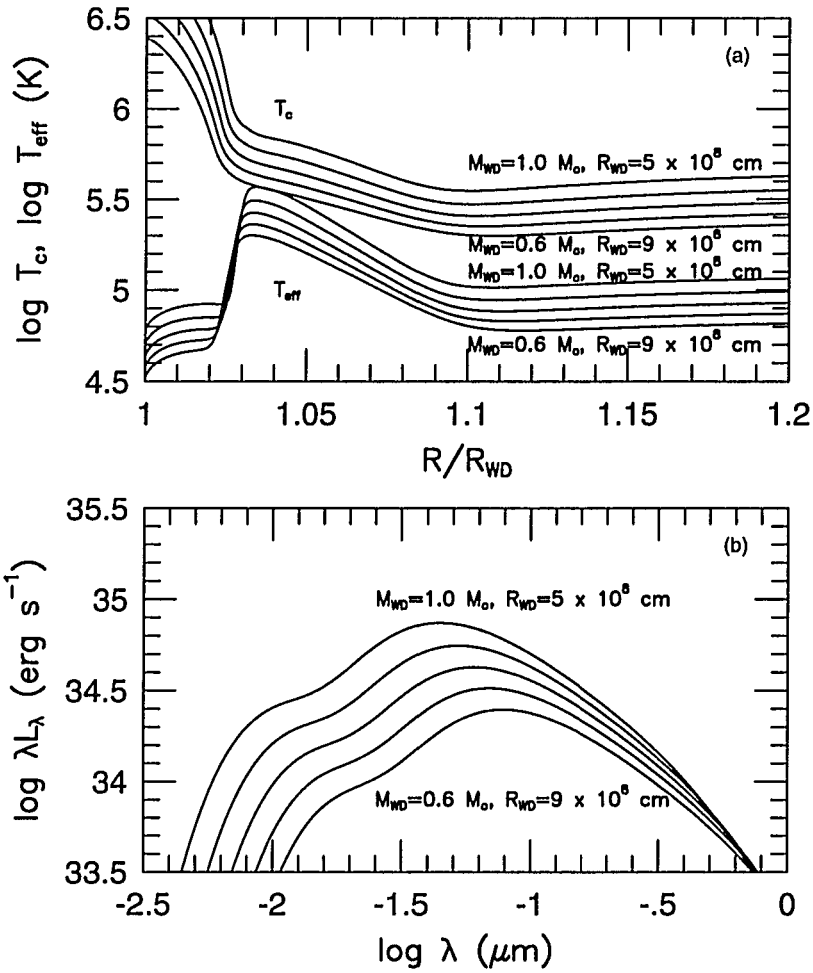

Fig. 9.2—(a) The central and effective temperatures and (b) the spectra of the solutions shown in Figure 9.1. The spectra include flux from the boundary layer and the disk, which extends out to 100 stellar radii.

have to lose in the boundary layer region before it is added to the star. In section 9.4.2, we examine the relationship between Ω_* and the boundary layer luminosity in more detail. Here, we present boundary layer solutions for five values of Ω_*: 0, 0.25, 0.50, 0.75, and 0.921 s^{-1}. Note that the Keplerian rotation rate at the stellar surface, where $R = R_{WD} = 5 \times 10^8$ cm, is 1.03 s^{-1}. Nonetheless, the highest stellar rotation rate for which solutions are available is 0.921 s^{-1}; this will be discussed further in section 9.3.

Figure 9.3 shows the angular and radial velocities for these five solutions. The angular velocities again drop rapidly in a narrow dynamical boundary layer; as Ω_* increases, the dynamical boundary layer widens slightly, even though the angular velocity is dropping less in these solutions. The radial velocity peaks in the boundary layer, but the peak is most dramatic in the $\Omega_* = 0$ (nonrotating) solution, where the radial velocity reaches nearly 100 km s^{-1}. As Ω_* increases, the peak radial velocity drops dramatically, so that it is less than 10 km s^{-1} in the $\Omega_* = 0.921 s^{-1}$ solution.

Figure 9.4 shows the central and effective temperatures and the combined spectra of the boundary layer and disk for the same five solutions. The temperature profiles change substantially as a function of Ω_*. Outside the boundary layer, all of the solutions are identical; the central temperature drops slowly as the material flows inward. In this region the flow is described well by the Shakura-Sunyaev equations, in which the central temperature reaches a local maximum at $R = 1.44R_*$ and then decreases. In the thermal boundary layer region, where the boundary layer luminosity is being released, the central temperature rises substantially, and finally,

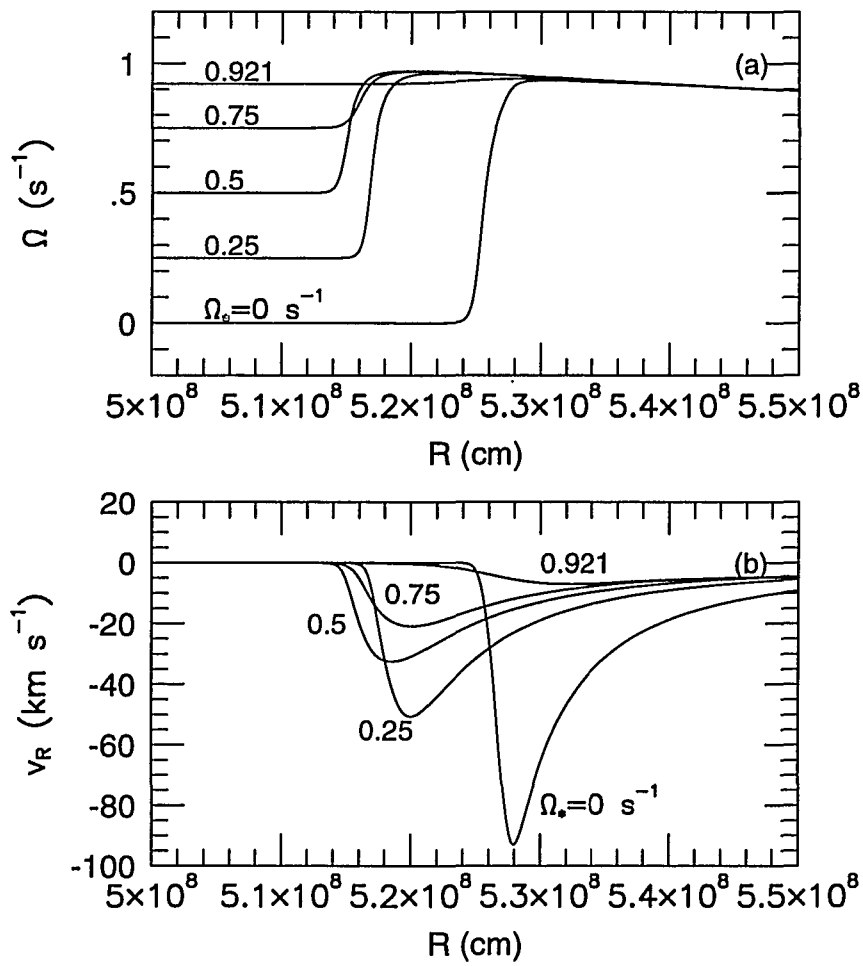

Fig. 9.3—(a) The angular and (b) radial velocities in the boundary layer as a function of the stellar rotation rate Ω_*. The solutions shown have rotation rates of 0, 0.25, 0.5, 0.75, and 0.921 s^{-1}. All of the solutions have a white dwarf mass of $1.0\,M_\odot$, a white dwarf radius of 5×10^8 cm, a mass accretion rate of $10^{-7.5}\,M_\odot\ yr^{-1}$, and an angular momentum accretion rate of 1.02 times the Keplerian rate.

at the inner edge of the boundary layer, it rises quite rapidly as the flow approaches the stellar surface.

The effective temperature follows a slightly different pattern. Outside the boundary layer, the effective temperatures are identical for all the solutions, following the Shakura-Sunyaev profile and reaching a local maximum at $R = 1.36R_*$. The effective temperature rises dramatically in the thermal boundary layer region, then drops quite rapidly at the inner edge of the region, and is relatively low inside the boundary layer. The central temperature, effective temperature, and thermal width of the boundary layer all decrease substantially as Ω_* increases. Moving from the $\Omega_* = 0.921\text{s}^{-1}$ solution to the $\Omega_* = 0$ solution, the central temperature ranges from about 300,000 K to 1,000,000 K, the effective temperature from about 100,000 K to 500,000 K, and the thermal width from about 3% to 10% of the stellar radius.

The effective temperature profile also develops a dip near its maximum in the slowly rotating solutions. This is caused by the large radial velocities and high temperatures reached in this region, which result in a very small absorptive optical depth, and a corresponding decline in the cooling efficiency. At a lower accretion rate, the total optical depth (absorption plus scattering) might become small in slowly rotating solutions, producing high-temperature, optically thin boundary layers like those seen in Chapter 8. In other words, the transition from optically thick to optically thin boundary layers would probably occur at a higher accretion rate for slowly rotating stars than for rapidly rotating stars.

The spectra also show dramatic changes as a function of Ω_*. The solution for a nonrotating star shows a strong boundary layer component at extreme ultraviolet and soft X-ray wavelengths. As Ω_* increases, this component rapidly disappears,

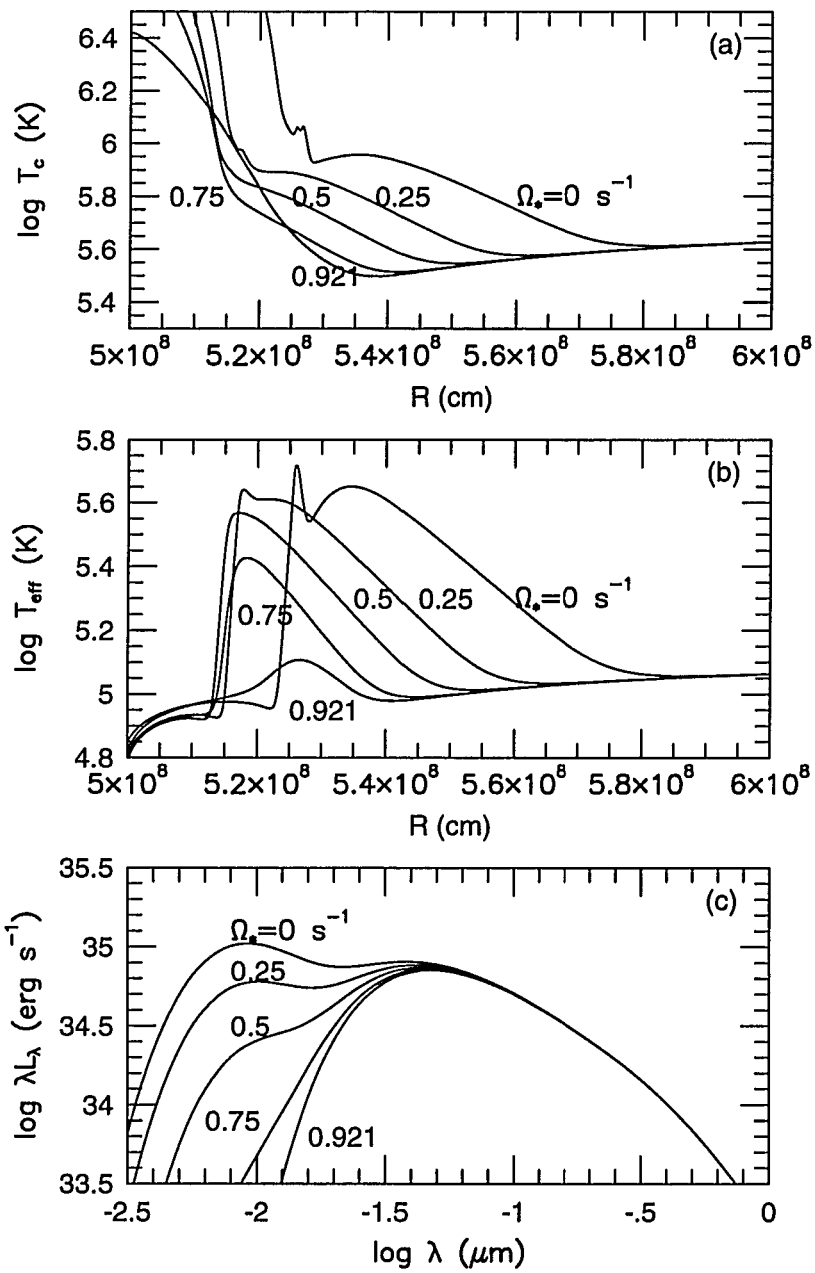

Fig. 9.4—The (a) central temperatures, (b) effective temperatures, and (c) spectra of the solutions shown in Figure 9.3.

leaving only a single disk component in the solutions for rapidly rotating white dwarfs.

9.3 The "Breakup Branch" for Rapidly Rotating Accreting White Dwarfs

In Chapter 5, using a simple polytropic disk model, we discovered the existence of a "breakup branch" of boundary layer solutions. These solutions occurred for accretion onto stars which were rotating at breakup speed, and they allowed the star to accrete mass while accreting little or no angular momentum, or even losing angular momentum to the surrounding disk. The existence of such solutions indicated that accretion could continue even after a star had spun up to breakup. Up to now, the existence of such solutions has not been demonstrated in a full disk model which includes an energy equation.

Figure 9.5 shows the angular and radial velocities of seven breakup branch solutions. All the solutions have $\Omega_* = 0.921\text{s}^{-1}$, but each has a different value of j, the angular momentum accretion rate scaled by the Keplerian angular momentum accretion rate at the stellar surface. The seven solutions have j = 1.02, 1.00, 0.95, 0.80, 0.50, 0.00, and -1.00. The $j = 1.02$ solution is almost identical to the solution with $\Omega_* = 0.921\text{s}^{-1}$ in Figure 9.3; this solution represents the transition between the slowly-rotating branch of solutions and the breakup branch. The angular velocity Ω of this solution reaches a maximum and then falls gradually to 0.921 s^{-1}. As j decreases, this maximum vanishes, and Ω simply flattens out when it reaches Ω_*, with the transition from Keplerian to constant Ω becoming more gradual as j continues to decrease. The lack of a maximum in Ω between the star and the

disk means that viscosity can transport angular momentum from the star to the disk; this viscously transported angular momentum offsets the angular momentum of the accreting material, and allows the net angular momentum accretion rate to be small or even negative.

The radial velocities in the breakup branch solutions are very small compared to those in the slowly-rotating solutions. Except for the transitionary $\Omega_* = 0.921\mathrm{s}^{-1}$ solution, the radial velocity profiles do not show a pronounced peak; rather, the radial velocity rises slowly in the disk, then drops gradually as the accreting gas approaches the star. These solutions have the same accretion rates as the slowly rotating solutions, so the surface density of the accreting material must be much larger to compensate for the small radial velocities. Thus, these solutions have large optical depths in the boundary layer. To demonstrate this, we calculated solutions with $\Omega_* = 0.921\mathrm{s}^{-1}$ and $j = 0$ for accretion rates from $10^{-7.5}\,\mathrm{M}_\odot\ \mathrm{yr}^{-1}$ to $10^{-10.5}\,\mathrm{M}_\odot\ \mathrm{yr}^{-1}$, and found that all of these solutions remained optically thick. This provides another demonstration that the boundary between optically thick and optically thin solutions depends strongly on the rotation rate of the accreting star, rather than simply falling at a particular value of the mass accretion rate. This dependence could be very useful in setting limits on Ω_* for CVs which emit hard X-rays.

Figure 9.6 shows the central temperatures, effective temperatures, and spectra for the solutions shown in Figure 9.5. Both sets of profiles are quite simple; apart from the $j = 1.02$ solution, none show any evidence for the presence of a boundary layer component. Instead, there is a smooth transition from disk to star, which becomes more and more gradual as j decreases. Both the central and effective

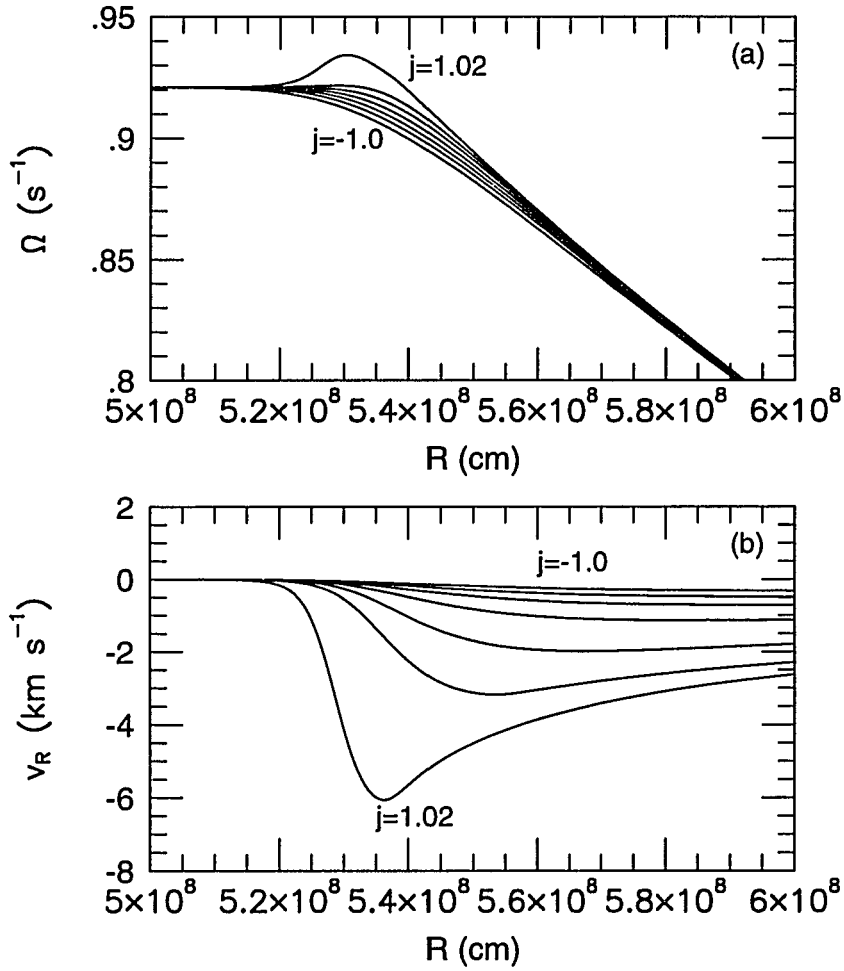

Fig. 9.5—(a) The angular and (b) radial velocities for solutions on the breakup branch, as a function of j, the angular momentum accretion rate in units of the Keplerian rate. The solutions shown have j = 1.02, 1.00, 0.95, 0.80, 0.50, 0.00, and -1.0. All of the solutions have a white dwarf mass of $1.0\,M_\odot$, a white dwarf radius of 5×10^8 cm, a white dwarf rotation rate of 0.5 s^{-1}, and a mass accretion rate of $10^{-7.5}\,M_\odot\ yr^{-1}$.

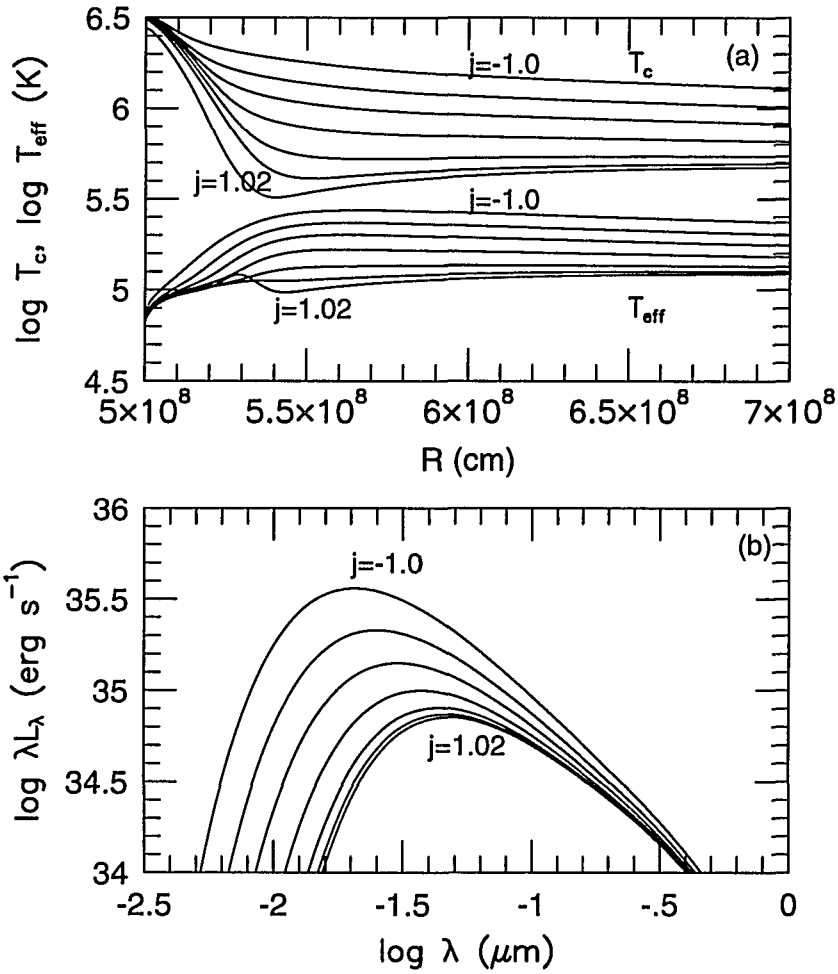

Fig. 9.6—(a) The central and effective temperatures and (b) the spectra of the solutions shown in Fig. 9.5.

temperatures increase substantially as j decreases. This is because energy which had been used to spin up the accreting star is now being dissipated and radiated in the disk. A more detailed description of the spin-up of the star and its effect on the boundary layer luminosity is given in section 9.4. The increase in the central and effective temperatures as j decreases extends out to large radii, unlike the temperature changes due to different stellar rotation rates, which occur only in the boundary layer region. The spectra of these solutions show only a single disk component, which gets hotter and more luminous as j decreases.

9.4 Energetics of Optically Thick Boundary Layers

9.4.1 *Energy Balance in the Boundary Layer Region*

The energetics of the boundary layer region tend to be somewhat more complex than those in the surrounding accretion disk. In the disk, it is assumed that a simple balance exists between energy dissipated by viscosity and energy radiated by the disk surface, so that the dissipated energy is radiated locally. In the boundary layer, however, it is necessary to include the effects of radial energy transport. One reason for this is that the radial extent of the dynamical boundary layer, where the boundary layer luminosity is generated, may be smaller than the disk height at that point. Thus, most of the energy radiated from the region will be directed radially rather than vertically. The entropy of the accreting gas is also transported by the accretion flow itself.

We have included these terms in our energy equation, which reads

$$\dot{M}T\frac{dS}{dR} - \dot{M}\frac{\nu}{v}\left(R\frac{d\Omega}{dR}\right)^2 - \frac{d}{dR}(4\pi RHF_R) - 4\pi RF_V = 0. \qquad (1)$$

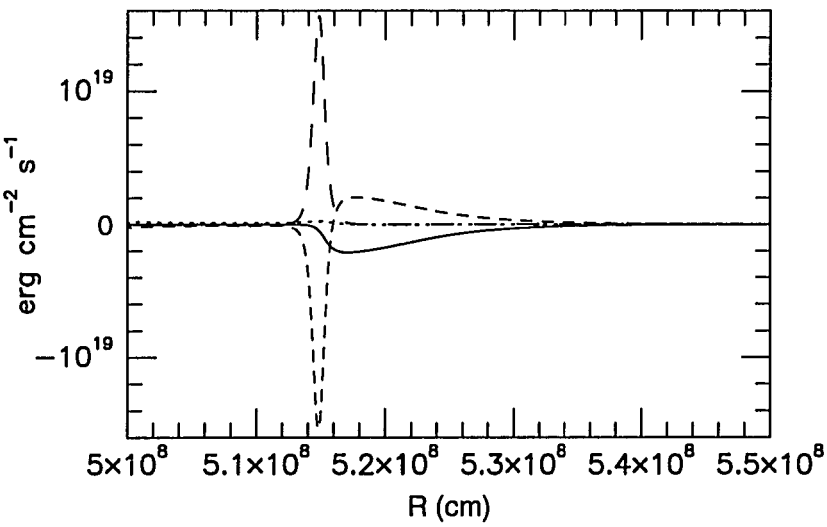

Fig. 9.7—The energy balance in the boundary layer region for a solution with $\dot{M} = 10^{-7.5}\,\mathrm{M}_\odot\ \mathrm{yr}^{-1}$ and $\Omega_* = 0.5\mathrm{s}^{-1}$. The four terms in the energy equation are shown: the vertical flux from the disk surface as a solid line, the energy added or lost as radial luminosity as a short-dashed line, the viscous dissipation of energy as a long-dashed line, and the advection of the entropy of the accreting gas as a dotted ine.

The first term in this equation represents the advection of the entropy of the accreting gas by the accretion flow. The second term is the dissipation of energy by shear viscosity, where ν is the kinematic viscosity coefficient. The third term is the divergence of the radially-directed luminosity, which gives the amount of energy gained or lost by the disk via radial transport of radiation per radial width dR. Finally, the fourth term represents energy radiated from the disk surface.

These four energy terms are shown in Figure 9.7 for the boundary layer region in the solution with $\dot{M} = 10^{-7.5}\,\mathrm{M}_\odot\ \mathrm{yr}^{-1}$, $\Omega_* = 0.5\mathrm{s}^{-1}$, and $j = 1.02$, which was also shown in Figures 9.1-9.4. The boundary layer and the region around it can

be divided into zones based on which pair of energy terms dominates in each zone. Outside the boundary layer, in the disk, viscous dissipation and vertical flux balance each other, as is assumed in the Shakura-Sunyaev equations. The boundary layer luminosity is dissipated in the dynamical boundary layer, as evidenced by the fairly narrow spike in the viscous dissipation rate. The matching spike in the divergence of the radial luminosity shows that the great majority of this energy is radiated in the radial direction. The reason for this is fairly clear: the radial extent of the dynamical boundary layer is only about 2×10^6 cm, while the full disk height in the same region is about 2×10^7 cm, so that the shape of the emitting region ensures that most of the radiation will go in the radial direction. The density of the accreting gas is around $10^{-5}\mathrm{gcm}^{-3}$ just outside the dynamical boundary layer, but increases rapidly within the dynamical boundary layer, and continues to increase rapidly as it approaches the star. This ensures that most of the radiation ends up traveling radially outward rather than inward toward the star. This radiation is absorbed and converted into vertical radiation over a wider region, the thermal boundary layer. In this region, the divergence of the radial luminosity is a source of energy which is balanced by vertical flux from the disk surface. The thermal boundary layer extends over a radial distance which is comparable to the full disk height. Finally, as the accreting gas settles into the star, the entropy it carries inward becomes the dominant energy source, which is balanced by the radial flux.

9.4.2 *The Total Luminosity of the Boundary Layer and Disk*

By ignoring the boundary layer and making some simple assumptions, it is simple to find the total luminosity of an accretion disk (e.g., Pringle 1981). If one

assumes that the disk angular velocity is Keplerian all the way in to the stellar radius R_*, and that the luminosity is equal to the total energy per unit time dissipated by viscosity, the flux from the disk surface can been written

$$F(R) = \nu\Sigma(R\frac{d\Omega}{dR})^2 = \frac{3GM_*\dot{M}}{4\pi R^3}\left[1-\left(\frac{R_*}{R}\right)^{1/2}\right], \qquad (2)$$

where Σ is the surface density of the accreting gas. By integrating this flux over the disk area, assuming that the disk extends from R_* to infinity, we obtain the total luminosity of the disk, $L_{disk} = \frac{1}{2}GM_*\dot{M}/R_*$. Thus, only half of the gravitational potential energy $GM_*\dot{M}/R_* \equiv L_{acc}$ is radiated away by the disk. The other half is in the form of the rotational kinetic energy of the accreting gas.

Some of this kinetic energy is dissipated in the boundary layer, where the angular velocity of the accreting gas decreases rapidly. The amount which is dissipated depends on the rotation rate of the accreting star. Since the gas at the stellar surface has kinetic energy per unit mass $\frac{1}{2}\Omega_*^2R_*^2$, it has long been incorrectly assumed that the remaining kinetic energy per unit mass $\frac{1}{2}(\Omega_K^2(R_*)-\Omega_*^2)R_*^2$ is dissipated and radiated by the boundary layer, which gives a boundary layer luminosity (Pringle 1981)

$$L_{bl} = \frac{1}{2}\dot{M}(\Omega_K^2(R_*)-\Omega_*^2)R_*^2 = \frac{GM_*\dot{M}}{2R_*}\left(1-\frac{\Omega_*^2}{\Omega_K^2(R_*))}\right). \qquad (3)$$

Under this assumption, the boundary layer luminosity would vary quadratically with the stellar rotation rate, such that $L_{bl}/L_{acc} = \frac{1}{2}[1-(\Omega_*/\Omega_K(R_*))^2]$, which gives $L_{bl} = 0.5L_{acc}$ for a nonrotating star, $L_{bl} = 0$ for a star with $\Omega_* = \Omega_K(R_*)$, and $L_{bl} = 0.375L_{acc}$ for a star with $\Omega_* = 0.5\Omega_K(R_*)$.

This formula for the boundary layer luminosity neglects to account for the energy which goes into spinning up the accreting star, as was pointed out by Kluzniak

(1987). The correct formula can be derived in an approximate way as follows. Accretion adds angular momentum to the star at a rate $\dot{J} = j\dot{M}\Omega_K(R_*)R_*^2$. Since the accreting gas arrives at the stellar surface rotating at the stellar rotation rate Ω_*, it carries angular momentum to the star at a rate $\dot{M}\Omega_* R_*^2$. The remainder of the angular momentum is added by the viscous torque at a rate $\dot{M}(j\Omega_K(R_*) - \Omega_*)R_*^2$, which is generally positive, but can be negative in some breakup branch solutions where $j\Omega_K(R_*) < \Omega_*$. Both the accreting gas and the torque also add rotational energy to the star. The rotational kinetic energy of the accreting gas increases the star's rotational kinetic energy at a rate $\frac{1}{2}\dot{M}\Omega_*^2 R_*^2$. The torque spins the star up, adding rotational energy at a rate $\dot{M}(j\Omega_K(R_*) - \Omega_*)\Omega_* R_*^2$. Thus, the total rate at which rotational energy is added to the star is $\dot{M}(j\Omega_K(R_*)\Omega_* - \frac{1}{2}\Omega_*^2)R_*^2$. If we assume that all of the energy $\frac{1}{2}\dot{M}\Omega_K^2(R_*)R_*^2$ is either radiated or imparted to the rotation of the central star, then the boundary layer luminosity is just

$$L_{bl} = \dot{M}\left(\frac{1}{2}\Omega_K^2(R_*) - j\Omega_K(R_*)\Omega_* + \frac{1}{2}\Omega_*^2\right)R_*^2$$

$$= \frac{GM_*\dot{M}}{R_*}\left(\frac{1}{2} - j\frac{\Omega_*}{\Omega_K(R_*)} + \frac{1}{2}\frac{\Omega_*^2}{\Omega_K^2(R_*)}\right). \qquad (4)$$

If we also assume that the disk luminosity is simply $\frac{1}{2}GM_*\dot{M}/R_*$, the total luminosity of the boundary layer and disk is

$$L_{tot} = \frac{GM_*\dot{M}}{R_*}\left(1 - j\frac{\Omega_*}{\Omega_K(R_*)} + \frac{1}{2}\frac{\Omega_*^2}{\Omega_K^2(R_*)}\right). \qquad (5)$$

Thus, when the energy expended in spinning up the star is accounted for, the quadratic dependence of the boundary luminosity on Ω_* is reversed: for $j \simeq 1$, $L_{bl}/L_{acc} \simeq \frac{1}{2}[1 - (\Omega_*/\Omega_K(R_*))]^2$, so that $L_{bl} = 0.125L_{acc}$ when $\Omega_* = 0.5\Omega_K(R_*)$.

Thus, contrary to the old eq. (3), eq. (5) shows that most of the decrease in the boundary layer luminosity occurs in the early stages of spin-up, when the star is rotating slowly, rather than the late stages when it is nearing breakup.

The derivation given here makes a number of simplifying assumptions. A more formal derivation for the total luminosity of the boundary layer and disk is given in Appendix C; it arrives at a similar result

$$L_{tot} = \frac{GM_*\dot{M}}{R_*}\left(1 - j\frac{\Omega_*}{\Omega_K(R_*)} + \frac{1}{2}\frac{\Omega_*^2}{\Omega_K^2(R_*)}\right) - \frac{GM_*\dot{M}}{R_{out}}\left(\frac{3}{2} - j\frac{R_*^{1/2}}{R_{out}^{1/2}}\right)$$
$$+\frac{1}{2}\dot{M}v_R^2(R_{out}) - \frac{1}{2}\dot{M}v_R^2(R_*) + \dot{M}\int_{P_{in}}^{P_{out}}\frac{dP}{\rho}. \qquad (6)$$

The first term is identical to eq. (5), and the remaining terms are generally comparatively small.

Equation (4) shows that the boundary layer luminosity depends on a number of factors: the stellar mass M_* and radius R_*, the mass accretion rate $\dot{M}$, the stellar rotation rate Ω_*, and the appropriately scaled angular momentum accretion rate j. In this chapter, we have presented a variety of boundary layer solutions in which these parameters were varied. In Table 2, we show the total luminosities for the disk and boundary layer for each of these solutions, along with the total luminosity predicted by eq. (6).

We find good agreement with equation (6) for all the parameters. Note that eq. (6) gives the luminosity dissipated by the disk and boundary layer, which may differ slightly from the luminosity which is actually radiated due to factors not included in eq. (6), such as the flux entering the disk at the inner boundary. We have included both the dissipated and radiated luminosities from our numerical

TABLE 2

TOTAL LUMINOSITY OF THE DISK AND BOUNDARY LAYER

Ω_*	j	M_{WD}	R_{WD}	$L^1_{predicted}$	L^1_{visc}	L^1_{rad}
0.00	1.02	1.0	5×10^8	4.946	4.948	5.088
0.25	1.02	1.0	5×10^8	3.892	3.893	3.967
0.50	1.02	1.0	5×10^8	3.098	3.100	3.122
0.75	1.02	1.0	5×10^8	2.612	2.614	2.631
0.921	1.02	1.0	5×10^8	2.467	2.468	2.488
0.921	1.02	1.0	5×10^8	2.465	2.466	2.487
0.921	1.00	1.0	5×10^8	2.554	2.556	2.581
0.921	0.95	1.0	5×10^8	2.789	2.790	2.817
0.921	0.80	1.0	5×10^8	3.493	3.495	3.528
0.921	0.50	1.0	5×10^8	4.906	4.908	4.950
0.921	0.00	1.0	5×10^8	7.262	7.264	7.322
0.921	-1.00	1.0	5×10^8	11.977	11.980	12.071
0.36	1.02	0.9	6×10^8	2.326	2.327	2.339
0.27	1.02	0.8	7×10^8	1.773	1.774	1.782
0.21	1.02	0.7	8×10^8	1.359	1.359	1.364
0.16	1.02	0.6	9×10^8	1.036	1.036	1.040

[1] $L_{predicted}$ is from equation (6); L_{visc} and L_{rad} are the luminosity dissipated by viscosity and the luminosity radiated by each of the models listed. All luminosities are in units of 10^{35} ergs.

solutions in Table 2; the dissipated luminosities agree to high precision with the predictions of eq. (6). The radiated luminosities also agree quite well, generally to within a percent or so.

The luminosities in Table 2 also follow the dependences on the stellar parameters and the mass and angular momentum accretion rates quite accurately. The total luminosity decreases as the white dwarf mass decreases and the white dwarf radius increases. As the stellar rotation rate increases, the star follows the predicted quadratic dependence quite accurately, confirming that eq. (4) rather than eq. (3)

is the correct expression for the boundary layer luminosity. Finally, as we decrease j along the breakup branch, the total luminosity rises dramatically, since the energy which had been expended in spinning up the star is now being dissipated by viscosity and radiated by the disk and boundary layer. In fact, in the $j = 0$ and $j = -1$ solutions, the total luminosity exceeds the accretion luminosity, since the disk removes some of the rotational energy from the star and radiates it away.

10. BOUNDARY LAYERS IN PRE-MAIN SEQUENCE ACCRETION DISKS

Abstract

We present self-consistent solutions, using α-viscosity, for the flow and energetics of optically thick boundary layers in accretion disks around pre-main sequence stars. The solutions span a range of accretion rates from $\dot{M} = 10^{-7}\,M_\odot\ yr^{-1}$ to $10^{-4}\,M_\odot\ yr^{-1}$ and are in qualitative agreement with observations of T Tauri and FU Orionis stars. The boundary layers in the solutions have two radial zones. The viscous dissipation occurs in a relatively narrow dynamical boundary layer, but most of the energy is actually radiated over a wider thermal boundary layer which extends to larger radii. We find that at low accretion rates, the boundary layer emission is clearly visible as a separate hot component in the combined spectrum of the disk and boundary layer, but this component is more difficult to distinguish at higher accretion rates.

10.1 Introduction

In recent years it has become clear that many pre-main sequence stars undergo disk accretion as they evolve toward the main sequence. Accretion produces a substantial luminosity in these systems, dominating the intrinsic stellar luminosity at high accretion rates, as in the FU Orionis stars, and contributing significantly even at the relatively modest accretion rates found in T Tauri stars.

Up to half of the luminosity of an accretion disk should be produced by the boundary layer region, the interface between the disk and the star where the rotational velocity of the accreting material slows from nearly Keplerian to the stellar

rotation rate (Lynden-Bell & Pringle 1974). It is here that most of the rotational kinetic energy of the accreting material is dissipated by viscosity and radiated. Recent observations of the spectra of accreting pre-main sequence stars (Bertout, Basri, & Bouvier 1988, Basri & Bertout 1989, Hartigan *et al.* 1989, 1991) have provided evidence of boundary layer emission, and have led to crude estimates of the sizes and temperatures of the emitting region. However, detailed interpretation of the observations has been impossible in the absence of self-consistent models of the boundary layer flow.

In this paper, we report physically self-consistent solutions for boundary layers around pre-main sequence stars for accretion rates ranging from $\dot{M} = 10^{-7}\,\mathrm{M}_\odot\ \mathrm{yr}^{-1}$ to $10^{-4}\,\mathrm{M}_\odot\ \mathrm{yr}^{-1}$.

10.2 Disk and Boundary Layer Model

We model the entire accretion flow in the disk, the boundary layer and the central star by a single set of equations, which are similar to the standard disk equations developed by Shakura & Sunyaev (1973), but with additional terms to account for the more complex physics of the boundary layer. We assume that the disk is axisymmetric and in a steady state, and solve for the radial structure. The local vertical structure is treated in the usual vertically-averaged approximation.

10.2.1 *Dynamical Equations*

The dynamics of the accretion flow are described by two components of the momentum equation. The steady state angular momentum equation can be used

to find the variation of the angular velocity Ω with radius R:

$$\frac{d\Omega}{dR} = \frac{v_R}{\nu}\left(\Omega - \frac{\dot{J}}{\dot{M}R^2}\right), \tag{1}$$

where v_R is the radial velocity, ν is the kinematic shear viscosity coefficient, and $\dot{J}$ is the rate of accretion of angular momentum. We use a modified α-prescription for the viscosity, as described in Narayan (1992) and Popham & Narayan (1992).

The radial momentum equation gives

$$v_R\frac{dv_R}{dR} + \frac{1}{\rho}\frac{dP}{dR} = \left(\Omega^2 - \Omega_K^2\right)R, \tag{2}$$

where P is the pressure, ρ is the density, and Ω_K is the Keplerian angular velocity at radius R. This equation describes the transition from rotational support ($\Omega^2 R$) to pressure support ($-\nabla P/\rho$) as the accreting material moves from the disk to the star. We use an equation of state which includes gas and radiation pressure.

In the vertical direction, we assume that the material is in hydrostatic equilibrium. This gives rise to the usual expression for the vertical scale height of the fluid, $H = c_s/\Omega_K$, where the sound speed $c_s \simeq (P/\rho)^{1/2}$.

10.2.2 *Energy Balance*

The standard disk equations (Shakura & Sunyaev 1973) assume that energy dissipated by viscosity is radiated locally by the disk surface. In order to model the boundary layer region, we need to include additional terms in the energy balance to account for radial transport of energy. Since the height of the boundary layer may be comparable to or greater than its radial extent, most of the energy dissipated here may go into radial rather than vertical flux. Also, since the radial infall velocity

may be large, advection of the entropy of the accreting material may be significant. Thus, we use the "slim disk" energy balance equation (Abramowicz *et al.* 1988)

$$\dot{M}T\frac{dS}{dR} - \dot{M}\frac{\nu}{v_R}\left(R\frac{d\Omega}{dR}\right)^2 - \frac{d}{dR}(4\pi RHF_R) - 4\pi RF_V = 0, \tag{3}$$

where S is the entropy, F_R is the radial flux, and F_V is the vertical flux from the disk surface.

We calculate the radial flux F_R using a simple two-stream radiative transfer, so that

$$F_R = -\frac{4\pi}{3}\frac{du}{d\tau}, \quad \frac{d}{dR}\left(RH\frac{du}{d\tau}\right) = 3\kappa_{abs}\rho RH(u - B), \tag{4}$$

where u is the mean intensity, B is the frequency-integrated Planck function, κ_{abs} is the absorptive opacity, and $d\tau = \kappa\rho dR$, where κ is the total opacity. For the vertical flux we use an approximate relation due to Hubeny (1990):

$$F_V = \sigma T_{eff}^4 = \frac{\sigma T_c^4}{\frac{3}{4}\left(\frac{\tau_c}{2} + \frac{1}{\sqrt{3}} + \frac{1}{3\tau_{abs,c}}\right)}, \tag{5}$$

where T_{eff} is the effective temperature, and T_c, $\tau_c = \kappa\rho H$, and $\tau_{abs,c} = \kappa_{abs}\rho H$ are the temperature, total optical depth, and absorptive optical depth at the midplane of the disk or boundary layer.

We calculate Rosseland mean opacities assuming a pure hydrogen gas and including H and H^- bound-free and free-free absorption and electron scattering. We tabulate and interpolate these opacities at each radial position as a function of the midplane density and temperature. At relatively low temperatures, where the Rosseland mean opacity drops below 1 cm^2 g^{-1}, we simply assume that $\kappa = \kappa_{abs} = 1$ cm^2 g^{-1}. Although this prescription is a reasonable approximation at

temperatures below about 1500 K, where the opacity is due to dust grains (Pollack, McKay, & Christofferson 1985), it substantially overestimates the opacity in the range 1500 K $\lesssim T \lesssim$ 5000 K where molecules are the dominant opacity source (Alexander, Augason, & Johnson 1989). However, in the boundary layer region, the midplane temperature is generally hotter than 5000 K, so this simplification has no effect on our main results.

10.2.3 *Boundary Conditions*

The equations described above include five coupled differential equations. At the inner edge R_{in} of our radial computational grid we adopt the following boundary conditions: $\Omega = \Omega_*$, the stellar rotation rate, and $F_R = \sigma T_*^4$, where T_* is an assumed photospheric temperature of the star. We take the outer edge to be at $R = 100 R_{in}$, and there the boundary conditions are $\Omega = \Omega_K$, $u = B$, and $T_c = T_{SS}$, where T_{SS} is the Shakura-Sunyaev temperature, i.e. the temperature assuming that there is local balance between viscous energy dissipation and vertical flux.

We solve the resulting boundary-value problem numerically using a relaxation code. For each solution, we specify the values of the stellar mass, rotation rate, and photospheric temperature, M_*, Ω_*, and T_*, the mass accretion rate $\dot{M}$, the angular momentum accretion rate $\dot{J}$, and the viscosity parameter α. We adjust $\dot{J}$ until we obtain the required "stellar radius" R_*. Note that R_* cannot be defined precisely (cf. Popham & Narayan 1991); in this paper, we take R_* to be the radius in the boundary layer where Ω drops to one half its maximum value.

10.3 Results

We have calculated boundary layer and disk solutions for stellar masses, radii and accretion rates similar to those estimated from observations of T Tauri and FU Orionis stars: $M_* = 1\,M_\odot$, $R_* \sim 2 - 7R_\odot$, $\dot{M} = 10^{-7} - 10^{-4}\,M_\odot$ yr^{-1} (Kenyon, Hartmann, & Hewett 1988, Bertout, Basri, & Bouvier 1988, Basri & Bertout 1989, Hartigan *et al.* 1989, 1991). We display four solutions corresponding to $\dot{M} = 10^{-7}, 10^{-6}, 10^{-5}$, and $10^{-4}\,M_\odot$ yr^{-1} for $\alpha = 0.1$ (solid lines in the figures) and one solution for $\dot{M} = 10^{-4}\,M_\odot$ yr^{-1} with $\alpha = 0.001$ (dashed lines). In all cases we assume a nonrotating star, $\Omega_* = 0$, and a stellar temperature $T_* = 5000$ K.

Figure 10.1(a) shows Ω as a function of R in the boundary layer region of these solutions. We define the dynamical width of the boundary layer, ΔR_d, to be the radial extent of the region where Ω drops from $\sim \Omega_K$ to $\Omega_* = 0$. This is also the region where the boundary layer luminosity is generated by viscous dissipation. We find that ΔR_d scales as H^2/R. For $\dot{M} = 10^{-7}\,M_\odot$ yr^{-1}, ΔR_d is fairly small compared to the stellar radius, $\sim 0.02R_*$, but as $\dot{M}$ increases, ΔR_d increases rapidly, so that $\Delta R_d \sim 0.1R_*$ at $10^{-5}\,M_\odot$ yr^{-1} and $\Delta R_d \sim 0.3R_*$ at $10^{-4}\,M_\odot$ yr^{-1}.

For observational purposes, the most useful measure of the size of the boundary layer is not the dynamical width, but rather the thermal width, ΔR_t, the radial width over which the boundary layer luminosity is radiated. Figure 10.1(b) shows plots of the effective temperature T_{eff} for the solutions. In general, we find that $\Delta R_t \sim 2H$, the "full-thickness" of the disk, which agrees with some previous estimates (e.g., Pringle 1977), so that $\Delta R_t \sim (R/H)\Delta R_d \gg \Delta R_d$ for thin disks. In the $\dot{M} = 10^{-7}\,M_\odot$ yr^{-1} solution, $\Delta R_t \sim 0.2R_*$, and the peak T_{eff} reaches 8500 K. As the accretion rate increases, ΔR_t gets progressively larger, and in general

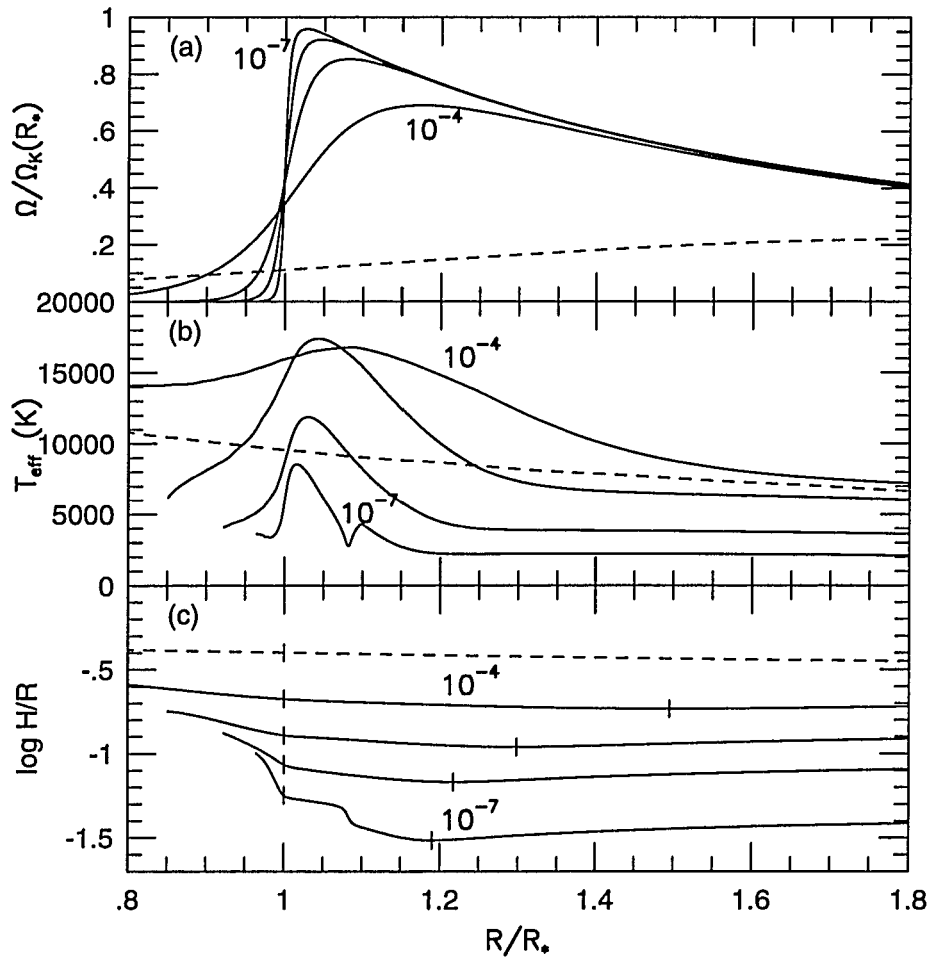

Fig. 10.1—The variation of (a) Ω, (b) T_{eff}, and (c) log H/R in five boundary layer solutions around pre-main sequence stars. The four solutions shown by solid lines have accretion rates $\dot{M} = 10^{-7}$, 10^{-6}, 10^{-5}, and $10^{-4}\,M_\odot\ yr^{-1}$, stellar radii of $R_* = 2.23$, 2.33, 2.53, and 4.53 $R_\odot$, respectively, and $\alpha = 0.1$. The dashed line shows a solution with $\dot{M} = 10^{-4}\,M_\odot\ yr^{-1}$, $R_* = 6.58R_\odot$, and $\alpha = 0.001$. All of the solutions are for nonrotating stars, $\Omega_* = 0$, with stellar temperatures $T_* = 5000$ K. The feature in T_{eff} and H/R at $R \simeq 1.08R_*$ in the $10^{-7}\,M_\odot\ yr^{-1}$ solution is due to the strong temperature dependence of the opacity in this temperature regime.

T_{eff} also increases. However, the peak T_{eff} at $\dot{M} = 10^{-4}\,\mathrm{M}_\odot\ \mathrm{yr}^{-1}$ is lower than at $\dot{M} = 10^{-5}\,\mathrm{M}_\odot\ \mathrm{yr}^{-1}$. In the $\dot{M} = 10^{-4}\,\mathrm{M}_\odot\ \mathrm{yr}^{-1}$, $\alpha = 0.001$ solution, the boundary layer is so wide that there is no peak in T_{eff}, and it is difficult to tell where the boundary layer ends and the disk begins.

Figure 10.1(c) shows the ratio H/R for the various solutions. It is clear that H/R increases steadily with increasing $\dot{M}$, but remains small enough that the thin disk (or, more accurately, "slim disk", cf. Abramowicz *et al.* 1988) formulation is reasonable. We have marked the approximate regions corresponding to the star, boundary layer, and disk for each solution. At lower $\dot{M}$, these regions are easy to recognize, since H/R reaches a minimum near the outer edge of the thermal boundary layer, increases gradually within the boundary layer, and increases more rapidly as the flow reaches the stellar surface. However, in the $10^{-4}\,\mathrm{M}_\odot\ \mathrm{yr}^{-1}$ solution, particularly for $\alpha = 0.001$, the three regions are quite difficult to distinguish.

We show blackbody spectra for the various models in Figure 10.2. These spectra include flux from the stellar radius R_* out to $10^4 R_*$, covering the boundary layer and a large region of the disk, but not the central star. (The numerical solutions displayed in Figs. 10.1(a)-(c) extend only to $R_{out} = 100 R_{in} \lesssim 100 R_*$. To compute the spectrum out to $10^4 R_*$, we assume that T_{eff} is given by the Shakura-Sunyaev solution outside of R_{out}.) The general characteristics of the spectra are not surprising: as the accretion rate increases, the boundary layer gets hotter and the spectrum gets bluer. However, the shape of the spectrum clearly changes with accretion rate. In the $10^{-7}\,\mathrm{M}_\odot\ \mathrm{yr}^{-1}$ solution, the contributions to the spectrum from the boundary layer and from the disk are clearly distinguishable, with an inflection around 1 μm.

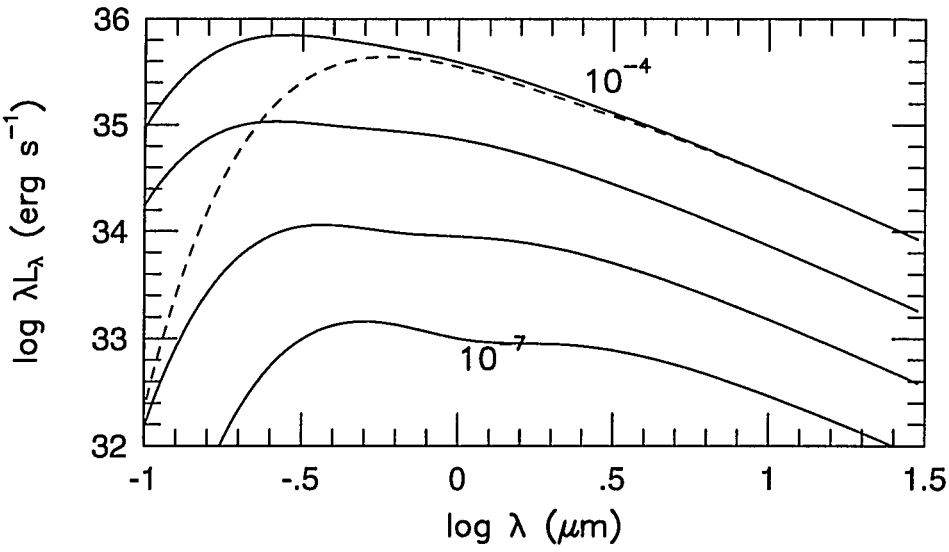

Fig. 10.2—The blackbody spectra of the solutions shown in Figure 10.1. The spectra include flux emitted by the boundary layer and disk from $R = 1R_*$ to $R = 10^4 R_*$.

The two components are only marginally visible at $10^{-6}\,M_\odot\,yr^{-1}$, and at higher $\dot{M}$ they have essentially merged into one.

10.4 Summary and Discussion

The main result that we wish to emphasize is that we have obtained self-consistent numerical solutions of optically thick boundary layers in pre-main sequence accretion disks. We have developed robust techniques whereby we can find solutions for accretion rates ranging from $\dot{M} = 10^{-7} - 10^{-4}\,M_\odot\,yr^{-1}$, corresponding to the rates estimated in T Tauri and FU Orionis stars. The solutions provide a description of the flow of the accreting material and the energy balance in the disk

and boundary layer, including radial transport terms.

An interesting aspect of the solutions involves the apparent disappearance of the boundary layer component from the overall spectrum at high accretion rates. Our results show that as $\dot{M}$ increases from $10^{-7}\,M_\odot\ yr^{-1}$ to $10^{-4}\,M_\odot\ yr^{-1}$, it becomes progressively more difficult to distinguish the boundary layer and disk components in the overall spectrum. This can be understood by observing that as the accretion rate increases, the vertical optical depth becomes larger and the disk thickens, and as a consequence the radial extent of the boundary layer increases. The boundary layer luminosity is then spread over such a large area that its temperature is no longer very different from that of the adjoining disk and it becomes difficult to distinguish it as a separate component in the spectrum. Kenyon *et al.* (1989) examined ultraviolet spectra of FU Orionis systems, with $\dot{M} \sim 10^{-4}\,M_\odot\ yr^{-1}$, and found very little evidence for boundary layer emission. This is in contrast to T Tauri systems (discussed below), with $\dot{M} \sim 10^{-7}\,M_\odot\ yr^{-1}$, where there is clear evidence in the spectra for a separate hot component. Our solutions reproduce this difference quite well.

At accretion rates around $10^{-4}\,M_\odot\ yr^{-1}$, the material in the midplane of the inner disk and boundary layer approaches virial temperatures because the large optical depth inhibits cooling. Therefore, even within the star, the entropy carried in by the accretion flow is significant. This large flux of energy into the star would be expected to increase the stellar radius substantially (Prialnik & Livio 1985). In this context it is interesting that disk models for FU Orionis objects suggest inner disk radii $\sim$ twice as large as the typical radii of T Tauri stars (Kenyon, Hartmann, & Hewett 1988).

Our models may also help to interpret observations of several symbiotic binaries through an eruption cycle. Quiescent observations of both CI Cyg and AX Per suggest a "standard" boundary layer temperature of $\sim 10^5$ K for an estimated accretion rate of $\sim 10^{-5}\,M_\odot\ yr^{-1}$ (Kenyon *et al.* 1991; Mikołajewska & Kenyon 1992). As these systems evolve to a mass transfer rate of $\sim$ a few $\times 10^{-4}\,M_\odot\ yr^{-1}$ during an outburst, the boundary layer temperature initially tracks the increase in $\dot{M}$ but then falls dramatically. The solutions presented here show a similar drop in the boundary layer temperature, due to both the increase in the boundary layer width and the larger stellar radius at high accretion rates.

Another important result of our calculations is that the boundary layer has two distinct widths, which define different regions of the accretion flow. The boundary layer luminosity is generated within the relatively narrow dynamical boundary layer, where Ω drops from Keplerian to the stellar rotation rate. However, this luminosity is not radiated locally from the disk surface at the same radius as where it is generated. Instead, most of the energy goes into radial flux, and is transported outward and re-radiated from the disk surface at a larger disk radius. The region which radiates the luminosity is the thermal boundary layer, and it has a radial width comparable to the full thickness of the disk (Pringle 1977). The two-zone boundary layers in our solutions are quite different from those obtained by Bertout & Regev (1992) using the matched asymptotic method. Their method constrains the radial flux to be zero at the point where Ω reaches its maximum value, the outer edge of our dynamical boundary layer. This forces all of the energy dissipated in the boundary layer to be radiated inward, toward the star, which in turn requires the temperature to decrease inward. Because of these constraints, they were able

to find solutions for only a restricted range of $\dot{M}$, and even these solutions required them to invoke an *ad hoc* mass loss from the boundary layer.

Although the solutions presented here are primarily intended to illustrate the general features of boundary layers in pre-main sequence accretion disks, a brief quantitative comparison with observations is instructive. Basri & Bertout (1989) and Hartigan *et al.* (1991) derived estimates of boundary layer widths and temperatures and mass accretion rates for T Tauri stars by modeling the blue continuum excess emission observed in these systems as flux from a slab of material at a single temperature and density. They derived accretion rates of about $10^{-7}\,M_\odot\ yr^{-1}$, temperatures in the range from 7000 to 10,000 K, and boundary layer widths of 1-10% of the radius of the star. The $10^{-7}\,M_\odot\ yr^{-1}$ solution presented here reaches a maximum effective temperature of about 8500 K in the boundary layer. The full thermal width of the boundary layer in this solution is about 15-20% of the stellar radius, but the width of the region above 7000 K is only a few percent of the stellar radius. Thus our $10^{-7}\,M_\odot\ yr^{-1}$ solution matches general T Tauri boundary layer parameters fairly well. However, it has been suggested that the inner portions of accretion disks in T Tauri stars may be disrupted by the magnetic field of the central star (Königl 1991, Calvet & Hartmann 1992). If this is correct, then the resulting boundary layer will be quite different from those we have modeled here.

Kenyon, Hartmann, & Hewett (1988) used standard disk models to fit spectra of two FU Orionis stars, and derived accretion rates $\dot{M} \sim 10^{-4}\,M_\odot\ yr^{-1}$ and stellar radii $R_* \sim 4 - 5R_\odot$. The disk models did not include any boundary layer, and the best-fit maximum disk temperatures were around 7000 K. Thermal instability models for FU Orionis outbursts indicate that $\alpha \sim 0.001$ for these systems (Clarke,

Lin, & Pringle 1990, Bell & Lin 1993). Our $10^{-4}\,M_\odot\ yr^{-1}$ solution for this value of α has a boundary layer effective temperature of around 7000–9000 K, quite close to the observed temperatures. The solution with $\alpha = 0.1$ is significantly hotter, suggesting that for this choice of accretion rate and stellar parameters, a low value of α is favored.

The work reported here includes only optically thick disks and boundary layers. There are indications that boundary layers in some T Tauri stars may be optically thin; both Basri & Bertout (1989) and Hartigan *et al.* (1991) derived optical depths $\tau \sim 1$ in some systems. Our models indicate that for accretion rates $\dot{M} < 10^{-7}\,M_\odot\ yr^{-1}$, the "opacity gap" in the 1500–5000 K temperature range will begin to affect the boundary layer. In particular, when $\dot{M} \lesssim 3 \times 10^{-8}\,M_\odot\ yr^{-1}$, the dynamical boundary layer may become optically thin, which could produce important changes in the overall structure of the boundary layer (Narayan & Popham 1993). We hope to examine optically thin boundary layer solutions in the near future. We also plan to make a detailed comparison of observed spectra of T Tauri and FU Orionis stars to solutions calculated with the model described here, incorporating a more sophisticated treatment of the vertical disk structure and a wavelength-dependent opacity in order to generate better model spectra.

11. APPENDIX A—POLYTROPIC FLUIDS

11.1 Two-Dimensional Fluid

We assume that the height-integrated two-dimensional fluid has an equation of state of the form

$$P = K\Sigma^{\gamma}, \tag{A1}$$

where K and γ are constants. This leads to a relation between the two-dimensional sound speed, c_s, and the radial infall velocity, v_R, (cf. equation [4])

$$c_s^2 = \frac{dP}{d\Sigma} = C_o(R|v_R|)^{1-\gamma}, \tag{A2}$$

where C_o is a constant.

Consider now the outer regions of the disk, where $\Omega(R)$ is very nearly equal to the Keplerian $\Omega_K(R) = \sqrt{GM/R^3}$. Further, assume that $j/R^{1/2} \ll 1$. Then, equations (3), (10), (11) and (A2), show that v_R, Σ and c_s scale as follows with radius,

$$v_R \propto R^{-(2\gamma-3)/2\gamma}, \tag{A3}$$

$$\Sigma \propto R^{-3/2\gamma}, \tag{A4}$$

$$c_s \propto R^{-3(\gamma-1)/4\gamma}. \tag{A5}$$

In the detailed theory of thin accretion disks, the regime of the "outer disk" is defined as the region where gas pressure dominates over radiation pressure and free-free opacity dominates over electron scattering (Shakura & Sunyaev 1973). In

this regime it can be shown that $v_R \propto R^{-1/4}$, $\Sigma \propto R^{-3/4}$ (cf. Frank, King & Raine 1985). We see that we can simulate this dependence with our two-dimensional fluid by choosing

$$\gamma = 2. \tag{A6}$$

Since most accretion disks do have an extended "outer disk," we specialize to this value of γ in all our calculations. We thus hope to obtain "realistic" behavior over at least some part of our simulated fluid.

11.2 Three-Dimensional Fluid

Let the fluid have a three-dimensional equation of state of the form

$$P_3 = K_3 \rho^{\gamma_3}, \tag{A7}$$

where P_3 is the pressure, ρ is the density, γ_3 is assumed to be constant, and K_3 is in general a function of R. Vertical hydrostatic equilibrium requires

$$\frac{GMz}{(R^2+z^2)^{3/2}} = -\frac{1}{\rho}\frac{\partial P_3}{\partial z} = -\frac{K_3\gamma_3}{\gamma_3 - 1}\frac{d(\rho^{\gamma_3 - 1})}{dz} \tag{A8}$$

where M is the mass of the central star. Integrating, and writing the result in terms of the Keplerian frequency,

$$\Omega_K(R) = \sqrt{GM/R^3}, \tag{A9}$$

we have

$$\rho(z) = \left[\frac{(\gamma_3 - 1)\Omega_K^2}{2K_3\gamma_3}(H^2 - z^2)\right]^{1/(\gamma_3 - 1)}, \tag{A10}$$

where H is the vertical half-thickness of the fluid, and we have assumed $H \ll R$. Similarly, we obtain

$$P_3(z) = K_3 \left[\frac{(\gamma_3 - 1)\Omega_K^2}{2K_3\gamma_3} (H^2 - z^2) \right]^{\gamma_3/(\gamma_3-1)}. \tag{A11}$$

We now calculate the height-integrated surface density, Σ, and two-dimensional pressure, P, of the fluid:

$$\Sigma = \int_{-H}^{H} \rho(z) dz = \sqrt{\pi} \frac{\Gamma[\gamma_3/(\gamma_3 - 1)]}{\Gamma[(3\gamma_3 - 1)/2(\gamma_3 - 1)]} \left(\frac{\gamma_3 - 1}{2K_3\gamma_3} \right)^{1/(\gamma_3-1)} H^{(\gamma_3+1)/(\gamma_3-1)}, \tag{A12}$$

$$P = \int_{-H}^{H} P_3(z) dz = \sqrt{\pi} \frac{\Gamma[(2\gamma_3 - 1)/(\gamma_3 - 1)]}{\Gamma[(5\gamma_3 - 3)/(\gamma_3 - 1)]} K_3 \left(\frac{\gamma_3 - 1}{2K_3\gamma_3} \right)^{\gamma_3/(\gamma_3-1)} \Omega_K^{2\gamma_3/(\gamma_3-1)} H^{(3\gamma_3-1)/(\gamma_3-1)}. \tag{A13}$$

If P and Σ are to have a polytropic relation as in equation (A1), then we require K_3 to scale as

$$K_3 = K_o \Omega_K^{2(\gamma-\gamma_3)/(\gamma-1)} H^{(1+\gamma-3\gamma_3+\gamma\gamma_3)/(\gamma-1)}, \tag{A14}$$

with K_o a constant. Substituting this in (A12) and (A13) we find

$$\Sigma = \sqrt{\pi} \frac{\Gamma[\gamma_3/(\gamma_3 - 1)]}{\Gamma[(3\gamma_3 - 1)/2(\gamma_3 - 1)]} \left(\frac{\gamma_3 - 1}{2\gamma_3 K_o} \right)^{1/(\gamma_3-1)} \Omega_K^{2/(\gamma-1)} H^{2/(\gamma-1)}, \tag{A15}$$

$$P = \sqrt{\pi} \frac{\Gamma[(2\gamma_3 - 1)/(\gamma_3 - 1)]}{\Gamma[(5\gamma_3 - 3)/(\gamma_3 - 1)]} \left(\frac{\gamma_3 - 1}{2\gamma_3} \right) \left(\frac{\gamma_3 - 1}{2\gamma_3 K_o} \right)^{1/(\gamma_3-1)} \Omega_K^{2\gamma/(\gamma-1)} H^{2\gamma/(\gamma-1)}. \tag{A16}$$

The two-dimensional sound speed then becomes

$$c_s^2 = \frac{dP}{d\Sigma} = \frac{\gamma(\gamma_3 - 1)}{(3\gamma_3 - 1)} \Omega_K^2 H^2,$$

$$\text{i.e.} \qquad \frac{c_s}{\Omega_K R} = \left[\frac{\gamma(\gamma_3 - 1)}{(3\gamma_3 - 1)}\right]^{1/2} \frac{H}{R}. \tag{A16}$$

This relation allows us to estimate the vertical thickness of the fluid in terms of the sound speed c_s.

The above relations are written for arbitrary γ and γ_3. We have already specified the value of γ in equation (A6). To fix γ_3, we need some other criterion. We decided that we would like K_3 to be independent of H for given Ω_K. This permits our fluid to behave like a star with a three-dimensionally polytropic equation of state in the transition region between the disk and the star. For $\gamma = 2$, this corresponds to

$$\gamma_3 = 3. \tag{A17}$$

Equation (A16) then becomes

$$\frac{c_s}{\Omega_K R} = \frac{1}{\sqrt{2}} \frac{H}{R}. \tag{A18}$$

This relation is used in Chapter 5 to estimate the vertical thickness of the fluid. Note that when equation (A18) is combined with equation (A5) we obtain a scaling of the form,

$$H/R \propto R^{1/8}, \tag{A19}$$

a standard result for the regime of the outer accretion disk.

12. APPENDIX B—THE CONDITION FOR A SUBSONIC BOUNDARY LAYER

Although the following analysis can easily be done for an arbitrary Ω_*, we will for simplicity assume $\Omega_* = 0$. For such a star, the boundary layer will occur at $R \sim 1$, and the disk solution will correspond to $j \sim 1$. Consider a subsonic boundary layer with $v_R < c_s \ll \Omega_K R \sim 1$. Under these conditions, equations (7), (10) and (11) simplify to

$$\frac{d|v_R|}{dR} \sim \frac{|v_R|(1-\Omega^2)}{(c_s^2 - v_R^2)} > \frac{|v_R|(1-\Omega^2)}{c_s^2}, \tag{B1}$$

$$\frac{d\Omega}{dR} \sim \frac{|v_R|}{\alpha c_s^2}(1-\Omega). \tag{B2}$$

Combining these two equations, we find

$$\frac{d|v_R|}{d\Omega} > \alpha(1+\Omega) > \alpha. \tag{B3}$$

Now, in the boundary layer, Ω increases from 0 to ~ 1. Therefore, $|v_R|$, which is extremely small inside the star, will have a value outside the boundary layer given approximately by

$$|v_R| \gtrsim \alpha. \tag{B4}$$

The solution will be subsonic only if the above value of v_R is less than the sound speed. From equations (4) and (16), setting $R \sim 1$ and assuming $j/R_{\rm out}^{1/2} \ll 1$, we estimate the sonic $|v_R|$ to be

$$|v_R|_{\rm sonic} \sim C_o^{2/(\gamma+1)} \sim (3/2)^{(\gamma-1)/(\gamma+1)} R_{\rm out}^{-(3-\gamma)/2(\gamma+1)} \alpha^{(\gamma-1)/(\gamma+1)} X^{2\gamma/(\gamma+1)}. \tag{B5}$$

The condition for a subsonic boundary layer then becomes

$$\alpha < (3/2)^{(\gamma-1)/2} R_{\rm out}^{-(3-\gamma)/4} X^{\gamma}. \tag{B6}$$

For our particular choice of parameters, $\gamma = 2$, $R_{\rm out} = 100$, this gives

$$\alpha \lesssim 0.39 X^2. \tag{B7}$$

An inspection of the sense of the inequalities in equations (B1) and (B3) shows that the coefficient in equation (B7) is likely to be an overestimate, possibly by a factor $\sim$2.

13. APPENDIX C - THE TOTAL LUMINOSITY OF THE DISK AND BOUNDARY LAYER

The energy dissipated per unit area by viscosity is

$$D = \nu\Sigma\left(R\frac{d\Omega}{dR}\right)^2. \tag{C1}$$

Assuming that all of the dissipated energy is radiated from the disk surface, an annulus of radial width dR contributes a luminosity

$$dL = 2\pi R dR \cdot \nu\Sigma\left(R\frac{d\Omega}{dR}\right)^2. \tag{C2}$$

We know, e.g. from equation (1) of Chapter 10, that $d\Omega/dR$ can be written

$$\frac{d\Omega}{dR} = \frac{v_R}{\nu}\left(\Omega - \frac{\dot{J}}{\dot{M}R^2}\right) = \frac{v_R}{\nu}\left(\Omega - \frac{j\Omega_K(R_*)R_*^2}{R^2}\right), \tag{C3}$$

where $\dot{J} = j\dot{M}\Omega_K(R_*)R_*^2$. Eq. (C3) can be substituted into (C2) to give

$$\begin{aligned} dL &= 2\pi R dR \cdot \nu\Sigma R^2\frac{d\Omega}{dR}\cdot\frac{v_R}{\nu}\left(\Omega - \frac{j\Omega_K(R_*)R_*^2}{R^2}\right) \\ &= 2\pi R v_R\Sigma\cdot(\Omega R^2 - j\Omega_K(R_*)R_*^2)\frac{d\Omega}{dR}dR \\ &= -\dot{M}(\Omega R^2 - j\Omega_K(R_*)R_*^2)d\Omega. \end{aligned} \tag{C4}$$

This can be integrated to find the total luminosity of the disk and boundary layer,

$$L_{tot} = -\dot{M}\int_{\Omega_{in}}^{\Omega_{out}}(\Omega R^2 - j\Omega_K(R_*)R_*^2)d\Omega. \tag{C5}$$

Using the relation

$$\Omega R^2 d\Omega = \Omega R d(\Omega R) - \Omega^2 R dR, \tag{C6}$$

and using the radial momentum equation (e.g., eq. (2) in Chapter 10),

$$\Omega^2 R = \Omega_K^2 R + v_R \frac{dv_R}{dR} + \frac{1}{\rho}\frac{dP}{dR}, \tag{C7}$$

we can then write

$$L_{tot} = \dot{M}\left[\int_{R_{in}}^{R_{out}} \Omega_K^2 R dR + \int_{v_{R,in}}^{v_{R,out}} v_R dv_R + \int_{P_{in}}^{P_{out}} \frac{dP}{\rho}\right.$$
$$\left. - \int_{(\Omega R)_{in}}^{(\Omega R)_{out}} \Omega R d(\Omega R) + \int_{\Omega_{in}}^{\Omega_{out}} j\Omega_K(R_*) R_*^2 d\Omega\right], \tag{C8}$$

which gives

$$L_{tot} = \dot{M}\left\{-[\Omega_K^2(R_{out})R_{out}^2 - \Omega_K^2(R_{in})R_{in}^2] + \frac{1}{2}[v_{R,out}^2 - v_{R,in}^2] + \int_{P_{in}}^{P_{out}} \frac{dP}{\rho}\right.$$
$$\left. - \frac{1}{2}[\Omega_{out}^2 R_{out}^2 - \Omega_{in}^2 R_{in}^2] + j\Omega_K(R_*)R_*^2[\Omega_{out} - \Omega_{in}]\right\}. \tag{C9}$$

If we assume $R_{in} = R_*$, $\Omega_{in} = \Omega_*$, and $\Omega_{out} = \Omega_K(R_{out})$, and remember that $\dot{M}\Omega_K^2(R_*)R_*^2$ is just the accretion luminosity $GM_*\dot{M}/R_*$, we have the result

$$L_{tot} = \frac{GM_*\dot{M}}{R_*}\left(1 - j\frac{\Omega_*}{\Omega_K(R_*)} + \frac{1}{2}\frac{\Omega_*^2}{\Omega_K^2(R_*)}\right) - \frac{GM_*\dot{M}}{R_{out}}\left(\frac{3}{2} - j\frac{R_*^{1/2}}{R_{out}^{1/2}}\right)$$
$$+ \frac{1}{2}\dot{M}v_R^2(R_{out}) - \frac{1}{2}\dot{M}v_R^2(R_*) + \dot{M}\int_{P_{in}}^{P_{out}} \frac{dP}{\rho}. \tag{C10}$$

The first term is identical to equation (5) in Chapter 9, and the remaining terms are usually small.

14. REFERENCES

Abramowicz, M. A., Czerny, B., Lasota, J. P., & Szuszkiewicz, E. 1988, ApJ, 332, 646

Abramowicz, M. A., & Kato, S. 1989, ApJ, 336, 304

Adams, F., Lada, C. J., & Shu, F. 1987, ApJ, 312, 788

Alexander, D. R., Augason, G. C., & Johnson, H. R. 1989, ApJ, 345, 1014

Balbus, S. A., & Hawley, J. F. 1991, ApJ, 376, 214

Balbus, S. A., & Hawley, J. F. 1992, ApJ, 400, 610

Basri, G., & Bertout, C. 1989, ApJ, 341, 340

Basri, G., & Bertout, C. 1991, in Structure and Emission Properties of Accretion Disks, ed. C. Bertout, S. Collin, J.-P. Lasota, & J. Tran Thanh Van (Paris: Editions Frontières)

Bath, G. T. & Pringle, J. E. 1981, MNRAS, 194, 967

Bell, K. R., & Lin, D. N. C. 1993, in preparation

Bergeron, P., Saffer, R. A., & Liebert, J. 1992, ApJ, 394, 228

Bertout, C., Basri, G., & Bouvier, J. 1988, ApJ, 330, 350

Bertout, C., & Regev, O. 1992, ApJ, 399, L163

Calvet, N., & Hartmann, L. 1992, ApJ, 386, 239

Chanmugam, G., & Brecher, K. 1987, Nature, 329, 696

Clarke, C. J., Lin, D. N. C., & Pringle, J. E. 1990, MNRAS, 242, 439

Cordova, F. A., & Mason, K. O. 1983, in Accretion Driven Stellar X-ray Sources, ed. W. H. G. Lewin & E. P. J. van den Heuvel (Cambridge: Cambridge University Press), p. 147

Dewey, R. J., & Cordes, J. M. 1987, Ap. J., 321, 780

Ferland, G. J., Langer, S. H., MacDonald, J., Pepper, G. H., Shaviv, G., & Truran, J. W. 1982, ApJ, 262, L53

Frank, J., King, A. R., & Raine, D. J. 1985, Accretion Power in Astrophysics (Cambridge: Cambridge University Press)

Ghosh, P., & Lamb, F. K. 1979a, ApJ, 232, 259

Ghosh, P., & Lamb, F. K. 1979b, ApJ, 234, 296

Ghosh, P., Lamb, F. K., & Pethick, C. J. 1977, ApJ, 217, 578

Gold, T. 1975, private communication listed in Shapiro and Lightman (1976).

Goodman, J. 1993, ApJ, 406, 596

Grindlay, J. E., & Bailyn, C. D. 1988, Nature, 336, 48

Hachisu, I. 1986, ApJS, 61, 479

Hartigan, P., Hartmann, L., Kenyon, S. J., Hewett, R., & Stauffer, J. 1989, ApJS, 70, 899

Hartigan, P., Kenyon, S. J., Hartmann, L., Strom, S. E., Edwards, S., Welty, A. D., & Stauffer, J. 1991, ApJ, 382, 617

Hartmann, L., & Kenyon, S. J. 1985, ApJ, 299, 462

Hartmann, L., Kenyon, S., & Hartigan, P. 1991, in Protostars and Planets III, ed. E. H. Levy & J. Lunine (Tucson: University of Arizona Press)

Hawley, J. F., & Balbus, S. A. 1991, ApJ, 376, 223

Hawley, J. F., & Balbus, S. A. 1992, ApJ, 400, 595

Helfand, D. J., Ruderman, M. A., & Shaham, J. 1983, Nature, 304, 423

Hillenbrand, L. A., Strom, S. E., Vrba, F. J., & Keene, J. 1992, ApJ, 397, 613

Horne, K. 1991, in Structure and Emission Properties of Accretion Disks, ed. C. Bertout, S. Collin, J.-P. Lasota, & J. Tran Thanh Van (Paris: Editions Frontières)

Huang, M., & Wheeler, J. C. 1989, ApJ, 343, 229

Hubeny, I. 1990, ApJ, 351, 632

Königl, A. 1991, ApJ, 370, L39

Kenyon, S. J. 1986, The Symbiotic Stars (Cambridge: Cambridge University Press)

Kenyon, S. J., & Hartmann, L. 1987, ApJ, 323, 714

Kenyon, S. J., Hartmann, L., Imhoff, C. L., & Cassatella, A. 1989, ApJ, 344, 925

Kenyon, S. J., Hartmann, L., & Hewett, R. 1988, ApJ, 325, 231

Kenyon, S. J., Oliversen, N. A., Mikołajewska, J., Mikołajewski, M., Stencel, R. E., Garcia, M. R., & Anderson, C. M. 1991, AJ, 101, 637

Kley, W. 1989, A&A, 222, 141

Kley, W. 1991, A&A, 247, 95

Kluźniak, W. 1987, PhD Thesis, Stanford University

Kulkarni, S. R., & Narayan, R. 1988 ApJ, 335, 755

Levermore, C. D. & Pomraning, G. C. 1981, ApJ, 248, 321

Lewin, W. H. G, & van den Heuvel, E. P. J., eds. 1984, Accretion-driven Stellar X-ray Sources (Cambridge: Cambridge University Press)

Lin, D. N. C., & Shields, G. A. 1986, ApJ, 305, 28

Lüst, R. 1952, Z. Naturforsch., 7a, 87

Lynden-Bell, D. 1969, Nature, 223, 690

Lynden-Bell, D., & Pringle, J. E. 1974, MNRAS, 168, 603

Matsumoto, R., Kato, S., Fukue, J., & Okazaki, A. T. 1984, PASJ, 36, 71

McClintock, J. 1991, Ann N Y Acad Sci., 647, 495

Mikołajewska, J., & Kenyon, S. J. 1992, AJ, 103, 579

Muchotrzeb, B. 1983, Acta, 33, 79

Muchotrzeb-Czerny, B. 1986, Acta, 36, 1

Muchotrzeb, B., & Paczyński, B. 1982, Acta, 32, 1

Narayan, R. 1992, ApJ, 394, 261

Narayan, R., & Popham, R. 1989, ApJ, 346, L25 (Chapter 4)

Narayan, R., & Popham, R. 1993, Nature, 362, 820 (Chapter 8)

Nomoto, K. 1984, ApJ, 277, 791

Nomoto, K. 1987, in The Origin and Evolution of Neutron Stars, ed. D. J. Helfand & J.-H. Huang (Dordrecht: Reidel), p. 281

Novikov, I. D., & Thorne, K. S. 1973, in Black Holes, ed. C. DeWitt & B. S. DeWitt (New York: Gordon & Breach)

Paczyński, B. 1987, Nature, 327, 303

Paczyński, B. 1991, ApJ, 370, 597

Paczyński, B., & Bisnovatyi-Kogan, G. 1981, Acta, 31, 283

Paczyński, B., & Wiita, P. J. 1980, A&A, 88, 23

Paczyński, B., & Zytkow, A. 1978, ApJ, 222, 604

Papaloizou, J. C. B. & Stanley, G. Q. G. 1986, MNRAS, 220, 593

Patterson, J. 1984, ApJS, 54, 443

Patterson, J. & Raymond, J. C. 1985a, ApJ, 292, 535

Patterson, J. & Raymond, J. C. 1985b, ApJ, 292, 550

Peek, B. M. 1942, J. Brit. Astr. Assoc., 53, 23

Pollack, J. B., McKay, C. P., & Christofferson, B. M. 1985, Icarus, 64, 471

Popham, R. & Narayan, R. 1991, ApJ, 370, 604 (Chapter 5)

Popham, R., & Narayan, R. 1992, ApJ, 394, 255 (Chapter 6)

Popham, R., Narayan, R., Hartmann, L., & Kenyon, S. 1993, ApJ Letters, in press (Chapter 10)

Prendergast, K. H., & Burbidge, G. R. 1968, ApJ, 151, L83

Press, W. H., Flannery, B. P., Teukolsky, S. A., & Vetterling, W. T. 1986, Numerical Recipes, (Cambridge: Cambridge University Press)

Prialnik, D., & Livio, M. 1985, MNRAS, 216, 37

Pringle, J. E. 1977, MNRAS, 178, 195

Pringle, J. E. 1981, ARA&A, 19, 137

Pringle, J. E. 1989, MNRAS, 236, 107

Pringle, J. E., & Rees, M. J. 1972, A&A, 21, 1

Pringle, J. E., & Savonije, G. J. 1979, MNRAS, 198, 177

Rees, M. J. 1984, ARA&A, 22, 471

Rees, M. J. 1988, Nature, 333, 523

Regev, O. 1983, A&A, 126, 146

Regev, O., & Hougerat, A. 1988, MNRAS, 232, 81

Regev, O., & Shara, M. M. 1989, ApJ, 340, 1006

Ryu, D., & Goodman, J. 1992, ApJ, 388, 438

Schmidt, G. 1989, in White Dwarfs, ed. G. Wegner (Berlin: Springer-Verlag), p. 305

Shakura, N. I., & Sunyaev, R. A. 1973, A&A, 24, 337

Shapiro, S. L., Lightman, A. P. & Eardley, D. M. 1976, ApJ, 204, 187

Shapiro, S. L., & Lightman, A. P. 1976, ApJ, 207, 263

Shapiro, S. L., & Teukolsky, S. A. 1983, Black Holes, White Dwarfs, and Neutron Stars (New York: Wiley)

Shklovsky, I. S. 1966, ApJ, 148, L1

Shu, F. H., Lizano, S., Ruden, S. P., & Najita, J. 1988, ApJ, 328, L19

Smak, J. 1984, PASP, 96, 5

Spruit, H. C. 1987, A&A, 184, 173

Sunyaev, R. A. & Trumper, J. 1979, Nature, 279, 506

Taam, R. E., & van den Heuvel, E. P. J. 1986, ApJ, 305, 235

Tohline, J.E. 1984, ApJ, 285, 721

Tylenda, R. 1981, Acta, 31, 267

van den Heuvel, E. P. J., & Taam, R. E. 1984, Nature, 309, 235

von Weizsäcker, C. F. 1943, Z. Astrophys., 22, 319

von Weizsäcker, C. F. 1948, Z. Naturforsch., 3a, 524

Wade, R. A. 1984, MNRAS, 208, 381

Wade, R. 1988, ApJ, 335, 394

Wade, R. A., & Ward, M. J. 1985, in Interacting Binary Stars, ed. J. E. Pringle & R. A. Wade (Cambridge: Cambridge University Press), p. 129

Wang, Y.-M. 1987, A&A, 183, 257

Watson, M. G., & King, A. R. 1991, in Structure and Emission Properties of Accretion Disks, ed. C. Bertout, S. Collin, J.-P. Lasota, & J. Tran Thanh Van (Paris: Editions Frontières)

Webbink, R. F., Rappaport, S., & Savonije, G. J. 1983, ApJ, 270, 678